Universidade de Lisboa

Faculdade de Ciências

Departamento de Física

Dynamics of Large-Scale Brain Activity in Health and Disease

Maria Teresa Andrade Santos Costa Montez

Doutoramento em Engenharia Biomédica e Biofísica

2008

Universidade de Lisboa

Faculdade de Ciências

Departamento de Física

Dynamics of Large-Scale Brain Activity in Health and Disease

Maria Teresa Andrade Santos Costa Montez

Thesis supervised by

Dr. Klaus Linkenkaer-Hansen

Center for Neurogenomics and Cognitive Research,

Section Integrative Neurophysiology, VU University Amsterdam,

Netherlands

Prof. Doutor Eduardo Ducla-Soares

Instituto de Biofísica e Engenharia Biomédica, Faculdade de

Ciências, Universidade de Lisboa

Doutoramento em Engenharia Biomédica e Biofísica

2008

To the memory of
my grandmother Lídia
and my friend Luís Guisado.

Contents

List of Original Publications

P1 **Montez T**, Linkenkaer-Hansen K, van Dijk BW, Stam CJ. 2006.

Synchronization likelihood with explicit time-frequency priors.

NeuroImage 33: 1117–1125.

P2 Stam CJ, Jones BF, Manshanden I, van Cappellen van Walsum AM, **Montez T**, Verbunt JP, de Munck JC, van Dijk BW, Berendse HW, Scheltens P. 2006.

Magnetoencephalographic evaluation of resting-state functional connectivity in Alzheimer's disease.

NeuroImage 32: 1335–1344.

P3 **Montez T**, Poil S-S, Jones B, Manshanden I, Verbunt JPA, van Dijk BW, Brussaard AB, van Ooyen A, Stam CJ, Scheltens P, Linkenkaer-Hansen K.

Impaired temporal correlations in temporo-parietal oscillations in early-stage Alzheimer's disease.

(Submitted)

P4 Stam CJ, **Montez T**, Jones BF, Rombouts SA, van der Made Y, Pijnenburg YA, Scheltens P. 2005.

Disturbed fluctuations of resting state EEG synchronization in Alzheimer's disease.

Clin Neurophysiol 116: 708–715.

Abbreviations

ACF	Autocorrelation function
AD	Alzheimer's disease
CDF	Cumulative probability Distribution Function
CSF	Cerebrospinal Fluid
DFA	Detrended Fluctuation Analysis
ECG	Electrocardiographic
EEG/MEG	Electro- / Magnetoencephalography
FIR	Finite Impulse Response
FFT	Fast Fourier Transform
(f)MRI	(functional) Magnetic Resonance Imaging
iEEG	Intracranial Electroencephalography
LRTC	Long-range Temporal Correlations
MMSE	Mini Mental State Examination
PDF	Probability Distribution Function
PET	Positron Emission Tomography
PSD	Power Spectral Density
S	Interdependency measure
SOC	Self-Organized Criticality
TF-SL	Time-frequency Synchronization Likelihood
WM	Working Memory

Abstract

Cognition relies on the integration of information processed in widely distributed brain regions. Neuronal oscillations are thought to play an important role in the supporting local and global coordination of neuronal activity. This study aimed at investigating the dynamics of the ongoing healthy brain activity and early changes observed in patients with Alzheimer's disease (AD). Electro- and magnetoencephalography (EEG/MEG) were used due to high temporal resolution of these techniques. In order to evaluate the functional connectivity in AD, a novel algorithm based on the concept of generalized synchronization was improved by defining the embedding parameters as a function of the frequency content of interest. The time-frequency synchronization likelihood (TF-SL) revealed a loss of fronto-temporal/parietal interactions in the lower alpha (8–10 Hz) oscillations measured by MEG that was not found with classical coherence. Further, long-range temporal (auto-) correlations (LRTC) in ongoing oscillations were assessed with detrended fluctuation analysis (DFA) on times scales from 1–25 seconds. Significant auto-correlations indicate a dependence of the underlying dynamical processes at certain time scales of separation, which may be viewed as a form of "physiological memory". We tested whether the DFA index could be related to the decline in cognitive memory in AD. Indeed, a significant decrease in the DFA exponents was observed in the alpha band (6–13 Hz) over temporo-parietal regions in the patients compared with the age-matched healthy control subjects. Finally, the mean level of SL of EEG signals was found to be significantly decreased in the AD patients in the beta (13–30 Hz) and in the upper alpha (10–13 Hz) and the DFA exponents computed as a measure of the temporal structure of SL time series were larger for the patients than for subjects with subjective memory complaint. The results obtained indicate that the study of spatio-temporal dynamics of resting-state EEG/MEG brain activity provides valuable information about the

AD pathophysiology, which potentially could be developed into clinically useful indices for assessing progression of AD or response to medication.

Keywords

Alzheimer's disease, electro- and magnetoencephalography, generalized synchronization, temporal correlations, functional connectivity.

Doença de Alzheimer, electro- e magnetoencefalografia, sincronização generalizada, correlações temporais, conectividade funcional.

Sumário

A doença de Alzheimer é uma doença neurodegenerativa responsável pela maioria dos casos de demência no mundo ocidental. O aumento da prevalência da doença e os avultados custos económicos associados ao acompanhamento dos doentes colocam como prioridades nas agendas científicas mundiais questões como: a identificação das causas desta patologia; a descoberta de biomarcadores para o diagnóstico precoce; a compreensão dos mecanismos afectados que levam às deficiências progressivas nas memórias episódica e de trabalho e diminuição de capacidades cognitivas observadas nos doentes e a procura de tratamentos eficazes.

Mais de um século passou desde que o psiquiatra alemão Alois Alzheimer descobriu, através de autopsias a doentes seus, placas beta amilóide e tranças neurofibrilhares (resultantes de alterações na conformação da proteína tau no interior dos microtúbulos). Apesar de nos nossos dias se terem aprofundado conhecimentos relativos à epidemiologia, à sintomatologia clínica, ao prognóstico e às alterações a nível celular e molecular, a causa da doença de Alzheimer não foi ainda determinada e os medicamentos disponíveis limitam-se a actuar ao nível dos sintomas. As teorias actuais para as causas da doença são as hipóteses associadas à proteína amilóide e à proteína tau responsáveis respectivamente pelas placas e pelas tranças neurofibrilhares observados por Alois Alzheimer e a hipótese colinérgica que relaciona a patologia com uma diminuição do neurotransmissor acetilcolina.

Com o avanço das técnicas de imagiologia e dos métodos de análise desenvolvidos esperam-se também progressos que permitirão o diagnóstico da doença em fases menos avançadas. Por exemplo, recorrendo a Tomografia por Emissão de Positrões é hoje possível mapear a deposição de amilóide; através de análises ao líquido encefaloraquidiano podem ser

quantificadas as concentrações de amilóide e tau; a diminuição do volume de regiões cerebrais pode ser medida em imagens de Ressonância Magnética e deficiências ao nível de fluxo sanguíneo associadas a diminuição de activação neural podem ser estudadas utilizando Ressonância Magnética funcional. As técnicas referidas anteriormente são apropriadas para a análise de alterações estruturais graças às suas resoluções espaciais. No entanto, é provável que as mudanças que ocorrem no início da doença sejam mais facilmente detectadas pelas alterações provocadas na dinâmica da actividade cerebral do que através de modificações estruturais características de um estado mais avançado da doença.

As técnicas de Electro- e Magnetoencefalografia (EEG/MEG) são técnicas de electrofisiologia que medem de forma não invasiva os campos electromagnéticos criados pela actividade síncrona de redes neuronais distribuídas pelo córtex com uma resolução temporal na ordem dos milissegundos permitindo o estudo da dinâmica da actividade cerebral a uma escala macroscópica. A importância das oscilações observadas na actividade neuronal para o processamento de informação pelo cérebro tem vindo a ser empiricamente reforçada por uma série de estudos que estabelecem a correspondência entre actividade em determinadas regiões em certas bandas de frequência com diversas funções desempenhadas pelo cérebro. Estudos de EEG/MEG revelaram um abrandamento nos doentes de Alzheimer dos ritmos encontrados nos cérebros saudáveis, isto é, um aumento da amplitude das frequências mais baixas e uma diminuição da amplitude nas frequências mais elevadas. Entrando em mais detalhe, verifica-se aumento de amplitude na banda delta (2-4 Hz) nas zonas frontais e occipitais, aumento global na banda teta (4-7 Hz), diminuição na banda alfa (8-12 Hz) na zona occipital e parietal e diminuição da banda beta (12-30 Hz) na zona frontal. Este abrandamento foi correlacionado com diminuição do volume cerebral e com alterações genéticas e provavelmente está relacionado com alterações no sistema colinérgico. A dessincronização das oscilações está associada à libertação de acetilcolina. Nos cérebros dos

doentes de Alzheimer esta dessincronização é alterada constituindo a causa do aumento de amplitude nas bandas de frequência mais baixa.

Processos cognitivos dependem da integração de processamentos que ocorrem simultaneamente em áreas cerebrais distintas e fenómenos oscilatórios representam um mecanismo essencial para esta integração, quer a nível local quer a nível global. Este mecanismo tem de ter capacidade de adaptação rápida para responder a estímulos e ao mesmo tempo manter um nível de referência a partir do qual é dada uma resposta. Este comportamento é observado em redes neuronais próximas de um chamado estado crítico caracterizadas por uma actividade muito diversa em termos espaciais e temporais. Através do desenvolvimento de novos métodos capazes de detectar estas interacções não lineares foi possível identificar informação contida na amplitude da actividade numa dada região, conectividade local entre bandas de frequências diferentes e interacções não lineares entre regiões cerebrais. Se bem que têm sido observadas alterações na actividade oscilatória em várias patologias, incluindo a doença de Alzheimer, não é ainda claro se os sintomas estão directamente relacionados com estas alterações ou se as alterações nas oscilações são um efeito secundário da verdadeira causa da patologia, não tendo portanto uma consequência directa nos défices cognitivos. A análise quantitativa da actividade oscilatória pode levar à descoberta de biomarcadores para monitorizar a progressão da doença e a resposta à administração de fármacos.

Os objectivos desta tese são, por um lado, perceber como é que a dinâmica complexa das oscilações neuronais pode ser quantificada e, por outro, compreender como é que esta é alterada na doença, especialmente na doença de Alzheimer utilizando dados de EEG e MEG de doentes e sujeitos saudáveis de idade semelhante medidos no estado de repouso com os olhos fechados. O trabalho realizado foi divulgado em três publicações ao longo do doutoramento, estando a quarta publicação em processo de revisão.

Na primeira publicação foi desenvolvido um algoritmo baseado no conceito de sincronização generalizada denominado *Time-Frequency Synchronization Likelihood* (TF-SL) que permite detectar conectividade funcional entre regiões cerebrais envolvendo termos não lineares. O conceito de sincronização generalizada pressupõe a repetição síncrona de estados em duas regiões, isto é, sempre que uma determinada região repita um determinado estado, outra região que esteja sincronizada com esta repetirá um outro estado. Estes estados são representados por vectores que correspondem a padrões, sendo uma das vantagens deste método, comparativamente com outros métodos utilizados, como por exemplo a correlação, o facto de estes padrões poderem ser diferentes nas duas regiões. O desenvolvimento introduzido no algoritmo prende-se com a definição dos parâmetros utilizados para a construção dos vectores (*time-delay embedding*) em função das frequências mais baixa e mais alta que compõem os padrões de interesse. Testes realizados ao método de TF-SL com dados de EEG mostram que o algoritmo é mais adequado à detecção do início de uma crise epiléptica do que a coerência clássica, tem uma maior resolução temporal e permite seguir a sincronização entre sinais provenientes de duas zonas do cérebro apresentando padrões de actividade complexos e consideravelmente diferentes numa zona e noutra.

Na segunda publicação quantificaram-se alterações na conectividade funcional em doentes de Alzheimer através da aplicação do método desenvolvido na primeira publicação e validado empiricamente na segunda publicação a dados de MEG obtidos com os sujeitos em estado de repouso de olhos fechados e compararam-se os resultados com os obtidos com coerência. Observou-se uma diminuição significativa da conectividade funcional entre as regiões do hemisfério esquerdo frontal e parietal, bem como frontal e temporal, na banda alfa mais baixa (8–10 Hz) que não foi encontrada para a coerência. As alterações verificadas sugerem uma associação com a perda de ligações entre diferentes regiões anatómicas, a redução de actividade colinérgica e o consequente declínio cognitivo.

Na terceira publicação testou-se a hipótese da memória fisiológica indexada pelas auto-correlações temporais na banda alfa estarem relacionadas com memória cognitiva e alteradas nos doentes de Alzheimer num subconjunto da mesma base de dados de MEG medidos com os sujeitos em repouso de olhos fechados da qual foram retirados os sujeitos para a segunda publicação. A análise de flutuações através de *Detrended Fluctuation Analysis* (DFA) dos dados revelou uma diminuição nas auto-correlações em escalas de tempo de 1 a 25 segundos em oscilações espontâneas na banda alfa definida no intervalo 6–13 Hz na zona parietal fortalecendo a hipótese da importância da memória fisiológica na memória cognitiva. A escolha de uma banda alfa mais ampla pretende anular as diferenças entre os grupos devidas ao desvio para frequências mais baixas do pico do espectro nos doentes de Alzheimer.

Na quarta publicação avaliou-se se o expoente de DFA, como medida de complexidade de sincronização, poderia ser usado como biomarcador da doença de Alzheimer utilizando dados de EEG de sujeitos em estado de repouso e olhos fechados. Expoentes mais baixos foram obtidos para doentes de Alzheimer comparativamente aos obtidos para sujeitos com queixas de memória (*subjective memory complaints*) para a banda alfa mais baixa (8–10 Hz) e para a banda beta, mostrando que a complexidade da série temporal de sincronização pode discriminar os dois grupos.

No entanto, de forma a obter uma discriminação individualizada e o diagnóstico precoce, estudos longitudinais incluindo grupos mais alargados de sujeitos são necessários para evitar que factores genéticos, isto é, valores diferentes para o biomarcador nos sujeitos saudáveis, sejam confundidos com alterações provocadas pela doença, assim como atenuações devidas à medicação administrada. Esta tese pretendeu contribuir para realçar o papel que estudos de EEG/MEG com sujeitos em repouso poderão ter na descoberta de biomarcadores, ao nível de sistemas, para a doença de Alzheimer, assim como ampliar o nosso conhecimento dos

mecanismos subjacentes a esta patologia através do desenvolvimento e aplicação de métodos que permitem a detecção de alterações ténues na dinâmica da actividade cerebral em fases iniciais da doença.

Acknowledgments

I would like to thank Dr. Cornelius J. Stam from the Department of Clinical Neurophysiology and MEG Centre of the VU University Medical Centre for sharing the valuable database of MEG recordings of Alzheimer patients (and elderly age matched controls) and for all the support given on the analysis of the data and clinical background on the disease. It is difficult for me to put in words my gratitude to Dr. Klaus Linkenkaer-Hansen from the CNCR, Section Integrative Neurophysiology, VU, Amsterdam, The Netherlands as he was an exemplar supervisor in the guidance of research questions to address, always motivating me to find my own ways. I am also deeply thankful to Professor Ducla-Soares from the Institute of Biophysics and Biomedical Engineering (IBEB), Science Faculty, University of Lisbon who has supported me since my first steps in scientific research and had a fundamental incentive role in the final stage of the PhD. The teamwork with Simon-Shlomo Poil proved me that the show will go on: I wish you good luck with your further research, my friend. The results achieved would not have been possible if I had not been fortunate to have fruitful discussions with Philip Scheltens, Bob van Dijk, Bethany Jones, Ilonka Manshanden, Jeroen Verbunt, Jan de Munck and Andreas Daffertshofer. I thank my colleagues at the VUmc: Sandra, Patrik, Mafalda, Sónia, Izabella, Ilonka, Geert, Arent, Fetsje, Adam, Fabrice, Dennis, Keith and Linda for creating a warm atmosphere, for example while eating cold sandwiches in the cantina. I would like to express my gratitude to Sandra L. for her sympathy and solutions to housing issues during my stay in Amsterdam. Huge hugs to João Graciano, Sandra and Rui, Roman B. and Marjan, Zsofi and Roman K., Patrik and Mia, Alexis, Susie, Christiaan, Maria and Alexandre, Duarte, Miguel and Inês for drying me up in the rainy days.

I would like to thank the Professors at IBEB: Pedro Miranda, Pedro Almeida and Alexandre Andrade for all the teachings. I am grateful to my colleagues from the doctoral programme (particularly Ana Carolina, Lília, Paulo and Pedro) and the residents: Sandra, Nuno M., Mónica, Hugo, Luís J., Luís F., Sofia, Susana, Paula,

Ricardo, Nuno O., Patrícia and Carlos for cooling me down while eating warm dishes at lunch as well as during stress peaks. Specials thanks to Ana Sousa and Beatriz Lampreia for making me feel in a nest. I would like to express also my gratitude to Dr. Claúdio for the graph analysis of weekly working hours and to the neighbours in Benfica for the coffee breaks,

Finalmente, agradeço à minha família por "tudo" e um beijinho especial para o meu sobrinho.

This study was financially supported by grants from the ***Fundação para a Ciência e Tecnologia*** (SFRH/BD/10592/2002) financed by POCI 2010 and FSE and the ***Fundação Calouste Gulbenkian*** (Proc. 79037) and resulted from the collaboration between the VU University Amsterdam, The Netherlands and the University of Lisbon, Portugal.

1. Introduction

Synchronized neuronal activity is a prominent feature of cortical networks and gives rise to oscillatory electromagnetic fields, which can be non-invasively measured with electro- or magnetoencephalography (EEG/MEG). The EEG and MEG are particularly well suited for the study of temporal dynamics of large-scale brain activity, because of the high temporal resolution of these techniques (~ millisecond). The importance of neuronal oscillations for information processing in the brain remains debated (Buzsaki and Draguhn, 2004); however, the past decade has witnessed an explosion in empirical evidence and theoretical arguments supporting a crucial role of oscillations in diverse brain functions (Buzsaki, 2006). In particular, it is increasingly acknowledged that cognition depends on integration of simultaneous processing in spatially distinct brain areas and that oscillations may provide an important mechanism for orchestrating this activity both locally and globally (Varela et al., 2001; Fries, 2005).

If oscillations are to play a role in coordinating activity on different spatial scales, it seems that oscillations need to balance the needs to swiftly adapt to processing demands while also providing a stable reference for neuronal representations. In recent years, several authors have advanced the hypothesis that this balancing act is supported by neuronal networks operating near a so-called critical state, which is characterized by a large variability in spatio-temporal activity (Linkenkaer-Hansen et al., 2001; Chialvo, 2007; Plenz and Thiagarajan, 2007). Critical or "meta-stable" dynamics may also be important for the transient coupling and exchange of information in distributed neuronal populations (Friston, 1994; Tononi et al., 1998; Stam, 2000; Varela et al., 2001). Advances in algorithms that can

identify and quantify changes in "meta-stable" or nonlinear dynamics have made it evident that neuronal oscillations are neither stable sinusoidal waves nor a form of filtered noise; rather, oscillations carry information in their waxing and waning amplitude patterns (Linkenkaer-Hansen et al., 2007), exhibit cross-frequency coupling locally (Palva et al., 2005a) and nonlinear interactions across brain regions (Stam et al., 2003a).

Brain-related disorders are commonly associated with aberrant oscillatory activity and much effort has been devoted to the characterization of the impact of pathology on neuronal oscillations. It remains a challenge, however, to understand whether symptoms are directly related to these changes or whether altered oscillatory activity is a side-effect of the underlying pathology without consequences for the cognitive impairments. Quantitative analysis of oscillatory activity may nevertheless lead to biomarkers for monitoring disease progression or responsiveness to therapeutic intervention (Frank and Hargreaves, 2003; Matthews et al., 2006). Much of the work in this thesis is aimed at understanding how the complex dynamics of neuronal oscillations may be quantified and how it is impaired in disease, especially Alzheimer's disease.

Alzheimer's disease (AD) is a neurodegenerative disorder characterized by a progressive decline in episodic and working memories and cognition. Although much is known about the epidemiology, clinical presentation, prognosis and the pathology at the cellular and molecular level, the cause of AD has not been identified and available treatment is only symptomatic. Many techniques have been used to investigate how the brain is affected in AD. For example, magnetic resonance imaging (MRI) has revealed atrophy of the medial temporal lobe, including the hippocampus and entorhinal cortex (van der Flier and Scheltens, 2005); functional magnetic resonance imaging (fMRI) and positron emission tomography (PET) have pointed to deficits in blood flow and metabolism in the posterior cingulate gyrus and precuneus (Fox et al., 2001); analysis of CSF from AD patients showed a decrease in the concentration of amyloid Aβ42 and an increase of tau (Waldemar, 2000); and EEG/MEG studies have shown slowing of spontaneous oscillations in AD with a suggested anterior displacement of the sources (Jeong, 2004; Osipova et al., 2005).

None of these techniques, however, allow for individual discrimination and diagnosis in the early stages of the disease (Nestor et al., 2004). Nevertheless, it is hoped that by studying the disease with a multitude of techniques and experimental protocols as well as through continued progress in the development of signal processing algorithms, this situation may one-day change to the benefit of the patients and a better understanding of the pathophysiology underlying the cognitive deficits. As an important spin-off from these pre-clinical studies, we are likely to learn about the neural basis of cognitive functions in the healthy brain.

2. Overview of the literature

2.1 Electro- and Magnetoencephalography

Electroencephalography (EEG) and magnetoencephalography (MEG) are non-invasive measures of the electric activity in the brain. EEG measures electric potential differences on the scalp and MEG records extracranial magnetic fields both generated by postsynaptic currents (Lopes da Silva and Van Rotterdam, 1999). These techniques require the summation of synchronous activity of thousands of pyramidal neurons that are oriented parallel to each other and perpendicular to the surface of the cortex. The EEG voltages are generated by extracellular compensatory currents, whereas the MEG measures intracellular activity located in the sulci where the pyramidal neurons are parallel to the surface of the head.

The localisation of the sources producing the electrical potentials and the magnetic fields is called the inverse problem and has no unique solution as different distributions of sources can lead to the same measured EEG and MEG signals (Helmholtz, 1853). The derivation from Maxwell's laws of the basic equations for solving the forward problem, i.e., computing the magnetic field created outside of the head by the distribution of currents within the brain, can be found in a review article (Hämäläinen et al., 1993). A comparison between different methods for source localisation has recently been reported (Liljeström et al., 2005).

The conventional whole-head EEG electrode locations and names are specified by the 10-20 system, reflecting the distance between adjacent electrodes to be either 10% or 20% of the total front-back or right-left distances of the skull and

identifying the lobe and the hemisphere location. The voltage differences measured from the scalp typically range from 10 to 100 μV (much larger values can be found especially in young children during sleep, and in brain pathology). EEG always has to be measured against some reference. Different montages reflect different solutions to this problem: "bipolar" if the difference is computed between adjacent channels; "referential" if a reference electrode is subtracted from each channel; "average" if the average of all the channels is used as the reference; and "laplacian" if the reference used is a weighted average of the neighbouring channels. None of these montages is perfect since the reference is seldom neutral. In contrast to EEG, MEG measurements are reference-free so that the problem with montages does not arise here. Perhaps due to the reference-free character MEG is more sensitive to nonlinear correlations and thus may be more suitable than EEG to assess functional connectivity (Stam et al., 2003a; Guevara et al., 2005).

The detection of the weak magnetic fields created by the brain ranging from 50 to 500 femtoTesla (up to a thousand femtoTesla in the case of epileptic spikes) is only possible using Superconducting Quantum Interference Devices (SQUIDs) and by attenuating environmental magnetic noise (e.g., from car traffic, power lines and the Earth's field) by measuring inside magnetically shielded rooms. Flux-transformers couple the magnetic flux to the SQUID and are required to be immerged in liquid Helium. The simplest flux transformer is a magnetometer, which measures the projection of the magnetic field along the normal of a single coil. When two magnetometers of opposite polarities are connected together and oriented along the radial (Fig. 1a), they form a 1st-order axial gradiometer (Vrba and Robinson, 2001). If the two opposite coils are placed in the same plane tangential to the scalp they form a planar gradiometer and, unlike for axial gradiometers, the largest signal is obtained directly above a given neuronal source (Fig. 1b and 2).

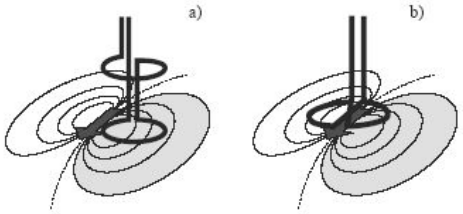

Figure 1 – Axial (a) and planar (b) gradiometers placed where the measured signal is maximal: on the side and just above the source, respectively. Simões (2002) adapted from Hari (1999).

Virtual Planar Gradiometers

The normal component of the magnetic field measured by axial gradiometers is considered a scalar field on a surface defined by the sensor array: $B(u,v)$ and may be transformed into virtual planar gradiometers by computing spatial derivatives (Fig. 2) for the two directions tangential to the scalp and orthogonal to each other: $\partial B/\partial u$ and $\partial B/\partial v$ using a 3D spline interpolation (Bastiaansen and Knösche, 2000).

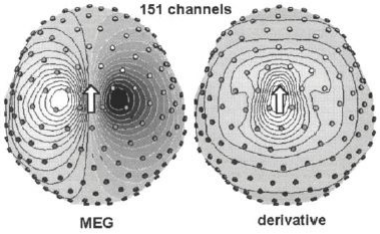

Figure 2 –Topographic representations of the magnetic field measured by axial gradiometers (left) and the gradient field representing the spatial derivative (right). (Bastiaansen and Knösche, 2000)

The decay of the gradient fields as a function of distance is more pronounced than the decay of electric fields, therefore MEG is more sensitive to superficial cortical activity and EEG detects more easily activity from deep sources than currents near the skull.

EEG and MEG share a temporal resolution of the order of milliseconds. EEG has a poorer spatial resolution than MEG due to smearing of the potentials caused by the different conductivities of the grey matter, cerebrospinal fluid, skull and scalp that do not affect the magnetic fields (i.e., volume conduction). However, EEG can be acquired simultaneously with functional magnetic resonance imaging (fMRI) taking advantage of the high spatial resolution of this technique.

Artefact removal using Independent Component Analysis

Since the first application of independent component analysis (ICA) to EEG (Makeig et al., 1996), the method is often used to detect and remove electrocardiographic (ECG), eye movements and muscular artefacts in EEG and MEG recordings (Jung et al., 2000).

The signals measured $x_1(t)$, $x_2(t)$, …, $x_m(t)$ corresponded to a sum of the independent components $s_1(t)$, $s_2(t)$, …, $s_n(t)$, and can thus be written as :

$$x_i = a_{i1}s_1 + a_{i2}s_2 + \ldots + a_{in}s_n = \sum_{j=1}^{n} a_{ij}s_j \quad \text{with } i = 1, \ldots, m.$$

The ICA model is given by $\boldsymbol{x} = A\,\boldsymbol{s}$, where A is the matrix of weights a_{ij}. It follows that $\boldsymbol{s} = W\,\boldsymbol{x}$, where W is the inverse of A. The components are assumed to be nongaussian, and are found by maximizing their nongaussianity. The outputs of the algorithm are time courses of the magnitude of each component and weights expressing the contribution of each channel signal to that component allowing a topographical representation (Fig. 3).

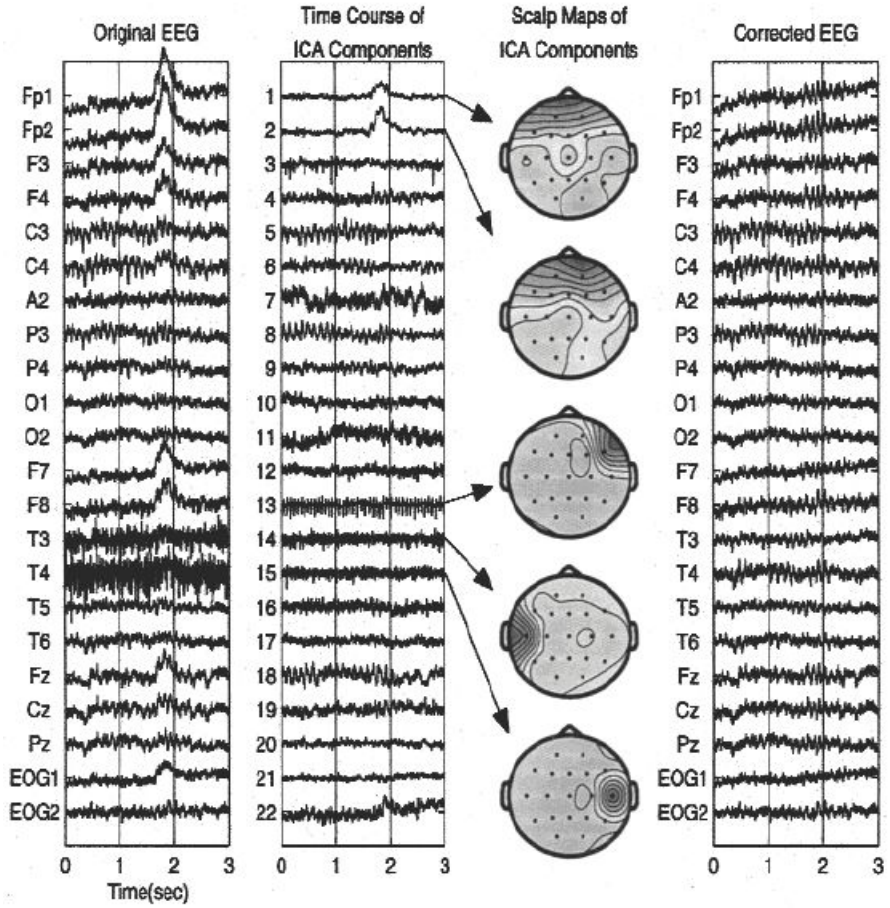

Figure 3 – Artefact removal by ICA. EEG time series (left), the corresponding ICA component activation (left middle), scalp maps of five of the components (right middle) and the EEG corrected for artefacts by removing the five selected components (right). (Jung et al., 2000)

Several algorithms are developed for computation of ICA, such as JADE (Cardoso et al., 1993) and the infomax (Bell and Sejnowski, 1995). Improved versions of the infomax, the so-called extended infomax (Amari et al., 1996; Makeig et al., 1997; Lee et al., 1999) and fixed-point ICA (Hyvarinen and Oja, 2000), have been implemented in the EEGLAB open source toolbox (Delorme and Makeig, 2004).

2.2 Alzheimer's Disease

Three studies in this thesis have investigated large-scale neuronal activity in Alzheimer's disease with the aim of identifying abnormal neurophysiological processes that could underlie parts of the cognitive dysfunction associated with Alzheimer's disease (AD). By studying large-scale neuronal activities we hope to help bridge the gap between our understanding of disease changes at cellular and sub-cellular levels on one hand, and clinical behavioural levels on the other hand.

Prominence and characteristics

The essential feature of dementia has been defined by the American Academy of Neurology as "impairment in short- and long-term memory, associated with impairment in abstract thinking, impaired judgement, other disturbances of higher cortical function, or personality change (…) severe enough to interfere significantly with work or usual social activities" (American Psychiatric Association, 1987).

The most important cause of dementia in the Western world was named after Alois Alzheimer, the German psychiatrist who discovered amyloid senile plaques and neurofibrillary tangles (formed by hyperphosphorylation of a microtubule-associated protein known as tau) in the atrophied brains of his patients while performing autopsies. Two competing theories attribute the cause of the disease to these two proteins, and are known as the amyloid (Hardy and Allsop, 1910) and the tau (Mudher and Lovestone, 2002) hypotheses. A third theory, the cholinergic hypothesis, associates AD with a decrease of the acetylcholine neurotransmitter (Shen, 2004).

A certain diagnosis of Alzheimer's disease continues to require post-mortem analysis, although nowadays we can track changes due to a probable AD in vivo, e.g., using MRI to measure the brain atrophy (Karas et al., 2004); PET to map the amyloid deposition; analysis of CSF for quantifying the concentration of amyloid

and tau (Jeong, 2004; Waldemar et al., 2007), and EEG (Boerman et al., 1994; Jonkman, 1997; Jeong, 2004) and MEG (Berendse et al., 2000; Maestu et al., 2001; Fernandez et al., 2002; Osipova et al., 2005) to follow electrophysiological changes that will be addressed in more detail in this thesis.

Early affected regions in AD are the medial temporal lobe, retrosplenial and posterior cingulate cortex. The retrosplenial cortex has dense reciprocal projections to the hippocampus and parahippocampal gyrus, where morphological changes occur in AD patients (Hyman et al., 1984; Braak et al., 1993) and are likely to be the cause of the prominent memory deficits characterizing the disease.

Posterior and frontal regions showing a consistent decrease of activity during attention demanding cognitive tasks have been identified in a PET study (Raichle et al., 2001), suggesting the existence of a default mode of brain function. The functional connectivity of these regions was addressed for the first time in a later study (Greicius et al., 2003) using fMRI. The same regions have shown metabolism differences (Fig. 4) and amyloid deposition (Fig. 5) in older adults with AD.

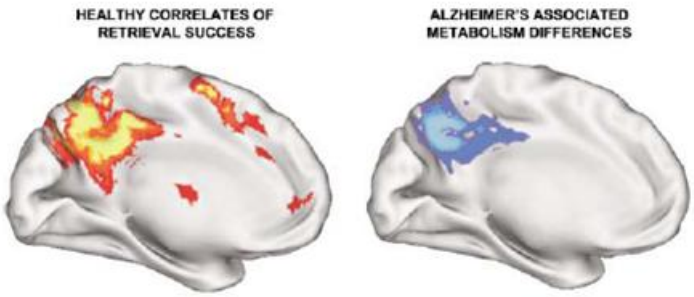

Figure 4 – Precuneus activity correlates with successful recall of items in healthy subjects (left) and show reduced metabolism in AD (right). (Buckner, 2004)

Decreased fMRI resting-state activity was also found with ICA in the posterior cingulate cortex and hippocampus of patients of AD, distinguishing them from healthy aging controls (Greicius et al., 2004). The disrupted connectivity between these two regions is in agreement with the posterior cingulate cortex hypo-metabolism reported in PET studies.

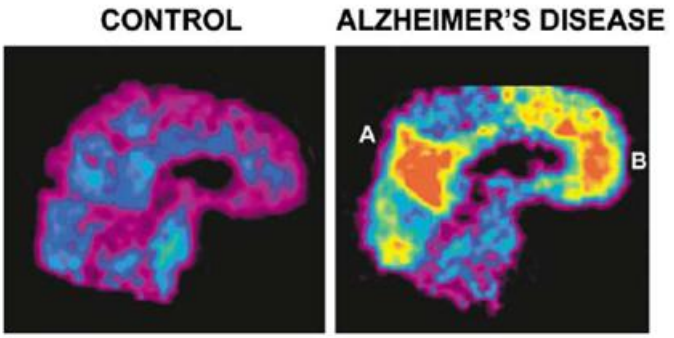

Figure 5 – Amyloid deposition in AD in the posterior parietal (A) and fontal cortex (B). (Buckner, 2004)

At later stages of the disease, distributed neocortical areas are affected (Braak et al., 1999) giving rise to other cognitive dysfunctions. EEG (Jonkman, 1997; Jeong, 2004) and MEG may allow the study of dynamical changes at early stages of AD (Stam, 2007).

EEG and MEG studies of AD

EEG dominant rhythms found in the healthy human brain (Berger, 1929) have been known for many years to be affected in AD (Weiner and Schuster, 1956; Letemendia and Pampiglione, 1958; Liddell, 1958; Gordon and Sim, 1967; Soininen et al., 1982; Coben et al., 1983; Penttila et al., 1985).

EEG studies have shown a slowing of the dominant rhythms in AD, meaning that an increase of power was observed in the delta (2-4 Hz) and theta (4-7 Hz) frequencies, and a decrease was reported for the alpha (8-12 Hz) and beta (12-30 Hz) bands (Jeong, 2004). MEG studies have confirmed these findings (Fig. 6) and suggested an anterior displacement of the sources of these rhythms (Berendse et al., 2000; Maestu et al., 2001; Fernandez et al., 2002; Fernandez et al., 2003; Maestu et al., 2003; Maestu et al., 2004; Maestú et al., 2005; Osipova et al., 2005; Fernandez et al., 2006).

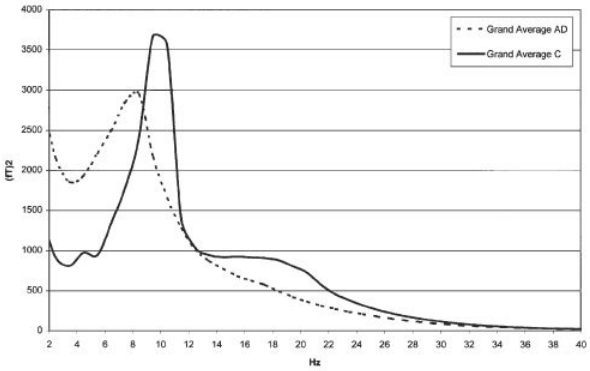

Figure 6 – MEG slowing in AD. Grand averages of spectra for 20 AD patients and 20 controls for 117 MEG channels (van Walsum et al., 2003).

AD patients showed an increase in delta power in the frontal and occipital regions; overall increase in theta power and decrease in beta power in the frontal region (Fig. 7).

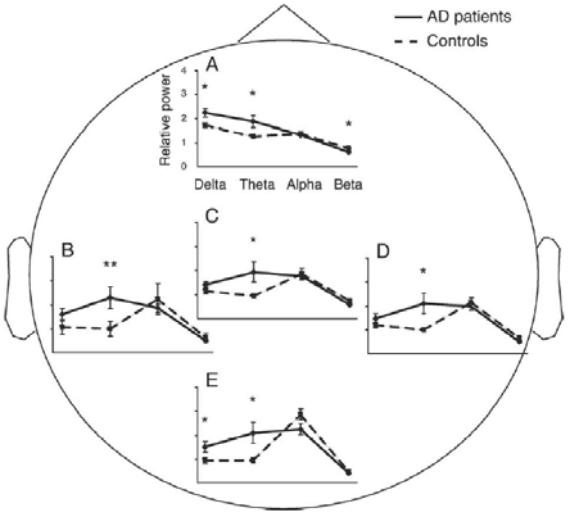

Figure 7 – Mean relative power and standard errors in the delta (2–4 Hz), theta (4–7 Hz), alpha (7–12 Hz), and beta (12–30 Hz) bands for 11 AD patients and 12 controls in the 22 frontal (A), 38 left temporal (B), 32 central (C), 38 right temporal (D) and 32 occipital (E) channels. * $p < 0.05$; ** $p < 0.01$. The mean relative power was obtained by dividing the mean band power by the total power at 2–30 Hz (Osipova et al., 2005).

The EEG and MEG slowing has been correlated with brain atrophy and the APOE genotype and is likely to be caused by the loss of cholinergic innervation of the cortex (Riekkinen et al., 1991; Lehtovirta et al., 1996). The desynchronization of spontaneous oscillations across various brain regions in the waking stage is associated with the release of acetylcholine (Celesia and Jasper, 1911; Kanai and Szerb, 1965). Pathological changes in the cholinergic system and the administration of pharmacological acetylcholine antagonists, by reducing the available acetylcholine, affect the desynchronization mechanisms and cause an increase of high amplitude slow-wave activity (Longo, 1966; Vanderwolf and Robinson, 1981).

Transient cognitive deficits caused by the administration of cholinergic antagonists to healthy subjects are reflected by similar changes in EEG and MEG signals (Sannita et al., 1987; Neufeld et al., 1994; Osipova et al., 2003).

2.3 Analysis of resting-state EEG and MEG data

The analysis of EEG and MEG data may be divided into stimulus-driven activity or intrinsically generated ongoing activity. Stimulus-driven activity leads to event-related potentials or fields and was not studied in this thesis. Here we focussed on the classical condition of eyes-closed rest, which is associated with prominent ongoing or spontaneous oscillations. Resting-state brain activity has also been studied intensively with metabolic techniques, e.g., PET and fMRI (Fox and Raichle, 2007) or the combination of EEG and fMRI (Mantini et al., 2007). Only little is known about the functional role of brain activity during rest (Raichle and Mintun, 2006), but the experimental condition has proven useful for clinical studies. The use of specific tasks aimed at activating brain regions assumed to be involved in AD might result in abnormally high as well as abnormally low task-related activation (Pijnenburg et al., 2004; Osipova et al., 2005).

Despite the general acceptance of the notion that synchronous oscillations present an important mechanism for integrating information processing in the brain (Singer, 1999), they are only a partial explanation of the relation between brain dynamics and cognition. Several authors have pointed out that information processing requires a self-organized dynamical process, whereby synchronous cell assemblies are continuously being formed and destroyed (Friston, 2000; Breakspear, 2002; Freeman and Rogers, 2002). Each synchronous cell assembly is hypothesized to be a fragile or "meta-stable" short-lived structure that may represent complex information; information processing required for cognition then consists of a succession of such short-lived synchronous cell assemblies exhibiting a scale-free spatial and temporal behaviour analogous to that of meta-stable patterns formed in equilibrium systems at the critical point of a phase transition (Beggs. 2007. Phil Trans R Soc. The criticality hypothesis; Chialvo DR (2007): The brain near the edge. Cooperative Behavior in Neural Systems: Ninth Granada Lectures. pp 1–12.). Analytical tools determining the level of synchronization with a high time resolution are required to study this ‘fragile binding’. Section 2.3.1 presents a brief explanation

of some methods for the evaluation of linear and nonlinear statistical dependencies that have been used in this thesis. A substantial part of this thesis consisted in the improvement of an algorithm based on generalized synchronization.

Optimal brain function has been suggested to require a suitable balance between local specialization and global integration of brain activity (Tononi et al., 1998). A large number of studies have aimed at identifying functional connectivity as defined by correlations between activity in different brain regions and interpreted this as a "functional coupling". Only little attention has been paid, however, to the potential importance of correlations over time, e.g., for ongoing mnemonic processes during resting-state periods. Spontaneous resting-state activity is characterized by amplitude modulation of ongoing oscillations in time-scales up to tens of seconds as indicated by long-range temporal auto-correlations (Linkenkaer-Hansen et al., 2001). The observed power-law form suggests existence of critical dynamics, supporting the theory of a critical state in the underlying neuronal network [see e.g. (Bak, 1997; Chialvo and Bak, 1999; Beggs and Plenz, 2003; Beggs and Plenz, 2004; Abbott and Rohrkemper, 2007; Mazzoni et al., 2007) (Kinouchi and Copelli, 2006; Levina et al., 2007; Poil et al., 2008b)]. In fact, the phenomenon of so-called self-organized criticality has been found in many manifestations of nature. Section 2.3.2 presents the definitions of different measures that can be used to quantify long-range temporal correlations (LRTC) in time series.

The measures used to quantify modulation of amplitude can also be used to follow temporal correlations of functional connectivity levels expressed by synchronization time series. It has been shown that the level of synchronization shows considerable fluctuations in healthy subjects (Gong et al., 2003), and that these fluctuations are affected by a working memory task (Stam et al., 2002a). Further support for the hypothesis of fluctuating synchronization levels comes from a study demonstrating nonlinear and non-stationary aspects of coupling in healthy subjects (Stam et al., 2003a). There seems to be increasing evidence that cognition depends not exclusively upon synchronization *per se*, but rather on the *dynamics of synchronization*.

Evaluation of functional coupling

Review of methods detecting nonlinear statistical dependencies

One key challenge in systems neuroscience is to develop tools to detect when, where, and how spatially distributed populations of neurons communicate. A large number of factors contribute to this challenge, e.g., the poor spatial resolution of non-invasive EEG/MEG data, an often low signal-to-noise ratio, and the fact that the function that governs the coupling of neuronal assemblies is not known *a priori* and may include nonlinear terms. Methods detecting linear statistical dependencies remain the most commonly used in studies on neuronal interactions; however, the nonlinear terms may reveal essential aspects of the coupling and require sensitive methods (Fig. 8) for their detection and quantification (Pereda et al., 2005; Stam, 2005).

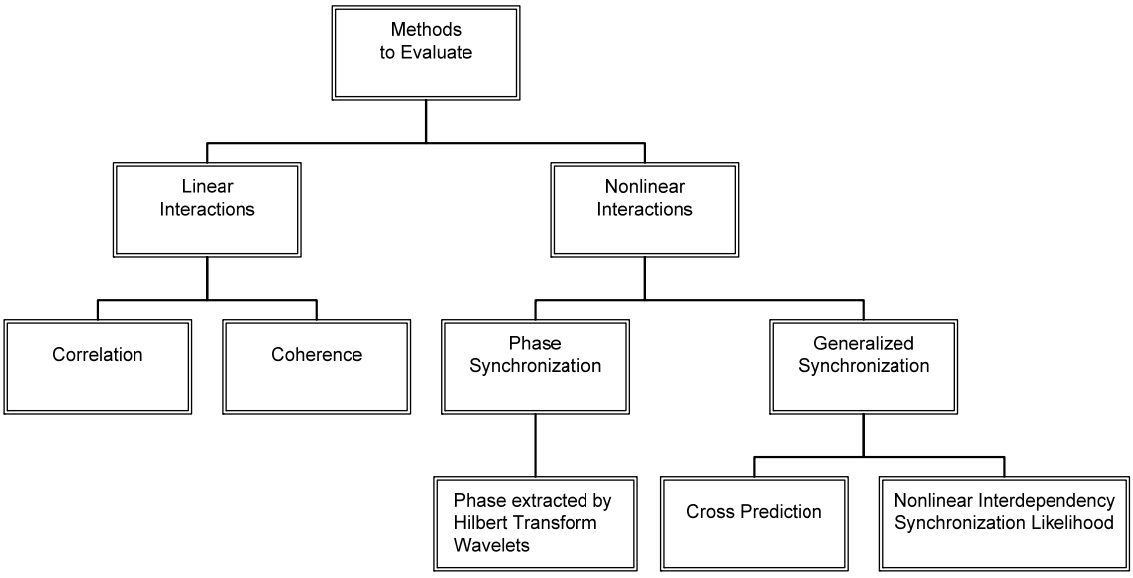

Figure 8 – Methods to evaluate linear and nonlinear statistical dependencies across sensors. Adapted with permission from *Onderzoek naar "functionele connectiviteit" met*

***EEG en MEG*, oral presentation by C.J. Stam at Medische Natuurwetenschappen, 6-6-2005.**

Correlation is the oldest and most classical measure of interdependencies between two time series and remains one of the mostly used measures. The cross-correlation function, C_{xy} between signals normalized to have zero mean and unit variance $x(t)$ and $y(t)$ is given by:

$$C_{xy}(\tau) = \frac{1}{N-\tau}\sum_{k=1}^{N-\tau} x(k+\tau)y(k) \qquad \textbf{(1)}$$

where N is the total number of samples and τ the time lag between the signals. The introduction of the fast Fourier transform (FFT) turned frequency-based measures increasingly popular. The coherence function gives the linear correlation between two signals as a function of the frequency. Coherence is a measure of linear phase correlations in a sliding window. The data set is divided into segments of length equal to the time resolution wanted and the spectra are estimated by averaging the periodogram over these segments (Welch, 1967). *Coherence* spectrum is normally computed as:

$$k_{xy}^2(f) = \frac{\left|\left\langle S_{xy}(f)\right\rangle\right|^2}{\left|\left\langle S_{xx}(f)\right\rangle\right|\left|\left\langle S_{yy}(f)\right\rangle\right|} \qquad \textbf{(2)}$$

where $\langle\cdot\rangle$ denotes average over the segments, f is the frequency, S is the periodogram and k_{xy} is the coherence. Coherence computation requires a large number of oscillation cycles to estimate the consistency of linear correlations between oscillations. The size of the sliding window gives the time resolution.

To detect statistical interdependencies that are not governed by simple linear functions methods able to detect nonlinear interdependencies are required. Phase synchronization in contrast to coherence is not dependent upon the amplitudes of the signals and can be computed using the Hilbert transform (Tass et al., 1998) or wavelet analysis (Lachaux et al., 1999). However, the concept of phase makes sense

only in oscillatory systems. Neurophysiological signals are often noisy and exhibit random phase slips, thus the phase-locking condition:

$$\varphi'_{n,m}(t) = \left| n\phi_x(t) - m\phi_y(t) \right| \bmod 2\pi \leq \text{constant} \qquad \textbf{(3)}$$

must be understood in a statistical sense, i.e., as the existence of a preferred value in the distribution of the relative phase (Rosenblum and Pikovsky, 2001).

Generalized Synchronization

Generalized synchronization is the most general form of interaction between two dynamical systems, where the state of a response system Y is a function of the state of the driver system X: $Y = F(X)$ (Rulkov et al., 1995). Generalized synchronization extends the study of coupling between identical systems to systems with different dynamics. Several algorithms have been proposed to measure Generalized synchronization defined from a state-space representation of the signals. One approach is based on cross prediction, i.e., the improvement in the prediction of X knowing Y (Schiff et al., 1996; Le Van Quyen et al., 1998). More reliable methods rely on the quantification of how embedding vectors that are close in the state space of one signal map on to vectors that are also close in the state space of the other signal, thus requiring the definition of a "critical distance". The interdependency measure (S) is sensitive to signals having different amplitudes or different degrees of freedom (Arnhold et al., 1999; Pereda et al., 2001).

Synchronization likelihood

A novel method referred to as synchronization likelihood (SL) was developed to solve the dependence of generalized synchronization measures on local power (Stam and van Dijk, 2002). The lack of a rigorous definition of SL parameters based on the frequency content of the neurophysiological data and an incomplete understanding of the influence of the parameter choices on the estimation of the interdependency

between signals motivated the introduction of an SL algorithm with explicit time-frequency priors (Montez et al., 2006) and Publication P1 of this thesis.

Signals are often bandpass filtered in a frequency band of interest: [*LF*, *HF*], before the computation of SL. The computation of SL can be divided into steps that will be explained in detail in this section: (*i*) state-space representation; (*ii*) detection of recurrences within each channel; (*iii*) computation of the likelihood of simultaneous recurrences in the two channels; and finally (*iv*) repetition of steps *i*–*iii* for different time points.

I. From time series to state-space representations of data: time-delay embedding

Patterns of activity can be represented by vectors in the state space (Fig. 9) by time-delay embedding (Takens, 1981). The embedding vectors are defined by two parameters: the lag L (the time interval between time-series samples used for the embedding vector); and the embedding dimension m (the number of samples taken from the time series for every embedding vector).

From the time series $x_{k,i}$ of channel k, the state vector $X_{k,i}$ is given by:

$$X_{k,i} = (x_{k,i}; x_{k,i+L}; x_{k,i+2*L}; \ldots x_{k,i+(m-1)*L}) \qquad \textbf{(4)}$$

Note that $X_{k,i}$ represents the state of the system in a time interval of length $L*(m-1)$, but for convenience we will refer to this interval as the state at time i, i.e., the beginning of the interval.

Several definitions of the embedding parameters have been proposed (Cellucci et al., 2003). The embedding dimension must be sufficiently high (more than twice the dimension of the system's attractor) to preserve the dynamical properties of the system (Whitney, 1936). In the context of finite, noisy and non-stationary signals, the lag can be chosen equal to the time interval after which the autocorrelation function (or the mutual information) of the time series drops to $1/e$ of its initial value, and repeat the analysis for increasing values of m until the result of the analysis is stable. Other approaches can be found for the definition of the lag

(Rosenstein et al., 1994) and the embedding dimension (Kennel et al., 1992). It has also been suggested to define the embedding window to be equal to the time after which the autocorrelation function of the times series becomes zero (Albano and Rapp, 1993).

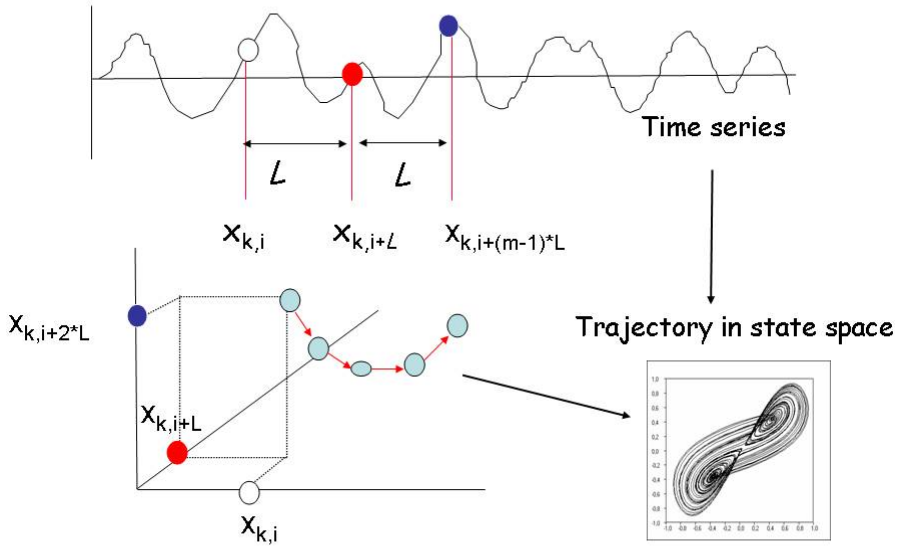

Figure 9 – Schematic representation of time-delay embedding. Adapted with permission from *Onderzoek naar "functionele connectiviteit" met EEG en MEG*, oral presentation by C.J. Stam at Medische Natuurwetenschappen, 6-6-2005.

Most of the previous studies did not deal with oscillatory processes. The choice of the embedding parameters will affect the frequency content of the patterns detected: the lag will determine the fastest oscillations sampled and the size of the embedding window, given by the product of the lag and $(m-1)$, will set the lowest limit. The awareness of these facts is crucial to the interpretation of the evaluation of functional connectivity in the brain using time-delay embedding methods.

II. Detection of recurrences of states in two potentially coupled systems

We start by constructing a reference vector in channel A at time i, $X_{A,i}$. Then we construct vectors $X_{A,j}$ along the time series at times j inside a time window W_2 and outside a time window W_1 (Fig. 10).

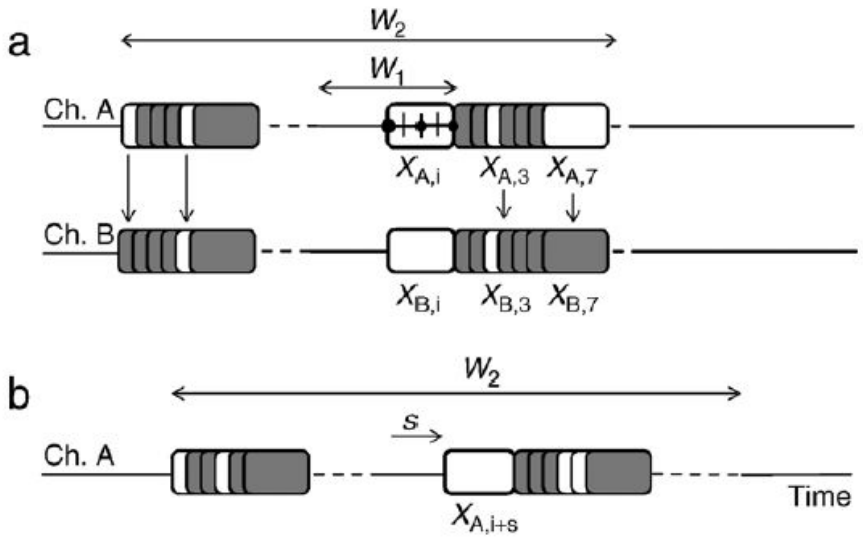

Figure 10 - State vectors and SL parameters (L, m, W_1, W_2 and s) with respect to the time series of channels A and B. (a) The reference vector of channel A, $X_{A,i}$ was obtained for m = 3 samples (small ticks) and L = 2 samples (dots). The state vectors (squares) are defined for times outside W_1 and inside W_2 and pairs for two time points $X_{A,3}$ and $X_{B,3}$,and $X_{A,7}$ and $X_{B,7}$ are marked. The time windows are centred at i. The time series of the channels are represented by solid horizontal lines and the range of the times of the state vectors is indicated with a dashed line. The vectors that are closer than the respective critical distances $r_{A,i}$ and $r_{B,i}$ are represented in white and the vectors that are not within the respective critical distance are represented in grey. The pair $X_{A,3}$ and $X_{B,3}$ is an example of a simultaneous recurrence. (b) A new reference vector is constructed for channel A at a time point with an increment s (arrow). The windows W_1 and W_2 are centred at $i + s$ and the state vectors close and distant from the reference vector are represented as in panel a (Montez et al., 2006).

W_1 is defined in order to prevent autocorrelation effects. Finally, we compute the Euclidean distance to the reference vector. The criterion for considering vectors close, meaning that they represent recurrences, is defined by the parameter p_{ref} equal to the ratio between the number of vectors considered close and the total number of vectors. The same procedure is applied to channel B.

The number of vectors considered close, referred to as recurrences, is the same for both channels and is given by:

$$n_{rec} = [W_2 - W_1 + 1] * p_{ref} \quad \textbf{(5)}$$

A vector $X_{A,j}$ is considered a recurrence of the reference vector $X_{A,i}$ if its distance to the reference vector given by $\left|X_{A,i} - X_{A,j}\right|$ is lower than the critical distance $r_{A,i}$. The same is valid for a vector $X_{B,j}$ and the critical distance $r_{B,i}$. The introduction of the parameter p_{ref} is the key improvement of SL when compared to the interdependency measure, because the critical distances are allowed to be different for each channel.

III. Computation of the likelihood (SL) that states recur simultaneously in the two systems

The times at which the recurrences occur in each channel are obtained and the number of simultaneous recurrences in both channels is determined:

$$n_{AB} = \sum_{j=i-W_2/2}^{i-W_1/2} n + \sum_{j=i+W_1/2}^{i+W_2/2} n \quad \textbf{(6)}$$

$$n = \theta(r_{A,i} - \left|X_{A,i} - X_{A,j}\right|)\theta(r_{B,i} - \left|X_{B,i} - X_{B,j}\right|)$$

where θ represents the Heaviside function which is equal to one if the argument is positive or zero and equal to zero if the argument is negative.

A better understanding of the advantages of the introduction of the parameter p_{ref} on the computation of SL can be facilitated by a schematic representation of the formulas and the mapping of the state vectors from channel A into the state space of channel B (Fig. 11).

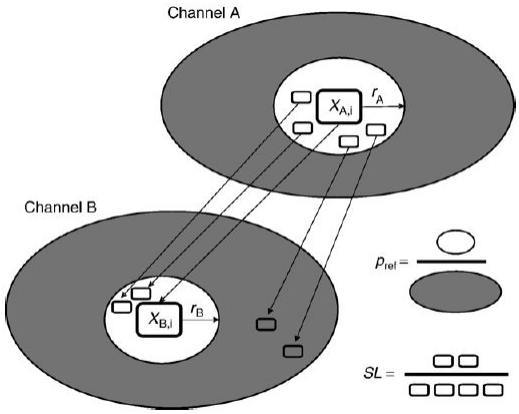

Figure 11 – Schematic representation of SL between two channels in terms of state vectors and critical distances. State vectors of channel A closer to the reference vector $X_{A,i}$ than the critical distances $r_{A,i}$ are shown inside white ellipses and connected by lines to state vectors of channel B, $X_B = F(X_A)$, at the same time points. Two out of four recurrences of $X_{A,i}$ in channel A are associated with simultaneous recurrences of $X_{B,i}$ in channel B, whereas the others fall outside the respective critical distance and are represented inside grey ellipses. P_{ref} is given by the ratio between the number of vectors close than the critical distance and the total number of state vectors. P_{ref} is the same for both channels whereas the critical distances are usually different. SL between channel A and B at time *i* is given by the ratio between the number of simultaneous recurrences and the total number of recurrences within channels, which per definition is n_{rec}. Adapted with permission (Posthuma et al., 2005) and included in P1 (Montez et al., 2006).

The parameter p_{ref} gives the ratio between the state space (strictly speaking the number of state-space vectors) that are defined by the critical distance to be closest to the reference vector, and the total state space (i.e., all state-space vectors). Generalized synchronization occurs when the state vectors at times *j* that are close to the reference vector in channel A are "mapped" into the state space of channel B, i.e., if recurrences of the references vector in channel A appear at the same times that recurrences of the reference vector of channel B appear in channel B (Fig. 10). SL is an index of the likelihood that recurrences of a reference state in channel A at certain

time points are associated with recurrences of a reference state in channel B at those same time points.

SL is given by the ratio between the number of simultaneous recurrences and the total number of recurrences in each channel, which per definition is n_{rec}.:

$$SL_i = \frac{n_{AB}}{n_{rec}} \tag{7}$$

Note once more that the value of SL for a time point i is a measure of the synchronization between the two channels based on the simultaneous repetition of states, represented by state vectors, within a time window of length W_2.

IV. Computation of SL for different time points

In order to obtain an SL time series, new reference vectors are constructed along the time series of the channels and the previous steps are repeated. The sampling frequency of SL is given by the ratio between the sampling frequency of the raw data and the time increment s. It is important to acknowledge that the temporal resolution of SL is high in the sense that SL values can vary dramatically from one reference time point to another, but that the time resolution is low in the sense that each SL value refers to the temporal structure of the signals in a window of length W_2, which is usually several orders of magnitude larger than the time increment s.

A conservative definition of s equal to one sample will lead to longer computational processing time and possibly redundant information, because the same states might be represented by several reference vectors, though it is the recommended procedure as it is the safest choice.

Boundary conditions must be taken into consideration, because it is not possible to fit a window $W_2/2$ on both sides of reference vectors at the beginning and at the end of the time series of data. In Publication P1, we dealt with this issue in a very pragmatic way as described in section 4.3 of this thesis.

Temporal correlations as an index of memory

In the previous section, we outlined recent developments for identifying correlations between neuronal signals obtained from different sensors or brain regions with the aim of revealing so-called "functional connectivity"—a coupling of activity that is thought to be crucial for parallel processing. Brain activity, however, may also be highly organized over time and it is therefore expected that a quantitative analysis of correlations in EEG/MEG signals on multiple time scales may reveal important information about the functional organization of the underlying neuronal networks (Linkenkaer-Hansen et al., 2005). Indeed, it has been observed that the amplitude envelope of neural oscillations exhibits a slow power-law decay of autocorrelations up to several tens of seconds, indicating that these rhythms carry a memory of their own dynamics (Linkenkaer-Hansen et al., 2001; Nikulin and Brismar, 2004). Further, LRTC are stronger in the vicinity of epileptic zones (Parish et al., 2004; Monto et al., 2007) and are influenced by genes (Linkenkaer-Hansen et al., 2007). Here we shall learn about the putative relevance of self-organized criticality for understanding the temporal correlation properties in ongoing oscillations.

Self-Organized Criticality: An explanation of $1/f$ Noise

The title of this chapter was taken from the paper introducing the self-organized criticality (SOC) theory (Bak et al., 1987). The authors used the dynamical response of a sandpile to small random perturbations to hypothesize about an explanation for the scale invariance observed in different manifestations of nature (Bak, 1997; Buchanan, 2000). The randomness of the perturbations introduced to the system, driving it to the critical state, reflects the feature of the ‘self-organization’ being an ‘internal’ phenomenon. The ‘criticality’ is characterized by spatial and temporal correlations of a power-law form, meaning that the system is scale-free, i.e., that event sizes are broadly distributed. SOC has been proposed as an explanation for

fractal structures observed in systems as diverse as earthquakes (Bak et al., 2002; Turcotte and Malamud, 2004; Lippiello et al., 2005); forest fires (Malamud et al., 1998; Turcotte and Malamud, 2004); financial markets (Mantegna and Stanley, 1995; Lux and Marchesi, 1999; Bartolozzi et al., 2005); avalanches in rice piles (Frette et al., 1996; Aegerter et al., 2003); epidemics (Rhodes and Anderson, 1996); evolution (Bak and Sneppen, 1993; Sneppen et al., 1995; Paczuski et al., 1996); solar flares (Charbonneau et al., 2001; Paczuski and Hughes, 2004); open source software evolution (Nakakoji et al., 2002; Wu, 2006) and, more important in the context of this thesis, also in neuronal activity (Jung et al., 1998; Linkenkaer-Hansen et al., 2001; Chialvo, 2004; de Arcangelis et al., 2006; Beggs, 2007; Plenz and Thiagarajan, 2007). In the next section, methods for the evaluation of the presence of SOC will be described and the range of time scales at which the temporal correlations are estimated will be clarified.

Assessment of long-range temporal correlations in time series

If the *autocorrelation function* (ACF) of a stationary stochastic process in discrete time $\{\xi_k\}$ with $\langle \xi_k \rangle = 0$ and $\langle \xi_k^2 \rangle = \sigma^2$, where $\langle\ \rangle$ denotes ensemble average, given by:

$$C(n) = \langle \xi_k \xi_{k+n} \rangle \quad \textbf{(8)}$$

scales with the lag n as:

$$C(n) \sim n^{-\gamma} \quad \textbf{(9)}$$

for large n, where $0 < \gamma < 1$, then the process is long-range correlated (Beran, 1994).

The *power spectrum* is defined as (Chatfield, 1989):

$$P(f) = C(0) + 2\sum_{n=1}^{\infty} C(n)\cos(2\pi f n) \quad \textbf{(10)}$$

and, in the presence of scaling of the ACF, given by:

$$P(f) \approx 2\sum_{n=1}^{\infty} n^{-\gamma}\cos(2\pi f n) \quad \textbf{(11)}$$

For small f we get a power-law form:

$$P(f) = \frac{1}{f^{\beta}} \quad \textbf{(12)}$$

where β is the power spectrum density (PSD) exponent.

In order to meaningfully apply detrended fluctuation analysis (DFA) to ongoing oscillations, we focus on their amplitude modulations. Thus, first we bandpass filter and extract the amplitude envelope, W, using the Hilbert transform (Fig. 13 B, thick line).
The mean value of the amplitude envelope is then subtracted and the cumulative sum is computed:

$$y(t) = \sum_{t'=1}^{t} (|W(t')| - \langle |W| \rangle) \quad \textbf{(13)}$$

The resulting y vector is then divided into time windows of size τ and in each window the local trend $y_{\tau}(t)$ computed by a least-square fit is subtracted (Fig. 12). Finally, the average fluctuation is evaluated as the average root-mean-square:

$$\langle F(\tau) \rangle = \sqrt{\frac{1}{N} \sum_{t=1}^{N} (y(t) - y_{\tau}(t))^2} \approx \tau^{\alpha} \quad \textbf{(14)}$$

The DFA exponent (α) is 0.5 for an uncorrelated signal; ranges from 0.5 and 1 for power-law correlated signals; and if α is above 1 the correlations are not ruled by power-scaling. For timescales larger than the period of repetition the DFA exponent will be zero, whereas anti-correlations are characterized by values between 0 and 0.5 (Peng et al., 1995).

The relationship between the DFA exponent (α), the PSD exponent (β), and the autocorrelation function exponent (γ) is given by (Rangarajan and Ding, 2000):

$$\alpha = \frac{1+\beta}{2} = \frac{2-\gamma}{2} \quad \textbf{(15)}$$

Whereas PSD analysis is particularly suited for identifying the presence of characteristic scales, DFA (Peng, et al. 1994) provides greater accuracy in estimating temporal (auto-)correlations when the amount of data available is limited (Gao, et al.

2006), which is particularly important at long time scales. Notice that DFA will give an incorrect estimation of correlations in the presence of sharp artefacts.

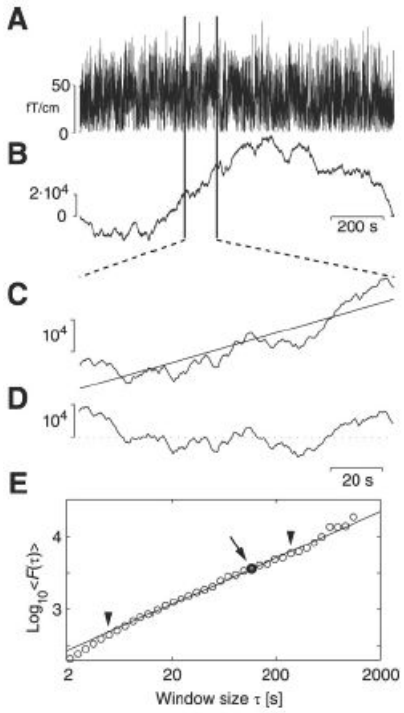

Figure 12 – DFA computation steps. The mean value of the signal is subtracted (A). The cumulative sum is computed (B). A time window with a certain length is selected from the integrated signal, a least-square line is fitted (C) and the linear trend is subtracted (D). The average of the root-mean-square fluctuation of the entire integrated and detrended signal is computed for that time scale and plotted in double logarithmic coordinates (arrow in E). The procedure starting in C is repeated for several window sizes to obtain the other data points in the plot (E). The power-law exponent is given by the slope of the line fitted within the indicated (arrowheads) bounds (Linkenkaer-Hansen et al., 2001).

Branching processes and brain oscillations

Critical networks may be simulated by ensuring that the average ratio of current to past activity, as expressed by the so-called *branching ratio* (σ), is close to one (Chialvo, 2006). Networks with a branching ratio larger than one are termed super-critical, whereas a ratio smaller than one prevents activity to propagate far in a so-called sub-critical network. In model networks with probabilistic activity propagation, the branching ratio corresponds to the average number of units activated by each active unit per time step and it has been observed that values not far from one as 1.06 and 0.96 are sufficient to induce, respectively, super-critical and sub-critical dynamics (Poil et al., 2008a).

The authors used MEG signals to introduce a novel method based on the definition of the duration or so-called '*life-time*' of an oscillation burst as the time that the amplitude envelope after bandpass filtering and Hilbert transform remains above its median level (Fig. 13).

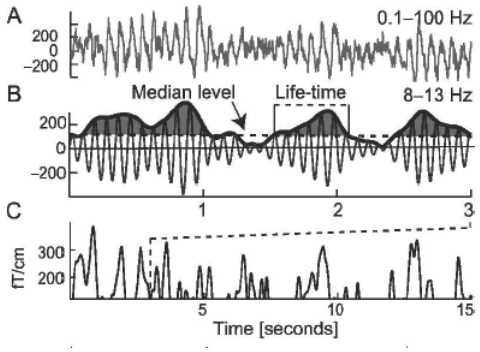

Figure 13 – Definition of the life-time of an oscillation burst. The MEG signal (A) is band-pass filtered in the frequency band of interest (thin line, B) and the amplitude envelope of the oscillations (thick line, B) is extracted with the Hilbert transform. The life-times of the bursts (shadowed) are defined by the length of the time intervals the amplitude envelope stays above a threshold (horizontal dashed line, B) defined as the median amplitude. C) On larger times scales the signal exhibits an oscillatory burst structure (Poil et al., 2008a).

Probability distributions of life-times decaying in a power-law form on time scales of 153–893 ms were found in spontaneous alpha oscillations in all subjects considered in the study measured by representative parietal and right sensorimotor channels. The same approach was used in the Publication P3 of this thesis.

The power-law exponents (slope in double-logarithmic coordinates) obtained for the life-times in the super-critical and sub-critical networks were significantly larger than for the critical network. Similar life-time exponents were found for the MEG channels in the sensorimotor and parietal regions and were not correlated with amplitude, indicating that the duration and amplitude of oscillations provide complementary indices of the underlying physiological process. Temporal correlations in time scales only up to the length of the longest avalanche were found in a model network with critical connectivity, whereas temporal correlations on time scales corresponding to several burst events could be observed in spontaneous alpha oscillations recorded with MEG. The authors speculate that temporal patterning on longer time scales are dependent also on mechanisms of sub-cortical modulation (Steriade 1990), or other mechanisms involved in slowly varying cortical excitability (Vanhatalo 2004), or activity-dependent plasticity (Marder and Goaillard 2006, van Ooyen 1994, Zhang and Linden 2003). Interestingly, there may be a relationship between the fractal temporal structure of oscillation amplitude and hemodynamic changes observed with fMRI (Bullmore 2004, Maxim 2005). Life-times, characterizing amplitude dynamics on short to intermediate time scales (< 1s), and DFA exponents, reflecting the temporal structure of tens of oscillations bursts, were significantly correlated in the sensorimotor region, but showed only a trend in parietal channels. The new life-time approach for the study of ongoing oscillations provides a more straightforward interpretation of changes in the temporal structure of oscillations than that of LRTC as indexed with the DFA algorithm.

Dynamical systems exhibiting SOC or 1/f power spectra are often said to have "memory", because fluctuations on many time scales are exhibiting a degree of dependence. In Publication P3 we investigated the intriguing possibility that this "physiological memory" would be important for cognitive memory and impaired in AD patients. Several studies, however, have shown that a modulation of oscillation

amplitudes on time scales of seconds occurs during working memory tasks in several frequency bands and brain regions, which provides an additional rationale for implementing indices of oscillation life-time in the study of AD as we did in Publication P3. Some of these studies are summarized below.

Oscillations are amplitude modulated on time scales of seconds in working-memory tasks

Modulation of the amplitude of oscillations during working memory tasks has been reported on several studies for several frequencies bands and brain regions. The amplitude of theta oscillations measured with EEG in the frontal midline increased with load in a '*n*-back' working memory (WM) task, whereas alpha activity in the posterior region decreased (Gevins, 1997). In a '*n*-back' task the subjects are presented with a continuous stream of items and have to indicate whether the probe matches the element presented *n* positions back. Measurements of intracranial EEG (iEEG) during a *Sternberg* working memory task revealed sustained theta activity during the entire duration of the trials, with an increase of power with the increase of the number of elements for a subdural electrode in the parietal cortex and a depth electrode in the left temporal lobe (Raghavachari et al., 2001). In a *Sternberg* task a series of items is presented; after a delay period a probe item is shown and subjects indicate if the probe was on the list. The main advantage of the *Sternberg* task over the '*n*-back' task is the separation in time of the encoding, retention and retrieval. When consonants (meaningful linguistic units) are used as items the task is considered a verbal working memory task (Baddeley, 1986). Sustained theta activity was also obtained in a MEG study using a similar WM task in a frontal brain region (Jensen et al., 2002). In addition an increase of the alpha amplitude was found with the increase of the number of items.

Temporal correlations of synchronization levels

Synchronization likelihood time-series obtained from EEG recordings of spontaneous activity during resting-state show a complicated structure (Stam and de Bruin, 2004).

The fluctuations observed at short time scales are a result of the high temporal resolution of the SL reflected in the ability to detect sharp changes of coupling between nonlinear systems. Though each value of the SL time series represents the degree of simultaneous repetition of patterns in two channels over a considerable long time window, the adaptive nature of SL allows consecutive reference vectors to be completely different and represent distinct dynamical states.

The algorithm of DFA can be used to quantify the extent to which the temporal structure of the SL time series differ from a random signal. This approach was pursued in Publication P4.

3. Aims of the study

The aim of this thesis was to investigate the complex spatio-temporal dynamics of brain activity in patients with Alzheimer's disease and healthy control subjects, using whole-head electro- or magnetoencephalographic recordings and novel algorithms.

The specific goals of each study were:

P1:

To develop and validate a "synchronization likelihood" algorithm for quantifying generalized synchronization, which is logically defined with respect to the time-frequency information of the signals of interest.

P2:

To assess resting-state functional connectivity in AD with TF-SL and to compare the results obtained with this measure able to detect nonlinear dependencies with the ones obtained with coherence.

P3:

To test the hypothesis that physiological memory as indexed by temporal correlations in ongoing alpha oscillations is related to cognitive memory and, therefore, impaired in AD.

P4:

To evaluate if the DFA exponent, as a measure of the complex temporal structure of Synchronization Likelihood time series, could be used as a biomarker for AD.

4. Materials and Methods

4.1 Subjects

For P1 EEG data of an epileptic patient showing an absence seizure was used.

The subjects studied in P2, P3 and P4 were chosen from databases of the Alzheimer Centre of the VU University Medical Center. Patients were diagnosed with probable AD according to the NINCDS-ADRDA criteria (McKhann, 1984). For P2, we selected 18 patients (mean age 72.1 ± SD 5.6 years; 11 males) and 18 healthy control subjects (69.1 ± 6.8 years; 7 males). In P3, we included 19 patients (73.9 ± 6.4 years; 11 males) and 16 healthy control subjects (70 ± 6.2 years; 7 males). In P4, we studied 24 patients (76.3 ± 7.8 years; 9 males) and 19 non-demented subjects with subjective memory complaints (76.1 ± 6.7 years; 9 males).

4.2 Recordings

During all the recordings the subjects sat comfortably, in sound attenuated and dimly lit environments, and were instructed to close their eyes. For P1, EEG data were acquired at 500 Hz with an OSG Brain Lab ® digital system with an common average reference electrode, involving all electrodes except Fp2 and Fp1. For P4, data was acquired at 200 Hz with a Nihon Kohden digital EEG apparatus (EEG 2100) against C3-C4. For P1 and P4, the impedance of the electrodes at 10-20

positions was kept below 5 kΩ. For P2 and P3, signals were acquired inside a magnetically shielded room (Vacuumschmelze GmbH, Hanau, Germany) using a 151-channel MEG system (CTF Systems Inc., Vancouver, Canada) at 625 Hz and band-pass filtered from 0.25 to 125 Hz. The head position relative to the coordinate system of the helmet was measured at the beginning and at the end of each recording by leading small alternating currents through three head position coils placed at left and right pre-auricular and nasion sites. Head position changes up to approximately 1.5 cm were accepted.

4.3 Data Analysis

In P1, the EEG signals of channels F7 and F8 were down-sampled off-line to 100 Hz and band-pass filtered with a 4th order Butterworth filter in the band 3-20 Hz. SL was computed with the set of parameters used in previous studies (L=10 samples, m=10 samples, W_1=100 samples, W_2/2=10% of the length of the data set and p_{ref}=0.01) and with embedding parameters defined with time-frequency priors (TF), the lag (L) as:

$$L = \frac{fs}{3 * HF} \quad \textbf{(16)}$$

where fs is the sampling frequency and HF the highest frequency; and the embedding dimension (m) as:

$$m = \frac{3 * HF}{LF} + 1 \quad \textbf{(17)}$$

where LF is the lowest frequency (giving: L=1/fs=0.01 s, m=21/fs=0.21 s and W_1=40/fs=0.4 s).

The window W_1 was defined as twice the length of the embedding vectors:

$$W_1 = 2 * L * (m - 1) \quad \textbf{(18)}$$

This definition of W1 was considered safe since it is well known that neuronal activity transients may emerge or fade away within one oscillation cycle (Palva et al., 2005b).

The same p_{ref} was used and we chose W_2=10 s in order to get 10 recurrences. A window $W_2/2$ was discarded from the beginning and the end of the raw data. SL and TF-SL were computed for two distances between references vectors s=1/fs and s=20/fs.

To study signals using coherence based on the Welch method, the windows are required to contain at least three periods of the lowest frequency and an overlap of half the size is advised; for a LF = 3 Hz (three periods ~ 1 s) the use of a window of 5 s = $W_2/2$ was appropriate. The time-frequency coherence was averaged in the 3–20 Hz frequency band and compared to TF-SL.

Unidirectionally coupled Hénon system time series were computer-generated with a total length of 4000 samples and different values of the coupling parameter (C) in a window between samples 1500 and 2500 (C was zero elsewhere). The power spectrum of the simulated data was computed to determine the frequencies of interest (9–16 Hz) and the TF embedding parameters (L=2/fs, m=7/fs, fs=100 Hz). SL and TF-SL were computed for all the time series and the mean value within the window where the signals were coupled was determined for each of the coupling strength.

In P2, the MEG data were down-sampled off-line to 312.5 Hz and zero-phase lag filtered for the frequency bands: delta (0.5–4 Hz), theta (4–8 Hz), alpha1 (8–10 Hz), alpha2 (10–13 Hz), beta (13–30 Hz) and gamma (30–45 Hz). SL was computed with TF parameters for all pair-wise combinations of the channels and averaged over three artefact-free visually selected epochs of 13,083 s for each subject and over groups of channels representing long distance intra- and inter-hemispheric and short distance connections. Similar analysis was performed with complex coherency. The cross-correlation was computed for the beta band.

In P3, the MEG signals were down-sampled off-line to 125 Hz, high-passed filtered at 1 Hz and low-pass filtered at 45 Hz using finite impulse response (FIR) filters. Non-periodic artefacts were visually selected and removed from the data. Independent components analysis was performed with EEGLAB (Delorme and Makeig, 2004) and components representing ECG, eye movements or muscular artefacts were removed. Bad channels were replaced by the average of their neighbours and planar synthetic gradiometers were computed using Fieldtrip

(Bastiaansen and Knösche, 2000). Bandpass FIR filters (with a Hamming window and filter order 28) at 6–13 Hz and the Hilbert transform were used to extract the amplitude envelope of the signal. Detrended fluctuation analysis accurately estimates the decay of LRTC in time scales of at least 10% of the total length of the signal; for the 4 min signals, we extracted scaling exponents of the time range of 1–25 s. Oscillation life- and waiting-times were defined as the length of the intervals where the amplitude envelope remains above or below the median value and probability distributions were computed using equidistant binning on logarithmic axis with 10 bins per decade. Visual inspection of probability distributions for parietal channels determined the least-square fitting time range (119–538 ms) for the computation of the power-law exponents.

In P4, epochs of 20.475 s were selected by visual inspection to avoid artefacts, such as eye-blinks, slow eye-movements, excess muscle activity and ECG, and SL was computed for delta, theta, alpha1, alpha2, beta (defined in the same way as in P2) and gamma (30–48 Hz) bands with the parameters used in previous studies (before the introduction of the TF definitions) and a distance *s* between the reference vectors of 16 samples / 200 Hz = 0.08 s. DFA was applied to the SL time series and exponents were computed for times scales of 0.32–10.48 s.

5. Results

This chapter summarizes the main results obtained in the four Publications that constitute the core of this thesis.

5.1 Time-delay embedding based on the frequency content of interest.

Complex and widely different patterns corresponding to spike wave discharges and their recurrences were identified by the TF-SL method in EEG data of an epileptic seizure on two channels: F7 and F8 (Fig. 14). The times of recurrences in channel F8 were similar to those expected on the basis of visual inspection.

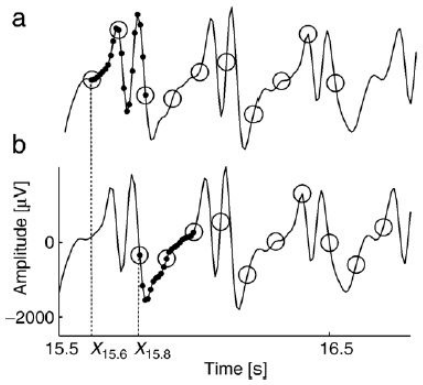

Figure 14 – State vectors obtained with TF parameters (black dots) and the parameters used in previous studies (white circles) for *i* = 15.6 s (a) and *i* = 15.8 s (b). A shift of 0.2 s corresponds to a window $W_1/2$ and translates in the tracking of completely different patterns by the TF parameters (Montez et al., 2006).

For channel F7, the reference patterns were different from those in channel F8, but its recurrences occasionally appeared at the same times as the recurrences in channel F8. At the onset of the seizure, when the channels visually seem to be synchronized, the TF-SL value increases reflecting the fact that the recurrences are occurring simultaneously in both channels and drops back at the end of the seizure to the baseline value it had before the seizure. We have shown that TF-SL is insensitive to the distance in time between consecutive reference vectors. This study thus gave empirical evidence for the advantage of TF-SL in tracking the onset and end of an epileptic seizure on EEG recordings compared to classical coherence.

The time-frequency coherence plot reflects the wide frequency content of the epileptic activity (Fig. 15).

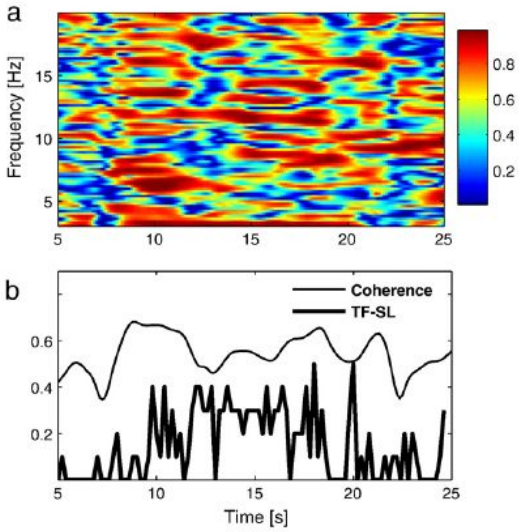

Figure 15 – Comparison between the classical coherence and TF-SL in the 3–20 Hz band. (a) The time-frequency coherence plot shows peaks for lower frequencies (5–10 Hz) around 10 s, higher frequencies (8–14 Hz) around 15 s and for frequencies above 15 Hz around 12 s. (b) Though the mean value of the classical coherence averaged in the 3–20 Hz is higher than the TF-SL values; classical coherence do not have a stable plateau during the seizure (10–20 seconds). The TF-SL increases on the onset of the seizure until a lower mean value compared to classical coherence and drops back at the end of the seizure to the baseline value it had before the seizure (Montez et al., 2006).

Classical coherence averaged in the same frequency band does not show stability during the seizure as the TF-SL.

Application to simulated data with manipulated coupling showed that the TF-SL based choice of the embedding parameters tracks the change of coupling strength between two unidirectionally coupled Hénon systems.

5.2 SL revealed loss of long distance intra-hemispheric interactions in the alpha band resting-state oscillations of AD patients measured by MEG.

Alzheimer patients showed a loss of long distance intra-hemispheric interactions in the alpha1 (8–10 Hz) and beta (13–30 Hz) bands with a focus on left fronto-temporal/parietal connections as revealed by significant SL group differences (Figs. 16 e 17). These changes may reflect loss of anatomical connections and/or reduced cholinergic activity.

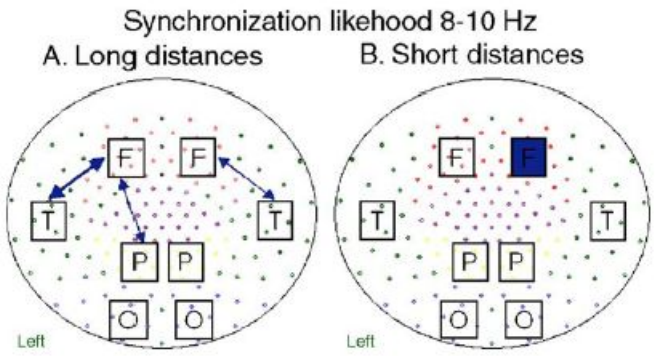

Figure 16 – Significantly lower SL in AD patients compared with healthy age-matched controls in the 8–10 Hz band for long (A) and short (B) distances. Lines correspond to significant changes of average SL between two regions and squares to significant changes of local SL. T-tests determined significant changes involving pairs of channels (arrows) in the left fronto-temporal (p = 0.009), left fronto-parietal (p = 0.012) and the right fronto-temporal (p = 0.015) regions. A significant (p < 0.01) local decrease of SL was observed for combinations of right frontal vectors (blue square). (Stam et al., 2006)

Positive correlations were found between mini-mental state exam score referred to as MMSE score (Folstein et al., 1975) and averaged inter-hemispheric SL in the alpha1 band (R = 0.727; P = 0.002) and in the beta band (R = 0.688; P = 0.005)

indicating that the decreased functional connectivity could underlie the cognitive impairment.

Coherence was significantly lower between the left fronto-temporal regions, but only in the beta band (Fig. 17).

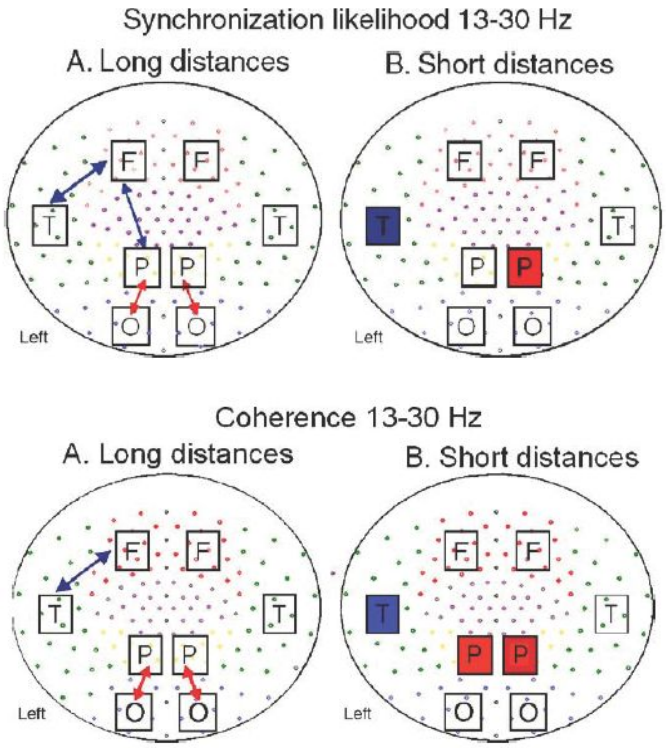

Figure 17 – Significant lower (blue) and higher (red) SL (up) and coherence (down) in AD patients compared with healthy age-matched controls in the 13-30 Hz band. The structure is the same as in the previous figure (thin line/light square: $p < 0.05$; thick line/dark square: $p < 0.01$). Both SL and coherence are significantly lower between the left fronto-temporal regions and significantly higher between the left parieto-occipital and right parieto-occipital regions with a local decrease in the left temporal region and local increase in the right parietal regions. SL is also significantly lower between the left fronto-parietal and coherence is locally increased in the left parietal region.

This study showed that both short distance interactions that might underlie specialization and long distance interactions that might be associated with global

integration (Tononi et al., 1998; van Walsum et al., 2003) are impaired in AD. This may reflect that the necessary balance between local specialization and global integration is compromised. Further, the study shows that short recordings (13 seconds of data) of resting-state activity are sufficient to detect AD-associated changes in large-scale brain networks.

5.3 Impaired temporal correlations in temporo-parietal oscillations in early-stage Alzheimer's disease.

A significant decrease in long-range temporal correlations was observed in AD patients in the alpha band (6–13 Hz) over temporo-parietal regions on time scales of 1–25 seconds as indexed by the DFA exponents obtained: 0.66 ± 0.01 for the AD patients and 0.71 ± 0.01 for the controls (Fig. 18). No significant group effect was found for the amplitude.

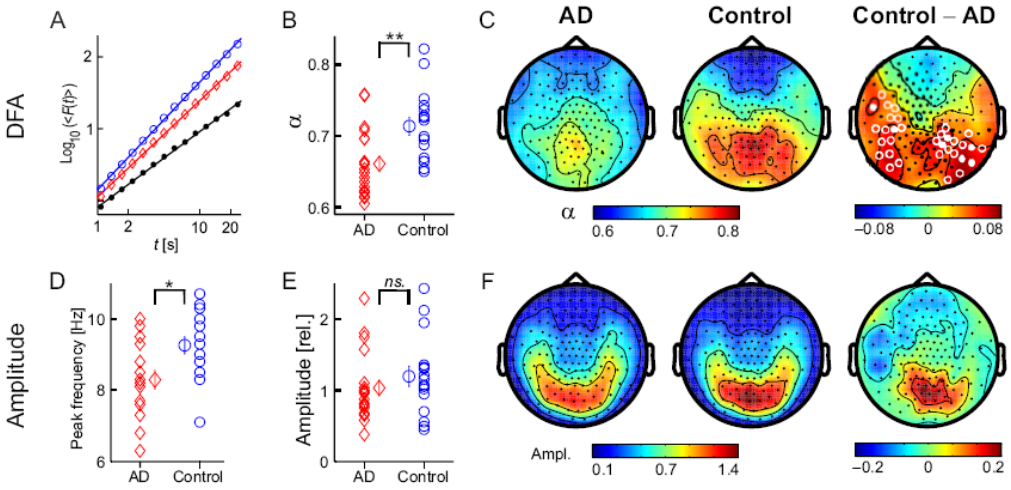

Figure 18 – Impaired LRTC in temporo-parietal oscillations in AD for the 6–13 Hz band. Grand-average plot of a parietal channel for AD patients (red diamonds), control subjects (blue circles) and an empty-room recording (black dots). (B) The individual DFA exponents averaged over the 33 channels marked in *C* with white circles are significantly lower for AD patients ($p < 0.005$). Mean ± SEM are represented in the middle. Grand-average topographies of the DFA exponents (C) and the amplitude (F) for the AD patients (left), control subjects (middle) and controls minus patients (right). White circles denote channels with $p < 0.05$ (open) and $p < 0.01$ (filled). (D) The individual peak frequencies in a parietal channel were significantly ($p < 0.05$) lower for patients. (E) Individual amplitudes averaged over the 12 channels showing the largest group difference.

Significantly reduced probability for the occurrence of bursts in alpha oscillations with long life- or waiting-times on shorter time scales (< 1 second) was found for the AD patients in the same temporo-parietal regions, as indicated by the respective power-law exponents obtained: life-times exponents of 1.91 ± 0.06 for the AD patients and 1.68 ± 0.04 for the controls; and waiting-times exponents of 1.77 ± 0.04 for the AD patients and 1.60 ± 0.04 for the controls (Fig. 19).

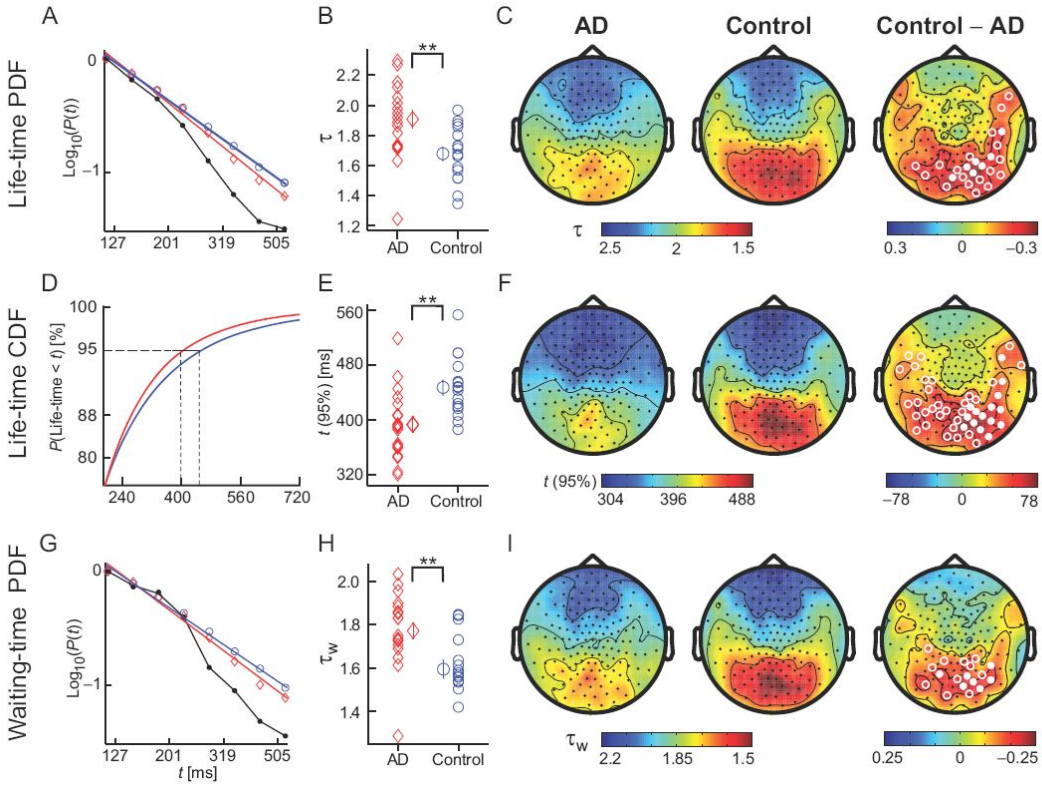

Figure 19 – Altered life- and waiting-times of temporal-parietal oscillations in AD. The colour coding and structure are the same as in the previous figure. (A) Grand-average probability distribution function (PDF) of oscillation life-times. (B) The individual life-time exponents averaged over the 25 channels marked with white circles in *C* are significantly ($p < 0.005$) higher for AD patients. Grand-average topographies of the life-time exponents (C), the cumulative life-times at the 95%-percentile (F) and the waiting-times (I). (D) Cumulative probability distribution function (CDF) of oscillation life-times. (E) The individual cumulative life-time averaged over the 45 channels

marked with white circles in *F*. (G) Grand-average probability distribution of waiting-times for channels with a significant group difference. (H) The individual waiting-times averaged over the 18 channels marked with white circles in *I*.

The cumulative probability distribution of life-times showed significant differences at percentiles around 88–100%. The 95%-percentile, e.g., was 383 ± 11 ms for the AD patients and 439 ± 12 ms for the controls. This decrease reflects the impaired generation of long-lasting oscillations by the disease.

The DFA, life- and waiting-time exponents were not significantly correlated (data not shown). Thus, the three methods provide complementary indices of abnormalities in the temporal structure of ongoing oscillations.

5.4 Disturbed fluctuations of resting state EEG synchronization in Alzheimer's disease.

Alzheimer's patients showed a significant decrease in the mean levels of EEG synchronization for the upper alpha (10–13 Hz) and beta (13–30 Hz) frequency bands (Fig. 20). These results are in agreement with the results of earlier EEG and MEG studies (Stam et al., 2002b; Stam et al., 2003b; Babiloni et al., 2004; Pijnenburg et al., 2004).

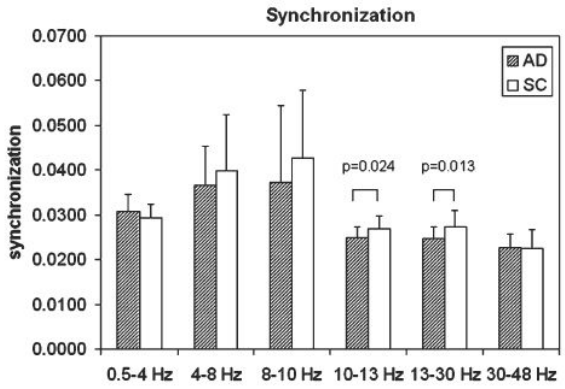

Figure 20 – Mean SL of AD patients and subjects with subjective memory complaints for different frequency bands. Error bars denote standard deviation and *p*-values correspond to two-tailed *t*-test (Stam et al., 2005).

Besides the decreased level of mean synchronization, the impaired functional connectivity was also indexed by disturbed fluctuations of the synchronization levels, extending the results obtained for healthy subjects in a previous study to longer time scales (Stam and de Bruin, 2004).

The study revealed trends for the lower (8–10 Hz) alpha ($p = 0.085$) and the beta ($p = 0.059$) bands in the direction of a smaller DFA exponent in the AD group compared to the group of subjects with subjective memory complaints (Fig. 21).

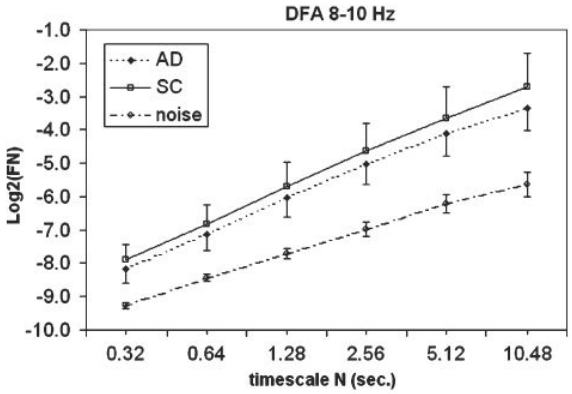

Figure 21 – Grand-average DFA plots for the AD patients and subjects with subjective memory complaints for the lower alpha band. For comparison, control white noise epochs were subjected to the same analysis (filtering, SL computation and DFA). The exponents obtained had a trend ($p < 0.10$) in the direction of smaller DFA exponents for the AD patients than for the subjects with subjective memory complaints (Stam et al., 2005).

6. Discussion

In this thesis, the SL algorithm was improved in P1 in order to account for the time-frequency content of the recurring patterns in the quantification of generalized synchronization and validated by tracking recurrences in EEG data of an epileptic seizure corresponding to those expected by visual inspection. The method was further applied in P2 to MEG data of AD patients and a decrease of left fronto-temporal and fronto-parietal resting-state functional connectivity was found in the lower alpha (8–10 Hz) band, whereas no significant differences were found in this band with coherence. DFA of MEG data from AD patients (P3) revealed a decrease in LRTC on time scales of 1–25 seconds in ongoing alpha oscillations (6–13 Hz), corroborating the hypothesis that physiological memory may be important for cognitive memory. Finally, DFA of SL time series obtained from resting-state EEG data (P4) resulted in trends towards smaller exponents for the AD patients than for subjects with subjective memory complaints for the lower alpha (8–10 Hz) and beta bands showing that the complexity of SL time series may capture differences in the spatio-temporal dynamics of oscillatory activity in these two groups.

6.1 Physiology of recurrent patterns in neuronal activity

Synchronization likelihood may become an important tool in cognitive research due to the ability to detect linear and nonlinear interactions between brain regions. SL may be used to study ongoing data since it automatically detects recurrences without *a priori* assumptions regarding the times of interactions. SL may

be a valuable algorithm for testing whether generalized synchronization is an important phenomenon in the human brain. Since the existence of recurrences is the assumption for studying generalized synchronization, it is recommended that special attention is paid to the visual inspection of patterns picked up by the algorithm as well as the temporal distribution of the occurrence of recurrences. SL is based on the search for a constant number of most similar patterns that represent the system at the same state in different time intervals. In some situations the method might pick up only random noise or recurrences representing the stability of the system in a certain state as opposed to the situation when the system comes back to a certain state after being in a different one.

Very similar patterns in neighbouring channels might be the result of volume conduction effects rather than synchronization. Strategies to avoid this situation should be considered in the decision of a SL analysis framework, though classical correlation analysis based on coherence suffers from the same problem. An option might be the use of source modelling, having the advantage of decreasing the computational time. It is in my opinion, a better option to look in more detail into pair-wise combination of sources, rather than computing SL for a large number of sensors and average the obtained time series over brain regions. Besides sparing time spent with redundant computations, i.e., computing SL for pairs of channels that reflect the same brain sources, the source approach would allow for visual inspection of the recurrent patterns and their temporal distribution as suggested above, which may reduce the probability of averaging out differences between groups of healthy controls and patients at specific channel combinations [that's what you mean?] and would bring advantages for the comparison between results obtained using MEG systems with axial or planar gradiometers. A deeper knowledge of the recurrent patterns possibly present in ongoing brain data would strengthen the interpretation of SL results and is likely to motivate a wider application of the algorithm.

6.2 The role of alpha oscillations

Several decades after the discovery of the so-called alpha activity there is still no consensus on the functional role of these oscillations and little is known about their mechanism of generation (Steriade, 2000). The initial idea that alpha oscillations were important for the maintenance of an 'idling' state of the brain (Adrian 1934) was based on attenuation by eye opening, visual stimuli and by increased attentiveness. An inhibition theory suggesting that alpha activity prevents flow of information into other active areas has become increasingly popular (Klimesch et al., 2007). A competing hypothesis is that not only alpha but simultaneous alpha, beta and gamma oscillations are directly involved in the selection and maintenance of neuronal object representation during working memory, perception and consciousness (Palva and Palva, 2007). In fact alpha desynchronization has been found to be accompanied by beta desynchronization and alpha synchronization by beta synchronization (Pfurtscheller and Klimesch, 1992).

Definition of "lower" and "upper" alpha and AD slowing

The definition of a lower alpha defined in the frequency band 8–10 Hz and an upper alpha of 10–13 Hz, used in Publications P2 and P4 of this thesis, was based on the definition by Klimesch that associated the lower alpha to attention and upper alpha (10–12 Hz) to stimulus encoding and long term memory processes (Klimesch, 1996). Differential reactivity of lower and upper alpha band may, however, also reflect differential involvement of alpha from different anatomical locations, because alpha activity from posterior sites tends to have a higher frequency than that of anterior sites (Hari and Salmelin, 1997; Klimesch et al., 2000). For P3, the alpha band was defined as a broad band from 6 to 13 Hz in order to include the peaks of the AD patients that were shifted to lower frequencies and thus avoid amplitude confounds on the DFA analysis.

6.3 Conclusion and Outlook

Longitudinal studies may give an important contribution to the evaluation of candidate Alzheimer's disease biomarkers, because they allow for tracking the evolution of the biomarker from a healthy value for that individual to normal aging or disease value and, thus, are not confounded by genetic variability. Genetic variance is presumably a leading cause for why several candidate biomarkers, e.g., based on blood tests, MRI or EEG, have not yet achieved a sensitivity that allows for diagnostic use. Another interesting avenue to explore in future studies is the power of the presented biomarkers to track the effects of medication, which should also be done in a longitudinal fashion by comparing biomarker values of the same patients before treatment started.

References

Abbott LF, Rohrkemper R (2007) A simple growth model constructs critical avalanche networks. Prog Brain Res 165:13-19.

Aegerter CM, Günther R, Wijngaarden RJ (2003) Avalanche dynamics, surface roughening, and self-organized criticality: Experiments on a three-dimensional pile of rice. Physical Review E 67:51306.

Albano AM, Rapp PE (1993) On the reliability of dynamical measures of EEG signals. The 2nd Annual Conference on Nonlinear Dynamics Analysis of the EEG, World Scientific, Singapore:117–139.

Amari S, Cichocki A, Yang HH (1996) A new learning algorithm for blind signal separation. Advances in Neural Information Processing Systems 8:757–763.

American Psychiatric Association (1987) Diagnostic and Statistical Manual of Mental Disorders, 3rd edition, revised. Washington, DC.

Arnhold J, Grassberger P, Lehnertz K, Elger CE (1999) A robust method for detecting interdependences: application to intracranially recorded EEG. Physica D: Nonlinear Phenomena 134:419-430.

Babiloni C, Ferri R, Moretti DV, Strambi A, Binetti G, Dal Forno G, Ferreri F, Lanuzza B, Bonato C, Nobili F, Rodriguez G, Salinari S, Passero S, Rocchi R, Stam CJ, Rossini PM (2004) Abnormal fronto-parietal coupling of brain rhythms in mild Alzheimer's disease: a multicentric EEG study. Eur J Neurosci 19:2583-2590.

Baddeley AD (1986) Working memory. Oxford, UK: Clarendon.

Bak P (1997) How nature works: The science of self-organized criticallity. Oxford: Oxford.

Bak P, Sneppen K (1993) Punctuated equilibrium and criticality in a simple model of evolution. Physical Review Letters 71:4083-4086.

Bak P, Tang C, Wiesenfeld K (1987) Self-organized criticality: An explanation of the 1/f noise. Physical Review Letters 59:381.

Bak P, Christensen K, Danon L, Scanlon T (2002) Unified Scaling Law for Earthquakes. Physical Review Letters 88:178501.

Bartolozzi M, Leinweber DB, Thomas AW (2005) Self-organized criticality and stock market dynamics: an empirical study. Physica A: Statistical Mechanics and its Applications 350:451-465.

Bastiaansen MCM, Knösche TR (2000) Tangential derivative mapping of axial MEG applied to event-related desynchronization research. Clinical Neurophysiology 111:1300-1305.

Beggs JM (2007) The criticality hypothesis: how local cortical networks might optimize information processing. Philos Transact A Math Phys Eng Sci.

Beggs JM, Plenz D (2003) Neuronal Avalanches in Neocortical Circuits. J Neurosci 23:11167-11177.

Beggs JM, Plenz D (2004) Neuronal Avalanches Are Diverse and Precise Activity Patterns That Are Stable for Many Hours in Cortical Slice Cultures. Journal of Neuroscience 24:5216-5229.

Bell AJ, Sejnowski TJ (1995) An Information-Maximization Approach to Blind Separation and Blind Deconvolution. Neural Computation 7:1129-1159.
Beran J (1994) Statistics for Long-Memory Processes: Chapman & Hall/CRC.
Berendse HW, Verbunt JPA, Scheltens P, van Dijk BW, Jonkman EJ (2000) Magnetoencephalographic analysis of cortical activity in Alzheimer's disease: a pilot study. Clinical Neurophysiology 111:604-612.
Berger H (1929) Über das Elektroenkephalogramm des Menschen. Arch Psychiatr Nervenkr 87:527-570.
Boerman RH, Scheltens P, Weinstein HC (1994) Clinical neurophysiology in the diagnosis of Alzheimer's disease. Clin Neurol Neurosurg 96:111-118.
Braak E, Griffing K, Arai K, Bohl J, Bratzke H, Braak H (1999) Neuropathology of Alzheimer's disease: what is new since A. Alzheimer? European Archives of Psychiatry and Clinical Neuroscience 249:14-22.
Braak H, Braak E, Bohl J (1993) Staging of Alzheimer-related cortical destruction. European neurology 33:403-408.
Breakspear M (2002) Nonlinear phase desynchronization in human electroencephalographic data. Human Brain Mapping 15:175-198.
Buchanan M (2000) Ubiquity. London.
Buckner RL (2004) Memory and Executive Function in Aging and AD: Multiple Factors that Cause Decline and Reserve Factors that Compensate. Neuron 44:195-208.
Buzsaki G (2006) Rhythms of the Brain. Oxford University Press.
Buzsaki G, Draguhn A (2004) Neuronal Oscillations in Cortical Networks. Science 304:1926-1929.
Cardoso JF, Souloumiac A, Paris T (1993) Blind beamforming for non-Gaussian signals. Radar and Signal Processing, IEE Proceedings F 140:362-370.
Celesia GG, Jasper HH (1911) Acetylcholine released from cerebral cortex in relation to state of activation. Neurology 1966:1053-1063.
Cellucci CJ, Albano AM, Rapp PE (2003) Comparative study of embedding methods. Physical Review E 67:66210.
Charbonneau P, McIntosh SW, Liu HL, Bogdan TJ (2001) Avalanche models for solar flares (Invited Review). Solar Physics 203:321-353.
Chatfield C (1989) The Analysis of Time Series: An Introduction, 4th ed. London: Chapman & Hall.
Chialvo DR (2004) Critical brain networks. Physica A: Statistical Mechanics and its Applications 340:756-765.
Chialvo DR (2006) Psychophysics: Are our senses critical? Nature Physics 2:301-302.
Chialvo DR (2007) The brain near the edge. Cooperative Behavior in Neural Systems: Ninth Granada Lectures:1-12.
Chialvo DR, Bak P (1999) Learning from mistakes. Neuroscience 90:1137-1148.
Coben LA, Danziger WL, Berg L (1983) Frequency analysis of the resting awake EEG in mild senile dementia of Alzheimer type. Electroencephalogr Clin Neurophysiol 55:372-380.
de Arcangelis L, Perrone-Capano C, Herrmann HJ (2006) Self-Organized Criticality Model for Brain Plasticity. Physical Review Letters 96:28107.

Delorme A, Makeig S (2004) EEGLAB: an open source toolbox for analysis of single-trial EEG dynamics including independent component analysis. Journal of Neuroscience Methods 134:9-21.

Fernandez A, Hornero R, Mayo A, Poza J, Gil-Gregorio P, Ortiz T (2006) MEG spectral profile in Alzheimer's disease and mild cognitive impairment. Clinical Neurophysiology 117:306-314.

Fernandez A, Arrazola J, Maestu F, Amo C, Gil-Gregorio P, Wienbruch C, Ortiz T (2003) Correlations of Hippocampal Atrophy and Focal Low-Frequency Magnetic Activity in Alzheimer Disease: Volumetric MR Imaging-Magnetoencephalographic Study. AJNR Am J Neuroradiol 24:481-487.

Fernandez A, Maestu F, Amo C, Gil P, Fehr T, Wienbruch C, Rockstroh B, Elbert T, Ortiz T (2002) Focal temporoparietal slow activity in Alzheimer's disease revealed by magnetoencephalography. Biol Psych 52:764-770.

Folstein MF, Folstein SE, McHugh PR (1975) "Mini-mental state": A practical method for grading the cognitive state of patients for the clinician. J Psych Res 12:189-198.

Fox MD, Raichle ME (2007) Spontaneous fluctuations in brain activity observed with functional magnetic resonance imaging. Nature Rev Neurosci 8:700-711.

Fox NC, Crum WR, Scahill RI, Stevens JM, Janssen JC, Rossor MN (2001) Imaging of onset and progression of Alzheimer's disease with voxel-compression mapping of serial magnetic resonance images. The Lancet 358:201-205.

Frank R, Hargreaves R (2003) CLINICAL BIOMARKERS IN DRUG DISCOVERYAND DEVELOPMENT. NATURE REVIEWS| DRUG DISCOVERY 2:567.

Freeman WJ, Rogers LJ (2002) Fine Temporal Resolution of Analytic Phase Reveals Episodic Synchronization by State Transitions in Gamma EEGs. Journal of Neurophysiology 87:937-945.

Frette V, Christensen K, Malthe-Soerenssen A, Feder J, Joessang T, Meakin P (1996) Avalanche dynamics in a pile of rice. Nature 379:49-52.

Fries P (2005) A mechanism for cognitive dynamics: neuronal communication through neuronal coherence. Trends Cogn Sci 9:474-480.

Friston KJ (1994) Functional and effective connectivity in neuroimaging: A synthesis. Hum Brain Mapp 2:56-78.

Friston KJ (2000) The labile brain. I. Neuronal transients and nonlinear coupling. Philosophical Transactions of the Royal Society B: Biological Sciences 355:215-236.

Gevins A (1997) High-resolution EEG mapping of cortical activation related to working memory: effects of task difficulty, type of processing, and practice. Cerebral Cortex 7:374-385.

Gong P, Nikolaev AR, van Leeuwen C (2003) Scale-invariant fluctuations of the dynamical synchronization in human brain electrical activity. Neuroscience Letters 336:33-36.

Gordon EB, Sim M (1967) The E.E.G. in presenile dementia. J Neurol Neurosurg Psychiatry 30:285-291.

Greicius MD, Krasnow B, Reiss AL, Menon V (2003) Functional connectivity in the resting brain: A network analysis of the default mode hypothesis. Proc Natl Acad Sci USA 100:253-258.
Greicius MD, Srivastava G, Reiss AL, Menon V (2004) Default-mode network activity distinguishes Alzheimer's disease from healthy aging: Evidence from functional MRI. Proc Natl Acad Sci USA 101:4637-4642.
Guevara R, Velazquez JLP, Nenadovic V, Wennberg R, Senjanovic G, Dominguez LG (2005) Phase synchronization measurements using electroencephalographic recordings. NeuroInformatics 3:301-313.
Hämäläinen M, Hari R, Ilmoniemi RJ, Knuutila J, Lounasmaa OV (1993) Magnetoencephalography—theory, instrumentation, and applications to noninvasive studies of the working human brain. Reviews of Modern Physics 65:413-497.
Hardy J, Allsop D (1910) Amyloid deposition as the central event in the aetiology of Alzheimer's disease. Trends Pharmacol Sci 1991:383-388.
Hari R (1999) Magnetoencephalography as a tool of clinical neurophysiology. In: Electroencephalography: Basic Principles, Clinical Applications, and Related Fields. 4th Edition (Niedermeyer E, Lopes da Silva F, eds), pp 1107-1134: Williams & Wilkins.
Hari R, Salmelin R (1997) Human cortical oscillations: a neuromagnetic view through the skull. Trends in Neurosciences 20:44-49.
Helmholtz H (1853) Ueber einige Gesetze der Vertheilung elektrischer Ströme in körperlichen Leitern, mit Anwendung auf die thierisch-elektrischen Versuche (Schluss.). Annalen der Physik 165:353-377.
Hyman BT, Van Hoesen GW, Damasio AR, Barnes CL (1984) Alzheimer's disease: cell-specific pathology isolates the hippocampal formation. Science 225:1168-1170.
Hyvarinen A, Oja E (2000) Independent component analysis: algorithms and applications. Neural Netw 13:411-430.
Jensen O, Gelfand J, Kounios J, Lisman JE (2002) Oscillations in the Alpha Band (9-12 Hz) Increase with Memory Load during Retention in a Short-term Memory Task. Cereb Cortex 12:877-882.
Jeong J (2004) EEG dynamics in patients with Alzheimer's disease. Clinical Neurophysiology 115:1490-1505.
Jonkman EJ (1997) The role of the electroencephalogram in the diagnosis of dementia of the Alzheimer type: an attempt at technology assessment. Neurophysiologie Clinique/Clinical Neurophysiology 27:211-219.
Jung P, Cornell-Bell A, Madden KS, Moss F (1998) Noise-Induced Spiral Waves in Astrocyte Syncytia Show Evidence of Self-Organized Criticality. In, pp 1098-1101: Am Physiological Soc.
Jung T-P, Makeig S, Humphries C, Lee T-W, McKeown MJ, Iragui V, Sejnowski TJ (2000) Removing electroencephalographic artifacts by blind source separation. Psychophysiology 37:163-178.
Kanai T, Szerb JC (1965) Mesencephalic reticular activating system and cortical acetylcholine output. Nature 205:80-82.

Karas GB, Scheltens P, Rombouts S, Visser PJ, van Schijndel RA, Fox NC, Barkhof F (2004) Global and local gray matter loss in mild cognitive impairment and Alzheimer's disease. Neuroimage 23:708-716.

Kennel MB, Brown R, Abarbanel HDI (1992) Determining embedding dimension for phase-space reconstruction using a geometrical construction. Physical Review A 45:3403-3411.

Kinouchi O, Copelli M (2006) Optimal dynamical range of excitable networks at criticality. Nature Physics 2:348-351.

Klimesch W (1996) Memory processes, brain oscillations and EEG synchronization. International Journal of Psychophysiology 24:61-100.

Klimesch W, Sauseng P, Hanslmayr S (2007) EEG alpha oscillations: The inhibition-timing hypothesis. Brain Research Reviews 53:63-88.

Klimesch W, Doppelmayr M, Röhm D, Pöllhuber D, Stadler W (2000) Simultaneous desynchronization and synchronization of different alpha responses in the human electroencephalograph: a neglected paradox? Neuroscience Letters 284:97-100.

Lachaux JP, Rodriguez E, Martinerie J, Varela FJ (1999) Measuring Phase Synchrony in Brain Signals. Human Brain Mapping 8:194-208.

Le Van Quyen M, Adam C, Baulac M, Martinerie J, Varela FJ (1998) Nonlinear interdependencies of EEG signals in human intracranially recorded temporal lobe seizures. Brain Research 792:24-40.

Lee TW, Girolami M, Sejnowski TJ (1999) Independent Component Analysis Using an Extended Infomax Algorithm for Mixed Subgaussian and Supergaussian Sources. Neural Computation 11:417-441.

Lehtovirta M, Partanen J, Kononen M, Soininen H, Helisalmi S, Mannermaa A, Ryynanen M, Hartikainen P, Riekkinen Sr P (1996) Spectral analysis of EEG in Alzheimer's disease: relation to apolipoprotein E polymorphism. Neurobiol Aging 17:523-526.

Letemendia F, Pampiglione G (1958) Clinical and electroencephalographic observations in Alzheimer's disease. J Neurol Neurosurg Psychiatry 21:167-172.

Levina A, Herrmann JM, Geisel T (2007) Dynamical synapses causing self-organized criticality in neural networks. Nature Physics 3:857-860.

Liddell DW (1958) Investigations of E.E.G. findings in presenile dementia. J Neurol Neurosurg Psychiatry 21:173-176.

Liljeström M, Kujala J, Jensen O, Salmelin R (2005) Neuromagnetic localization of rhythmic activity in the human brain: a comparison of three methods. Neuroimage 25:734-745.

Linkenkaer-Hansen K (2004) Long-range temporal correlations in brain activity in health and disease. ZonMW, VENI 016056181.

Linkenkaer-Hansen K, Nikouline VV, Palva JM, Ilmoniemi RJ (2001) Long-Range Temporal Correlations and Scaling Behavior in Human Brain Oscillations. J Neurosci 21:1370-1377.

Linkenkaer-Hansen K, Monto S, Rytsälä H, Suominen K, Isometsä E, Kähkönen S (2005) Breakdown of Long-Range Temporal Correlations in Theta

Oscillations in Patients with Major Depressive Disorder. J Neurosci 25:10131-10137.
Linkenkaer-Hansen K, Smit DJA, Barkil A, van Beijsterveldt TEM, Brussaard AB, Boomsma DI, van Ooyen A, de Geus EJC (2007) Genetic Contributions to Long-Range Temporal Correlations in Ongoing Oscillations. J Neurosci 27:13882-13889.
Lippiello E, de Arcangelis L, Godano C (2005) Memory in self-organized criticality. Europhysics Letters 72:678-684.
Longo VG (1966) Behavioral and electroencephalographic effects of atropine and related compounds. Pharmacol Rev 18:965-996.
Lopes da Silva F, Van Rotterdam A (1999) Biophysical aspects of EEG and magnetoencephalogram generation. Electroencephalography: basic principles, clinical applications, and related fields (4th ed) Lippincott: Williams & Wilkins p:93–109.
Lux T, Marchesi M (1999) Scaling and criticality in a stochastic multi-agent model of a financial market. Nature 397:498-500.
Maestu F, Fernandez A, Simos PG, Gil-Gregorio P, Amo C, Rodriguez R, Arrazola J, Ortiz T (2001) Spatio-temporal patterns of brain magnetic activity during a memory task in Alzheimer's disease. Neuroreport 12:3.917-913.922.
Maestu F, Arrazola J, Fernandez A, Simos PG, Amo C, Gil-Gregorio P, Fernandez S, Papanicolaou A, Ortiz T (2003) Do cognitive patterns of brain magnetic activity correlate with hippocampal atrophy in Alzheimer's disease? J Neurol Neurosurg Psychiatry 74:208-212.
Maestu F, Fernandez A, Simos PG, Lopez-Ibor MI, Campo P, Criado J, Rodriguez-Palancas A, Ferre F, Amo C, Ortiz T (2004) Profiles of brain magnetic activity during a memory task in patients with Alzheimer's disease and in non-demented elderly subjects, with or without depression. J Neurol Neurosurg Psychiatry 75:1160-1162.
Maestú F, García-Segura J, Ortiz T, Montoya J, Fernández A, Gil-Gregorio P, Campo P, Fernández S, Viaño J, Portera A (2005) Evidence of Biochemical and Biomagnetic Interactions in Alzheimer's Disease: An MEG and MR Spectroscopy Study. Dementia and Geriatric Cognitive Disorders 20:145-152.
Makeig S, Bell AJ, Jung TP, Sejnowski TJ (1996) Independent component analysis of electroencephalographic data. Advances in Neural Information Processing Systems 8:145-151.
Makeig S, Jung TP, Bell AJ, Ghahremani D, Sejnowski TJ (1997) Blind separation of auditory event-related brain responses into independent components. Proceedings of the National Academy of Sciences 94:10979.
Malamud BD, Morein G, Turcotte DL (1998) Forest Fires: An Example of Self-Organized Critical Behavior. Science 281:1840.
Mantegna RN, Stanley HE (1995) Scaling behaviour in the dynamics of an economic index. Nature 376:46-49.
Mantini D, Perrucci MG, Del Gratta C, Romani GL, Corbetta M (2007) Electrophysiological signatures of resting state networks in the human brain. PNAS 104:13170-13175.

Matthews PM, Honey GD, Bullmore ET (2006) Applications of fMRI in translational medicine and clinical practice. Nat Rev Neurosci 7:732-744.
Mazzoni A, Broccard FD, Garcia-Perez E, Bonifazi P, Ruaro ME, Torre V (2007) On the Dynamics of the Spontaneous Activity in Neuronal Networks. PLoS ONE 2:e439.
McKhann G (1984) Clinical diagnosis of Alzheimer's disease: report of the NINCDS-ADRDA Work Group under the auspices of Department of Health and Human Services Task Force on Alzheimer's Disease. In, pp 939-944: AAN Enterprises.
Montez T, Linkenkaer-Hansen K, van Dijk BW, Stam CJ (2006) Synchronization likelihood with explicit time-frequency priors. NeuroImage 33:1117-1125.
Monto S, Vanhatalo S, Holmes MD, Palva JM (2007) Epileptogenic Neocortical Networks Are Revealed by Abnormal Temporal Dynamics in Seizure-Free Subdural EEG. Cereb Cortex 17:1386-1393.
Mudher A, Lovestone S (2002) Alzheimer's disease–do tauists and baptists finally shake hands? Trends in Neurosciences 25:22-26.
Nakakoji K, Yamamoto Y, Nishinaka Y, Kishida K, Ye Y (2002) Evolution patterns of open-source software systems and communities. Proceedings of the International Workshop on Principles of Software Evolution:76-85.
Nestor PJ, Scheltens P, Hodges JR (2004) Advances in the early detection of Alzheimer's disease. Nat Med 10:S34-41.
Neufeld MY, Rabey MJ, Parmet Y, Sifris P, Treves TA, Korczyn AD (1994) Effects of a single intravenous dose of scopolamine on the quantitative EEG in Alzheimer's disease patients and age-matched controls. Electroencephalogr Clin Neurophysiol 91:407-412.
Nikulin VV, Brismar T (2004) Long-range temporal correlations in alpha and beta oscillations: effect of arousal level and test-retest reliability. Clinical Neurophysiology 115:1896-1908.
Osipova D, Ahveninen J, Jensen O, Ylikoski A, Pekkonen E (2005) Altered generation of spontaneous oscillations in Alzheimer's disease. NeuroImage 27:835-841.
Osipova D, Ahveninen J, Kaakkola S, Jaaskelainen IP, Huttunen J, Pekkonen E (2003) Effects of scopolamine on MEG spectral power and coherence in elderly subjects. Clinical Neurophysiology 114:1902-1907.
Paczuski M, Hughes D (2004) A heavenly example of scale-free networks and self-organized criticality. Physica A: Statistical Mechanics and its Applications 342:158-163.
Paczuski M, Maslov S, Bak P (1996) Avalanche dynamics in evolution, growth, and depinning models. Physical Review E 53:414-443.
Palva JM, Palva S, Kaila K (2005a) Phase Synchrony among Neuronal Oscillations in the Human Cortex. J Neurosci 25:3962-3972.
Palva S, Palva JM (2007) New vistas for [alpha]-frequency band oscillations. Trends in Neurosciences 30:150-158.
Palva S, Linkenkaer-Hansen K, Naatanen R, Palva JM (2005b) Early Neural Correlates of Conscious Somatosensory Perception. J Neurosci 25:5248-5258.

Parish LM, Worrell GA, Cranstoun SD, Stead SM, Pennell P, Litt B (2004) Long-range temporal correlations in epileptogenic and non-epileptogenic human hippocampus. Neuroscience 125:1069-1076.
Peng CK, Havlin S, Stanley HE, Goldberger AL (1995) Quantification of scaling exponents and crossover phenomena in nonstationary heartbeat time series. Chaos: An Interdisciplinary Journal of Nonlinear Science 5:82-87.
Penttila M, Partanen JV, Soininen H, Riekkinen PJ (1985) Quantitative analysis of occipital EEG in different stages of Alzheimer's disease. Electroencephalogr Clin Neurophysiol 60:1-6.
Pereda E, Quiroga RQ, Bhattacharya J (2005) Nonlinear multivariate analysis of neurophysiological signals. Prog Neurobiol 77:1-37.
Pereda E, Rial R, Gamundi A, González J (2001) Assessment of changing interdependencies between human electroencephalograms using nonlinear methods. Physica D: Nonlinear Phenomena 148:147-158.
Pfurtscheller G, Klimesch W (1992) Event-related synchronization and desynchronization of alpha and beta waves in a cognitive task. Induced Rhythms in the Brain:117-128.
Pijnenburg YAL, vd Made Y, van Cappellen van Walsum AM, Knol DL, Scheltens P, Stam CJ (2004) EEG synchronization likelihood in mild cognitive impairment and Alzheimer's disease during a working memory task. Clinical Neurophysiology 115:1332-1339.
Plenz D, Thiagarajan TC (2007) The organizing principles of neuronal avalanches: cell assemblies in the cortex? Trends Neurosci 30:101-110.
Poil S-S, van Ooyen A, Linkenkaer-Hansen K (2008a) Avalanche dynamics of human brain oscillations: relation to critical branching processes and temporal correlations. Human Brain Mapping In Press.
Poil SS, van Ooyen A, Linkenkaer-Hansen K (2008b) Avalanche dynamics of human brain oscillations: Relation to critical branching processes and temporal correlations. Human Brain Mapping 29:770-777.
Posthuma D, de Geus EJC, Mulder E, Smit DJA, Boomsma DI, Stam CJ (2005) Genetic components of functional connectivity in the brain: the heritability of synchronization likelihood. Hum Brain Mapp 26:191-198.
Raghavachari S, Kahana MJ, Rizzuto DS, Caplan JB, Kirschen MP, Bourgeois B, Madsen JR, Lisman JE (2001) Gating of Human Theta Oscillations by a Working Memory Task. J Neurosci 21:3175-3183.
Raichle ME, Mintun MA (2006) Brain Work and Brain Imaging. Annual Review of Neuroscience 29:449-476.
Raichle ME, MacLeod AM, Snyder AZ, Powers WJ, Gusnard DA, Shulman GL (2001) Inaugural Article: A default mode of brain function. Proc Natl Acad Sci USA 98:676-682.
Rangarajan G, Ding M (2000) Integrated approach to the assessment of long range correlation in time series data. Physical Review E 61:4991-5001.
Rhodes CJ, Anderson RM (1996) Power laws governing epidemics in isolated populations. Nature 381:600-602.

Riekkinen P, Buzsaki G, Riekkinen Jr P, Soininen H, Partanen J (1991) The cholinergic system and EEG slow waves. Electroencephalogr Clin Neurophysiol 78:89-96.

Rosenblum MG, Pikovsky AS (2001) Detecting direction of coupling in interacting oscillators. Physical Review E 64:45202.

Rosenstein MT, Collins JJ, De Luca CJ (1994) Reconstruction expansion as a geometry-based framework for choosing proper delay times. Physica D 73:82-98.

Rulkov NF, Sushchik MM, Tsimring LS, Abarbanel HDI (1995) Generalized synchronization of chaos in directionally coupled chaotic systems. Physical Review E 51:980-994.

Sannita WG, Maggi L, Rosadini G (1987) Effects of Scopolamine (0.25-0.75 mg im) on the Quantitative EEG and the Neuropsychological Status of Healthy Volunteers. Logo 17.

Schiff SJ, So P, Chang T, Burke RE, Sauer T (1996) Detecting dynamical interdependence and generalized synchrony through mutual prediction in a neural ensemble. Physical Review E 54:6708-6724.

Shen ZX (2004) Brain cholinesterases: II. The molecular and cellular basis of Alzheimer's disease. Medical Hypotheses 63:308-321.

Simoes C (2002) Neuromagnetic characterization of the human secondary somatosensory cortex.

Singer W (1999) Neuronal Synchrony: A Versatile Code Review for the Definition of Relations? Neuron 24:49-65.

Sneppen K, Bak P, Flyvbjerg H, Jensen MH (1995) Evolution as a self-organized critical phenomenon. Proceedings of the National Academy of Sciences of the United States of America 92:5209-5213.

Soininen H, Partanen VJ, Helkala EL, Riekkinen PJ (1982) EEG findings in senile dementia and normal aging. Acta Neurol Scand 65:59-70.

Stam CJ (2000) Brain dynamics in theta and alpha frequency bands and working memory performance in humans. Neuroscience Letters 286:115-118.

Stam CJ (2005) Nonlinear dynamical analysis of EEG and MEG: Review of an emerging field. Clinical Neurophysiology 116:2266-2301.

Stam CJ (2007) Electrophysiological tests. In: Clinical diagnosis and management of Alzheimer's disease, 3rd ed. (Gauthier S, ed), pp 111-123. Oxford: Informa Healthcare.

Stam CJ, van Dijk BW (2002) Synchronization likelihood: an unbiased measure of generalized synchronization in multivariate data sets. Physica D: Nonlinear Phenomena 163:236-251.

Stam CJ, de Bruin EA (2004) Scale-free dynamics of global functional connectivity in the human brain. Human Brain Mapping 22:97-109.

Stam CJ, van Cappellen van Walsum AM, Micheloyannis S (2002a) Variability of EEG synchronization during a working memory task in healthy subjects. International Journal of Psychophysiology 46:53-66.

Stam CJ, Breakspear M, van Walsum AMC, van Dijk BW (2003a) Nonlinear synchronization in EEG and whole-head MEG recordings of healthy subjects. Human Brain Mapping 19:63-78.

Stam CJ, van der Made Y, Pijnenburg YAL, Scheltens P (2003b) EEG synchronization in mild cognitive impairment and Alzheimer's disease. Acta Neurologica Scandinavica 108:90-96.

Stam CJ, van Walsum AMC, Pijnenburg YAL, Berendse HW, de Munck JC, Scheltens P, van Dijk BW (2002b) Generalized Synchronization of MEG Recordings in Alzheimer's Disease: Evidence for Involvement of the Gamma Band. Journal of Clinical Neurophysiology 19:562.

Stam CJ, Montez T, Jones BF, Rombouts SA, van der Made Y, Pijnenburg YA, Scheltens P (2005) Disturbed fluctuations of resting state EEG synchronization in Alzheimer's disease. Clin Neurophysiol 116:708-715.

Stam CJ, Jones BF, Manshanden I, van Cappellen van Walsum AM, Montez T, Verbunt JPA, de Munck JC, van Dijk BW, Berendse HW, Scheltens P (2006) Magnetoencephalographic evaluation of resting-state functional connectivity in Alzheimer's disease. NeuroImage 32:1335-1344.

Steriade M (2000) Corticothalamic resonance, states of vigilance and mentation. Neuroscience 101:243-276.

Takens F (1981) Detecting strange attractors in turbulence. In: Dynamical Systems and Turbulence, Warwick 1980, pp 366-381: Springer Berlin / Heidelberg.

Tass P, Rosenblum MG, Weule J, Kurths J, Pikovsky A, Volkmann J, Schnitzler A, Freund HJ (1998) Detection of n: m Phase Locking from Noisy Data: Application to Magnetoencephalography. Physical Review Letters 81:3291-3294.

Tononi G, Edelman GM, Sporns O (1998) Complexity and coherency: integrating information in the brain. Trends in Cognitive Sciences 2:474-484.

Turcotte DL, Malamud BD (2004) Landslides, forest fires, and earthquakes: examples of self-organized critical behavior. Physica A: Statistical Mechanics and its Applications 340:580-589.

van der Flier WM, Scheltens P (2005) Use of laboratory and imaging investigations in dementia. J Neurol Neurosurg Psychiatry 76:v45-52.

van Walsum AMC, Pijnenburg YAL, Berendse HW, van Dijk BW, Knol DL, Scheltens P, Stam CJ (2003) A neural complexity measure applied to MEG data in Alzheimer's disease. Clinical Neurophysiology 114:1034-1040.

Vanderwolf CH, Robinson TE (1981) Reticulo-cortical activity and behavior: a critique of the arousal theory and a new synthesis. Behav Brain Sci 4:459-514.

Varela F, Lachaux J-P, Rodriguez E, Martinerie J (2001) The brainweb: Phase synchronization and large-scale integration. Nature Rev Neurosci 2:229-239.

Vrba J, Robinson SE (2001) Signal Processing in Magnetoencephalography. Methods 25:249-271.

Waldemar G (2000) Diagnosis and management of Alzheimer's disease and other disorders associated with dementia. The role of neurologists in Europe. European Journal of Neurology 7:133.

Waldemar G, Dubois B, Emre M, Georges J, McKeith IG, Rossor M, Scheltens P, Tariska P, Winblad B (2007) Recommendations for the diagnosis and management of Alzheimer's disease and other disorders associated with dementia: EFNS guideline. European Journal of Neurology 14:e1.

Weiner H, Schuster DB (1956) The electroencephalogram in dementia. Some preliminary observations and correlations. Electroencephalogr Clin Neurophysiol 8:479-488.
Welch P (1967) The use of fast Fourier transform for the estimation of power spectra: A method based on time averaging over short, modified periodograms. Audio and Electroacoustics, IEEE Transactions on 15:70-73.
Whitney H (1936) Differentiable manifolds. Ann Math 37:645-680.
Wu J (2006) Open Source Software Evolution and Its Dynamics. In: University of Waterloo.

Appendix: Original Publications

P1

ELSEVIER

NeuroImage

www.elsevier.com/locate/ynimg
NeuroImage 33 (2006) 1117–1125

Technical Note

Synchronization likelihood with explicit time-frequency priors

T. Montez,[a,b,*] K. Linkenkaer-Hansen,[c] B.W. van Dijk,[a] and C.J. Stam[a]

[a]*Department of Clinical Neurophysiology and MEG Centre, VU University Medical Center, Amsterdam, The Netherlands*
[b]*Institute of Biophysics and Biomedical Engineering, Faculty of Sciences, University of Lisbon, Portugal*
[c]*Center for Neurogenomics and Cognitive Research (CNCR), Department of Experimental Neurophysiology, Vrije Universiteit Amsterdam, The Netherlands*

Received 24 November 2005; revised 29 May 2006; accepted 25 June 2006
Available online 3 October 2006

Cognitive processing requires integration of information processed simultaneously in spatially distinct areas of the brain. The influence that two brain areas exert on each others activity is usually governed by an unknown function, which is likely to have nonlinear terms. If the functional relationship between activities in different areas is dominated by the nonlinear terms, linear measures of correlation may not detect the statistical interdependency satisfactorily. Therefore, algorithms for detecting nonlinear dependencies may prove invaluable for characterizing the functional coupling in certain neuronal systems, conditions or pathologies. Synchronization likelihood (SL) is a method based on the concept of generalized synchronization and detects nonlinear and linear dependencies between two signals (Stam, C.J., van Dijk, B.W., 2002. Synchronization likelihood: An unbiased measure of generalized synchronization in multivariate data sets. Physica D, 163: 236–241.). SL relies on the detection of simultaneously occurring patterns, which can be complex and widely different in the two signals. Clinical studies applying SL to electro- or magnetoencephalography (EEG/MEG) signals have shown promising results. In previous implementations of the algorithm, however, a number of parameters have lacked a rigorous definition with respect to the time-frequency characteristics of the underlying physiological processes. Here we introduce a rationale for choosing these parameters as a function of the time-frequency content of the patterns of interest. The number of parameters that can be arbitrarily chosen by the user of the SL algorithm is thereby decreased from six to two. Empirical evidence for the advantages of our proposal is given by an application to EEG data of an epileptic seizure and simulations of two unidirectionally coupled Hénon systems.

Keywords: Nonlinear dynamics; Generalized synchronization; Synchronization likelihood; EEG; MEG; Time-delay embedding; Functional connectivity

Introduction

Cognition depends on coordinated neuronal activity in spatially distinct areas of the brain (Varela et al., 2001). Two central issues in cognitive neuroscience are to detect the brain areas that interact during various tasks and to reveal the nature of their interaction. It is natural to assume that the coordination of activity or exchange of information between brain areas gives rise to a statistical interdependence between the activities in these areas. In other words, we may reveal the spatial functional connectivity underlying cognitive processing by mapping the statistical interdependencies between time series of neuronal data recorded from different anatomical locations (Lee et al., 2003). The evidence suggests that functional interactions are mediated by synchronization of oscillations and that the frequency content of these oscillations has some specificity to the function that they serve (Sarnthein et al., 1998; von Stein and Sarnthein, 2000; Varela et al., 2001). Nevertheless, neuronal activity patterns may be related through nonlinear functions including strongly transient or cross-frequency phase locking (Friston, 2000; Stam et al., 2003; Palva et al., 2005a). To detect statistical interdependencies that are not governed by simple linear functions, so-called "nonlinear methods" are required.

Many coupling measures for detecting linear and nonlinear interdependencies have been proposed (for a review, see Stam, 2005). Currently, there is no consensus on how to best detect nonlinear interdependencies in neurophysiological data (Quiroga et al., 2002; David et al., 2004). In fact, different algorithms have been shown to detect nonlinear interactions between brain regions (Stam et al., 2003). The most general form of interaction between two dynamical systems is generalized synchronization, where the state of a response system Y is a function of the state of the driver system X: $Y=F(X)$ (Rulkov et al., 1995). For neural systems, this implies that if a given area generates a specific pattern of activity (X) at different times, the functionally connected brain areas are likely to generate specific patterns of activity $F(X)$ at those same points in time. Note that the patterns in the different areas may be widely different because of the potentially nonlinear coupling that governs the functional relationships (in other words, F may be a nonlinear

* Corresponding author. MEG Centre, VU University Medical Center, P.O. Box 7057, 1007 MB Amsterdam, The Netherlands. Fax: +31 20 444 4816.
E-mail address: t.montez@vumc.nl (T. Montez).
Available online on ScienceDirect (www.sciencedirect.com).

1053-8119/$ - see front matter © 2006 Elsevier Inc. All rights reserved.
doi:10.1016/j.neuroimage.2006.06.066

function). Moreover, one may be interested in the coupling between organs that produce qualitatively different signals, e.g., heart-rate variability and sleep EEG (Dumont et al., 2004).

A natural way to investigate generalized synchronization is to represent the state of dynamic systems in a given time window by vectors in the so-called state space formed by time-delay embedding (Takens, 1981; Ott, 1993). The problem of detecting similar dynamic states then translates into finding embedding vectors that are close in state space. This approach was used in the interdependency measure of generalized synchronization between two time series (Arnhold et al., 1999). However, as pointed out previously, the interdependency measure is sensitive to signals having different amplitudes or different degrees of freedom (Arnhold et al., 1999; Pereda et al., 2001). To solve this problem, Stam and van Dijk (2002) introduced a measure of generalized synchronization termed synchronization likelihood. In synchronization likelihood, the critical distances determining whether state vectors are close or not are defined separately for the two systems. The interdependency measure (S) and the synchronization likelihood (SL) share the problem, however, of having six parameters to be chosen by the user of the algorithms and little is known about their influence on the estimation of interdependency between coupled systems.

Here we argue that when choosing the values of the time-delay parameters, the SL algorithm is implicitly biased towards detecting patterns in certain frequency bands. Thus, we introduce lower or upper bounds for the values of SL parameters on the basis of the frequency range of interest and the sampling frequency of the signals. Moreover, we show for the first time examples of recurrent patterns detected by the SL algorithm and how these patterns are distributed in the time series. Finally, we explain the importance of having a lower bound for the number of recurrences and in what sense the temporal resolution of the SL algorithm is surprisingly good.

Methods

Time-frequency synchronization likelihood

Here we describe the synchronization likelihood method with explicit time-frequency priors. The differences between the present and the previous version of SL are addressed in the discussion.

The basic assumption of the method is that the state of the system at any given moment may be represented by an embedding vector, and thus that recurrent states are represented by similar embedding vectors (Takens, 1981). The computation of SL between two time series can be divided into the following five steps: (1) definition of the frequency band of interest and band-pass filtering; (2) construction of time-delay embedding vectors that represent dynamical states of the neural systems; (3) localization of the times of recurrent dynamical states in both systems; (4) computation of the likelihood (SL) that the recurrence of a state in one system is accompanied also by a recurrent state in the other system; and (5) repetition of steps 2–4 at different times in order to obtain a time series of SL values.

Definition of the frequency band of interest and band-pass filtering

Before applying the SL algorithm, one has to decide for the frequency band of interest, i.e., the lower and upper bounds of the frequency content of the patterns. Note that this does not imply that the patterns cannot have complex shapes, although this would usually require a broad range of frequencies. The signals are then filtered with a suitable band-pass filter.

Representation of the dynamical state of the neural systems with time-delay embedding vectors

Following the decision on the frequency range of interest, we use time-delay embedding to form a state-space representation of the system dynamics. The rationale in the present study is that the state vector must sample the signal at sufficiently short intervals to pick up the fastest oscillation and also to be long enough to sample the slowest oscillation. From the time series $x_{k,i}$ of channel k, the state vector $X_{k,i}$ representing the state of the system at time i is given by:

$$X_{k,i} = (x_{k,i}; x_{k,i+L}; x_{k,i+2*L}; \ldots; x_{k,i+(m-1)*L}) \quad (1)$$

Here, L is the lag and m is the dimension of the embedding vector in state space. Note that $X_{k,i}$ represents the state of the system in a time interval of length $L*(m-1)$, but for convenience we will refer to this interval as the state at time i, i.e., the beginning of the interval.

The SL method assumes that in a given period of time a pattern of activity will closely repeat itself a number of times in one signal and in the case of generalized synchronization between two signals another pattern tends to repeat itself in the other signal at those same times. The likelihood of repetition in the second signal may depend, e.g., on the strength of coupling between the two systems or on the signal-to-noise ratio of the data. The highest frequency in the patterns was defined above (step 1) and the embedding lag is chosen so as to sample the fastest oscillations. According to the Nyquist sampling theorem, a dynamical process must be sampled at minimum twice the highest frequency (HF) of its fluctuations in order for the discrete signal to adequately represent the dynamics of the underlying system. In practice, however, a factor of three is commonly used (Smith, 1999):

$$L = \frac{fs}{3*\mathrm{HF}} \quad (2)$$

where fs is the sampling frequency in Hz.

The lowest frequency (LF) has the longest period and thus determines the length of the state vector:

$$L*(m-1) = \frac{fs}{\mathrm{LF}} \Leftrightarrow m = \frac{3*\mathrm{HF}}{\mathrm{LF}} + 1 \quad (3)$$

Detection of recurrences of states in two potentially coupled systems

Having the dynamical states of a system A represented in state space, a criterion for when to consider states at different times similar or "recurrent" is needed. We construct a reference vector in channel A at time i, $X_{A,i}$, and vectors $X_{A,j}$ at times j, ranging from $i-W_2/2$ to $i-W_1/2$ and from $i+W_1/2$ to $i+W_2/2$ in steps of $1/fs$ (Fig. 1a). The time windows W_1 and W_2 are defined later in this section. The Euclidean distance between the state vectors $X_{A,j}$ and the reference vector is computed (other distance measures such as the maximum norm may also be used). The p_{ref} is now introduced to denote the percentage of vectors $X_{A,j}$ that are considered close enough to $X_{A,i}$ to represent the same state of the system (Fig. 2), which leads to the definition of a critical Euclidean distance, r_A, for which: $|X_{A,i}-X_{A,j}|<r_A$. A $p_{\mathrm{ref}}=0.05$ means that five percent of the vectors $X_{A,j}$ will be considered recurrences of $X_{A,i}$. The same procedure is applied to channel B at the same time point. The p_{ref} is generally associated with different critical distances (r_A and r_B)

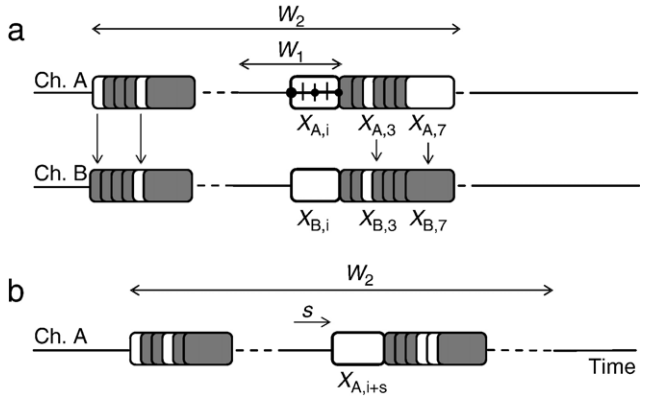

Fig. 1. Illustration of state vectors and synchronization likelihood parameters (L, m, W_1, W_2 and s) with respect to the time series of channels A and B. (a) The reference vector of channel A is denoted $X_{A,i}$ (thick line square) here chosen to have embedding dimension $m=3$ samples (small ticks) and lag $L=2$ samples (dots). The reference vector is compared with state vectors (squares) $X_{A,j}$ ($j=\pm 1,2 \ldots n$) within a window of W_2. State vectors starting at times j in the time interval outside the window W_1 and within the window W_2 (windows centered at time i) are compared with the reference vector. The time series is indicated with a solid horizontal line and the time intervals where the state vectors are constructed are indicated with a dashed line. The vectors $X_{A,j}$ closer to the reference vector $X_{A,i}$ than the critical distance, r_A (see also Fig. 2) are represented in white, whereas the vectors that are not within the critical distance are represented in grey. The white squares are termed recurrences. Similarly for channel B, a reference vector $X_{B,i}$ is compared with all state vectors $X_{B,j}$ ($j=1,2 \ldots n$). If the vectors are closer to $X_{B,i}$ than r_B they are represented in white, otherwise in grey. Synchronization likelihood is the number of simultaneous recurrences in channels A and B (e.g., at $j=3$) divided by the total number of recurrences within channels (b) In order to obtain a SL time series, a new reference vector is constructed at time point $i+s$ (the arrow represents the s increment), and the procedure in panel a is repeated with respect to the new time point (the windows W_1 and W_2 are now centered at $i+s$).

in the two channels, but the number of vectors within the critical distance is determined by p_{ref} and therefore the same for the two channels. The definition of critical distances separately for the two channels is a crucial difference between the SL algorithm and the nonlinear interdependency measure (Arnhold et al., 1999). Also note that the critical distance may as well differ at different time intervals, as it is determined for each $X_{A,i}$.

To prevent the inclusion of states that are similar because of autocorrelation effects, i.e., because states vary slowly relative to the sampling frequency, we define a window W_1 around time i, where state vectors are not compared for their possible similarity. The vectors starting inside the W_1 window are likely to not represent a recurrence of the reference state but the state itself (Theiler, 1986). If W_1 is twice the length of the embedding vectors, the overlap between the first vector $X_{A,j}$ and the reference vector is only one sample, i.e., $W_1/2$ is larger than the period of the lowest frequency in the signal after the filtering (cf. step 1):

$$W_1 = 2^*L^*(m-1) \tag{4}$$

This definition of W_1 represent a physiologically conservative lower bound as it is well known that neuronal activity transients may emerge or fade away within one oscillation cycle (Palva et al., 2005b).

The window W_2 defines the time interval where the similarity of any given state vector is compared with the reference vector. W_2 has to be large enough to allocate a sufficient number of vectors in order to make sense to take p_{ref} of them as recurrences. The relationship between W_2, p_{ref} and the number of recurrences (n_{rec}) is

$$n_{\text{rec}} = [W_2 - W_1 + 1]^*p_{\text{ref}}. \tag{5}$$

We consider $n_{\text{rec}}=10$ a lower bound for $p_{\text{ref}}=0.01$ and emphasize that it is safe to have a much higher value of n_{rec} because the selection of recurrences $X_{A,j}$ and $X_{B,j}$ that do not resemble the reference patterns $X_{A,i}$ and $X_{B,i}$, respectively, are unlikely to be coincident.

Computation of the likelihood (SL) that states recur simultaneously in the two systems

Having introduced a rational choice of the parameters L and m, we can now formulate the SL at time i as:

$$\text{SL}_i = \frac{n_{AB}}{[W_2 - W_1 + 1]^*p_{\text{ref}}} \tag{6}$$

where n_{AB} is the number of simultaneous repetitions in channels A and B given by:

$$n_{AB} = \sum_{j=i-w_2/2}^{i-w_1/2} n + \sum_{j=i+w_1/2}^{i+w_2/2} n$$
$$n = \theta\left(r_{A,i} - |X_{A,i} - X_{A,j}|\right)\theta\left(r_{B,i} - |X_{B,i} - X_{B,j}|\right) \tag{7}$$

θ is the Heaviside function, which attains the value of one if the argument is positive or zero, and the value of zero if the argument is negative.

Having p_{ref} constant means that the number of recurrences is fixed, whether they exist or not. It is possible that the SL algorithm

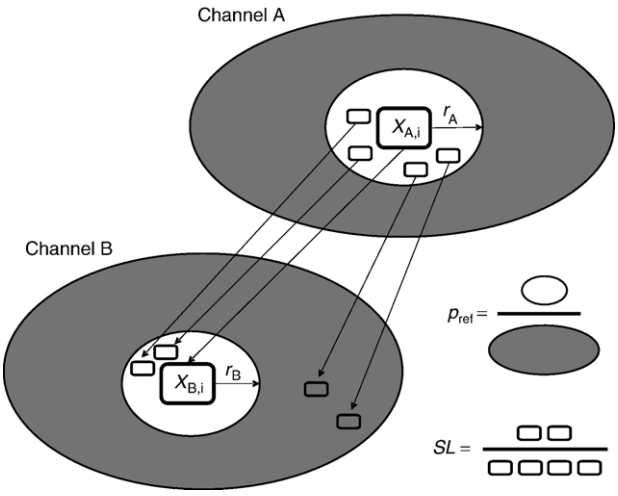

Fig. 2. Schematic representation of SL between two channels in terms of state vectors and critical distances (adapted with permission from Posthuma et al., 2005). $X_{A,i}$ and $X_{B,i}$ are the reference vectors of channels A and B, respectively. State vectors that are closer than the critical distance are shown inside white ellipses, whereas those that are not within the critical distance are represented inside grey ellipses. The lines connect pairs of state vectors at the same time point in both channels, i.e., state vectors $X_B=F(X_A)$. There are two simultaneous recurrences out of four possible. SL of channel A and B at time i is the ratio between the number of simultaneous recurrences and the total number of recurrences within channels. In order words, SL is an index of the likelihood that a recurrence of a reference state in channel A is associated also with a recurrence of a reference state in channel B. p_{ref} is the ratio between the number of vectors closer than the critical distance and the total number of state vectors. Note that p_{ref} is the same for A and B, while the critical distance for A and B is usually different.

considers a random pattern a recurrence because of its state vector coincidentally being close to that of the reference pattern. Nevertheless, the probability that such chance inclusion of random patterns as recurrences occur at identical times in the two time series is small (inversely proportional to the square of the number of state vectors considered) and only simultaneous recurrences contribute to higher values of SL. Therefore, using a higher p_{ref} will increase the number of possible values of SL without introducing spurious high values. Note, in the case of no coupling, the mean SL value over time will be equal to p_{ref}.

Computation of SL for different time points

To obtain a time series of SL values, a new reference vector, $X_{A,i+s}$, is chosen and steps (2) to (4) repeated, etc. (Fig. 1b). Choosing an increment, s, of one sample is safe; however, this is computationally demanding and provides redundant information. Empirical testing suggests that one may gain from s smaller than W_1 in the sense that reference patterns and SL values can vary radically on time scales smaller than W_1 (see Fig. 4). The sampling frequency of SL is the ratio between the sampling frequency of the raw data and s.

Reference vectors at the beginning and at the end of the data set lack data points to fit a window W_2 /2 on both sides. Necessarily, the algorithm must pay attention to these boundary conditions. In this paper, we solved the problem by not computing the SL within a window W_2 /2 from the beginning and the end of the time series. Another solution is to define periodic boundary conditions, i.e., to use the points in the end of the data set to fill the missing points in the beginning and vice versa.

In summary, the parameters necessary for computing the SL at time i can be classified in two groups. The first group includes the parameters related to the time-delay embedding (L and m), which are defined as a function of the frequency band of interest and sampling frequency. The second group includes the W_1, W_2 and p_{ref}, which are related to the process of finding recurrent states within a suitably defined window.

EEG data

EEG data of an absence seizure was acquired at 500 Hz with a OSG Brain Lab (R) digital system at the 10–20 positions. Electrode impedance was kept below 5 kΩ and an average reference electrode was used, involving all electrodes except Fp2 and Fp1. EEGs were recorded in a sound attenuated, dimly lit room while patients sat in a slightly reclined chair. The signals were down sampled offline to 100 Hz and band-pass filtered with a 4th order Butterworth filter. The data in EEG channels F8 and F7 were chosen for the present study and are displayed in Fig. 3a for the pass band: 3–20 Hz.

Simulated data

To test the performance of SL in data with controlled coupling a model of two unidirectionally coupled Hénon systems (Schiff et al., 1996) was used:

$$\begin{cases} x_{i+1} = 1.4 - x_1^2 + 0.3u_i \\ u_{i+1} = x_i \\ y_{i+1} = 1.4 - (Cx_i + (1-C)y_i)y_i + Bv_i \\ v_{i+1} = y_i \end{cases} \quad (7)$$

The state of the driver system X is given by x_i and the state of the response system Y is represented by y_i. For $B=0.3$ the systems

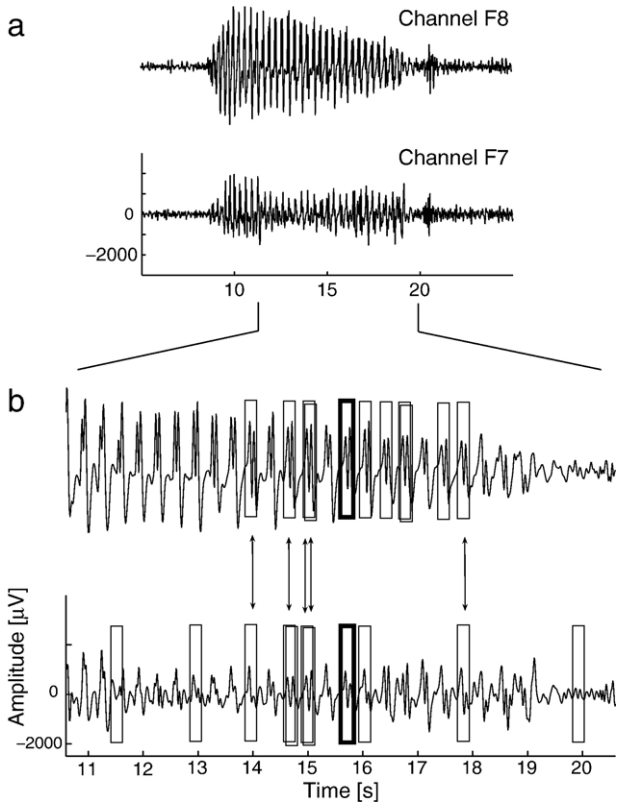

Fig. 3. An epileptic seizure filtered at 3−20 Hz, for channels F8 and F7 in an EEG average montage. (a) The signals represented for the time interval from 5 to 25 s. Note the clear onset of the seizure around 10 s, lasting until around 20 s shown in both channels. (b) Visualization of recurrences of a reference pattern occurring in EEG signals during an epileptic seizure. The reference vectors (thick-line boxes) are located at time 15.6 s and have the duration of 0.2 s. The number of state vectors considered close to the reference vector in each channel (thin-line boxes) is determined by p_{ref} (here $n_{\mathrm{rec}}=10$, see also Eq. (5)). The state vectors comprise complex patterns with multiple frequencies content. The vertical arrows indicate the simultaneous recurrences. SL at time 15.6 s is the ratio between the number of simultaneous recurrences and the number of vectors closer than the critical distance, i.e., SL=5/10=0.5.

are identical. The coupling parameter C gives the strength of the coupling, ranging from zero if the systems are uncoupled system to one if the coupling is complete.

Time series x_i and y_i of 4000 samples were simulated. C was equal to zero except for the time interval between 1500 and 2500 where different values were used. For each value of C, the first 5000 iterations were discarded. We averaged over 10 realizations considering random numbers between 0 and 1 for the initial values of x, u, y and v.

Results

Using EEG recordings of an epileptic seizure, we compare the performance of SL as implemented previously (Stam et al., 2003, 2005, Stam and de Bruin, 2004) and synchronization likelihood with explicit time-frequency (TF) priors as explained in the previous section. Previous studies used $L=10$ samples, $m=10$ samples, $W_1=100$ samples, $W_2/2=10\%$ of the length of the data set, $p_{\mathrm{ref}}=0.01$ or $p_{\mathrm{ref}}=0.05$ and different sampling frequencies (200,

250, 313 and 500 Hz). These parameter values are henceforth referred to as "previous parameters" as opposed to "TF parameters".

From recurrences of patterns of interest to SL

For the priors in the frequency band of 3–20 Hz and $fs=100$ Hz, the TF parameters follow from Eqs. (2), (3) and (4): $L=1/fs=0.01$ s, $m=21/fs=0.21$ s, $W_1=40/fs=0.4$ s, $W_2=10$ s and $p_{ref}=0.01$ corresponding to $n_{rec}=10$. A reference pattern and the corresponding recurrences as detected by the SL algorithm with TF priors are indicated in Fig. 3b. The times of recurrences in channel F8 were similar to those expected on the basis of visual inspection. For channel F7, the pattern at the reference time point is different from that in channel F8, but its recurrences occasionally appear at the same times as the recurrences in channel F8. SL is given by the ratio between the number of recurrences that occur simultaneously in both channels and the total number of recurrences considered in each channel.

SL depends on the choice of the time-delay embedding parameters: L and m

Fig. 4 shows a short segment of data and how different choices of L and m leads to the sampling of different patterns. At 15.6 s, the vector obtained with the TF parameters (samples represented with black dots) tracks the pattern of interest in channel F8, while the previous parameters do not (white circles), picking up points from three potential occurrences of the pattern of interest. The TF parameters also track the pattern well in the absence of high-frequency components as seen at 15.8 s, which is just a window

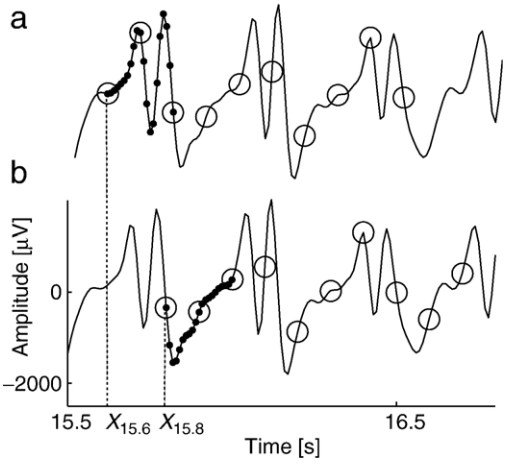

Fig. 4. The reference vectors of SL with TF priors track the patterns of interest. State vectors from Fig. 3b shown at a shorter time scale, at 15.6 s (a) and 15.8 s (b) for channel F8. White circles represent the samples that are selected for the reconstruction of the state vectors for the parameters used in previous studies ($L=10$ samples and $m=10$ samples) and black circles mark the samples of the state vectors based on time-frequency priors ($L=1/fs$ and $m=21/fs$, $fs=100$ Hz). The TF parameters pick up the pattern at 15.6 s with high frequency components, as well as the pattern at 15.8 s mostly comprising a low frequency component indicating the adaptive ability of the SL algorithm. Note that the shift of 0.2 s corresponds to a window $W_1/2$ with the TF parameters. Note that the previous parameters lead to under sampling and alias-type of problems in the context of sampling theorem and Nyquist- frequency.

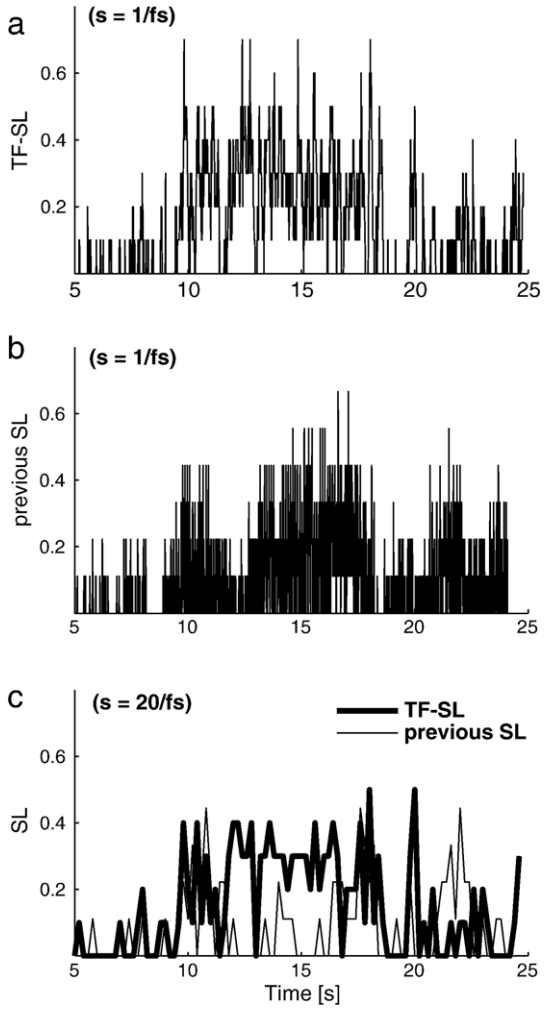

Fig. 5. Stability of the SL time series computed with the parameters based on the TF priors ($L=1/fs$ and $m=21/fs$, $fs=100$ Hz) and the ones used in previous studies ($L=10$ samples and $m=10$ samples). SL time series for a sampling frequency of 100 Hz and $s=1/fs$ for the TF parameters (a) and for the previous parameters (b) and for $s=20/fs$ for both sets of parameters (c). The TF-SL for $s=1/fs$ shows the onset and end of the seizure and when s is increased to $20/fs$, i.e., when the SL time series is re-sampled by a factor of 20, a mean value of 0.3 is maintained during the entire seizure. This means that the TF parameters are robust to changes in the spacing of consecutive reference vectors, i.e., the TF-SL is stable. The SL time series for the previous parameters and $s=1/fs$ increases from zero up to 0.6 in 0.02 s and is unstable, e.g., it is difficult to see where the middle of the seizure is. When the s is increased to $20/fs$ (0.2 s), previous SL mean value drops to 0.1 in the middle of the seizure and there is a peak around 22 s after the seizure.

$W_1/2$ away and thereby also pointing to a high temporal resolution and ability to adapt to changing patterns.

SL with TF priors is insensitive to the spacing of consecutive reference vectors

Fig. 5a shows the results obtained with the TF parameters for $s=1/fs$. The SL time series shows an increase at around 10 s, which lasts until around 18 s and then a brief increase around 20 s. Fig. 5b shows the results with the previous parameters. The SL time series is very unstable with large fluctuations on time scales

down to $2/fs = 0.02$ s. Fig. 5c shows the SL time series obtained with the TF and the previous parameters for $s = 20$. The results with the previous parameters are not robust to a change of s. The SL time series only shows a small increase around 10 s that ends before 15 s when the spacing of consecutive reference vectors increases. The highest values occur at around 18 and 22 s, times far after the onset of the seizure. At the latency of 15.6 s, the difference between the two SL time series is 0.6. The channels seem, by visual inspection of the signals, to be synchronized. Thereby, the TF parameters are sensitive to the onset of the seizure, while the previous parameters do not.

Comparison of SL with TF priors and classical coherence

The performance of SL with TF priors in tracing the emergence of a complex pattern of synchronized activity – as exemplified with an epileptic seizure – is compared with classical coherence, which is a measure of linear phase correlations in a sliding window (Welch, 1967). For this technical note, we consider it more important to contrast the performance of SL and a classical method than proving the presence of nonlinear dependencies *per se* with surrogate data tests (Theiler et al., 1992; Prichard and Theiler, 1994).

It should be emphasized that SL provides a statistical estimate of functional coupling and therefore is only applicable under the assumption that certain patterns are detected repeatedly in different sensors. This is completely analogous to coherence or phase-locking factors, which only provide useful indices of neuronal communication if a large number of oscillation cycles/trials are available to estimate the consistency of linear phase relations between oscillations.

The coherence method is based on dividing the data set into pieces of length equal to the time resolution wanted for the coherence method. In the present study, we were interested in frequencies with a lower bound of 3 Hz. To get averages for the application of the Welch method, windows with at least three periods (1 s), and overlapping at least half of the size, are shifted along time within the window determining the time resolution. For our data set 5 s is appropriate. Note that 5 s is $W_2/2$. Fig. 6a displays the time-frequency coherence of the signal band-pass filtered at 3–20 Hz and showing prominent coherence at all times and in all frequency bands.

To better compare coherence and synchronization likelihood performance in detecting the complex patterns and coupling in the frequency range of 3–20 Hz, we averaged the time-frequency coherence over the same frequencies (Fig. 6b). The coherence for the 3- to 20-Hz band is characterized by values between 0.5 and 0.7 s even outside the seizure period whereas the SL time series reaches values between 0.0 and 0.2, due to the better time resolution. The SL time series obtained for the signal filtered at 3–20 Hz with TF priors of the same range shows the onset of the epileptic seizure at around 10 s, lasting until around 20 s.

Application of SL to simulated data

Finally, the algorithm was applied to simulated data where the coupling has been manipulated in a time window (Stam and van Dijk, 2002). TF-SL increases rapidly with the sudden change of the coupling strength from zero to 0.5 achieving peaks of high value of synchronization (0.5), decreases in the same way when the coupling drops from 0.5 back to zero and fluctuates around p_{ref} when there is no coupling (Fig. 7a). The SL computed with the previous parameters never reaches values above 0.2 and has peaks of that amplitude outside the window where the systems are coupled.

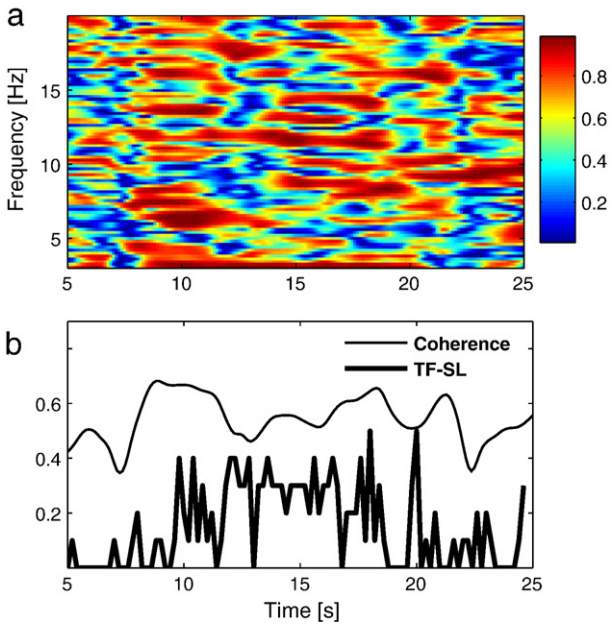

Fig. 6. Comparison between the classical coherence and the SL with TF priors for the signal filtered at 3−20 Hz. Time-frequency coherence plot (a) and classical coherence and TF-SL computed for the prior frequency bands of 3−20 Hz (b). The patterns in the time-frequency plot seem to be similar for the different frequencies. Peaks are found for lower frequencies (5−10 Hz) around 10 s and higher frequencies (8−14 Hz) around 15 s, also a peak in response for frequencies > 15 Hz is seen around 12 s. The classical coherence averaged in the 3−20 Hz has a higher mean value than the TF-SL; however, coherence does not show stability during the seizure. The TF-SL increases on the onset of the seizure around 10 s until a lower mean value compared to classical coherence and drops back at the end of the seizure to the baseline value it had before the seizure.

When the value of the coupling strength used in the time window increases, both the mean values obtained for that window with TF-SL and SL computed with the previous parameters increase (Fig. 7b). TF-SL increases slowly until $C = 0.5$ and abruptly reaches higher values for $C = 0.7$. SL computed with the previous parameters gave mean values close to p_{ref} for values of coupling strength up to 0.6.

Applying SL to a signal with a frequency content higher or lower than specified by the frequency priors inevitably renders the physiological interpretation of the results difficult and pre-processing the data by band-pass filtering in the frequency range of interest is therefore a crucial step when using the SL algorithm. The present paper has focused on defining parameters for short patterns, but we are aware that one may wish to let the SL algorithm search for patterns that are longer than one cycle of the lowest frequency. This is naturally achieved by a correspondingly higher value of m. The method is suited for the analysis of the dynamics of systems with complex patterns with broad frequency content.

Discussion

We have introduced a time-frequency approach to the synchronization likelihood algorithm, in order to investigate linear and nonlinear dependencies in physiological signals with only two

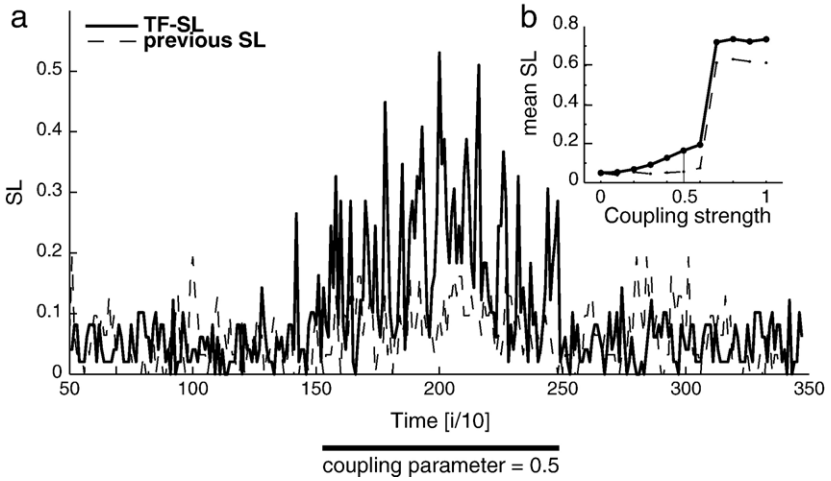

Fig. 7. TF-SL tracks the change of coupling strength between systems more accurately than previous SL. (a) The signals are coupled in a window between times $i=1500$ and 2500 with coupling parameter equal to 0.5. The frequencies of interest: 9–16 Hz (giving embedding parameters: $l=2/fs$ and $m=7/fs$, $fs=100$ Hz) were chosen after analysis of the power spectrum of the simulated time series (not shown). We used $W_2=1000$ samples and $p_{ref}=0.05$. (b) Mean values, between times $i=1500$ and 2500, of SL as a function of the value of the coupling strength. The results obtained with TF-SL are always larger than the ones obtained with the previous parameter for all values of coupling strength.

free parameters: W_2 and p_{ref}. We have shown that the method is robust to changes in the sampling frequency of the data and tracks recurrences of complex patterns with broad frequency content. Finally, our results indicate that SL is adaptive, i.e., the patterns may change radically as the reference window is moved through the time series, making SL a potentially powerful algorithm for the study of linear and nonlinear coupling between dynamical systems.

A rational choice of the embedding parameters: L and m

In previous applications of SL (Stam et al., 2003, 2005, Stam and de Bruin, 2004), the parameters L and m were fixed both to 10 samples (despite different studies using different sampling frequencies). Here, we have shown that this is not a suitable choice for low sampling frequencies because the L is then too large to sample the higher frequencies. Dumont et al. (2004) computed the embedding parameters: L was one-fourth of the time it takes for the normalized autocorrelation function to drop to $1/e$. L may then be different for each channel and, consequently, the state vectors will sample different higher frequencies. Our definition of the embedding parameters is based on the frequency range of interest. Considering a too low dimension may lead to "unfolding" of the state space and the existence of false neighbors, i.e., points that appear to be nearest neighbors because the embedded space is too small (Kennel et al., 1992). Theoretically, attractors are unfolded with an embedding dimension higher than twice the dimension of the attractor (Takens, 1981). In the case of the epileptic seizure, the TF approach leads to a higher m ($21/fs$) than the previous parameters ($10/fs$); in the case of the simulated data, m is equal to $7/fs$. A too high dimension makes the method more sensitive to influence of noise.

Parameters related to finding recurrent states: W_1, W_2 and p_{ref}

SL is not very sensitive to the choice of W_1, as long as W_1 is as long as it takes the system to change state and thereby prevent trivial recurrences caused by the reference state being sampled multiple times. The window W_1 is not applied around the other embedded vectors. If we get in one channel consecutive vectors for times j and $(j+1/fs)$ as recurrences they represent the same recurrence. However, if in the other channel we only get the vector embedded at time $(j+1/fs)$ as a recurrence, we would miss the simultaneous recurrence if W_1 was defined around time j.

We did not propose a strict definition of W_2 and p_{ref} because it depends on the data. W_2 has to be large enough to allocate a sufficient number of state vectors as potential recurrent states. From these vectors, a fraction p_{ref} is taken and considered to be recurrences (see also Eq. (5)). Choosing W_2 to be the entire data interval with periodic boundary conditions reduces the free parameters only to p_{ref}, with the only drawback of an increase of the computation time. Higher p_{ref} for the same W_2 implies a larger number of recurrences. We have shown that some recurrences are tracked more than once (at adjacent samples), so this might mean picking up the same number of recurrences, but each one more than once. This happens because, in some cases, the time increment ($1/fs$) is not enough for the system to change its state. It is naturally interesting to know how recurrences are clustering; suggesting that in future applications of SL the important patterns and the dynamics of their appearance should be explicitly studied, e.g., in pathologic subjects or different stages of sleep.

Physiology of recurrent patterns in neuronal activity

Recurrent patterns in neuronal activity have been recognized in neocortical circuits of rats *in vitro* (Beggs and Plenz, 2004; Rosanova and Ulrich, 2005); in primary visual cortex *in vivo* (Ikegaya et al., 2004, Kenet et al., 2003), cerebellum and red nucleus (Kalużny and Tarnecki, 1993) and in primary somatosensory cortex (Rosanova and Ulrich, 2005) of anesthetized cats, as well as in hippocampus of rats (Nádasdy et al., 1999). Altogether, these studies suggest that recurrent patterns are common in neuronal systems. SL and other algorithms that aim at quantifying generalized synchronization assume that when a given activity pattern is repeated in a certain area, functionally connected areas also tend to exhibit repetitions of a certain activity pattern.

Generally speaking, SL may detect spatiotemporally distributed processing that involves not only linear interactions between neuronal populations – such as coherence in distinct frequency bands (Fries, 2005) – but also nonlinear interactions. A nonlinear interaction between two brain regions may show up as radically different temporal activation patterns in recordings from these regions. This is a well-known phenomenon in the study of event-related fields, where the time-frequency profile of activations recorded over sensory and association cortices may differ significantly, although clearly a result of uni- or bi-directional neuronal communication. One advantage of SL, in addition to its potential of also detecting nonlinear interactions, is the absence of a priori assumptions regarding the times of interactions: recurrent patterns within channels and across channels are detected automatically and may therefore equally well be studied in ongoing data without well-defined stimulus- or task-induced activations. Nonlinear transient patterns are thought to mediate adaptive perceptual synthesis and sensorimotor integration (Friston, 2000) and the SL algorithm may therefore become an important tool in cognitive research.

The adaptive nature of SL

We showed that the SL method is better than classical coherence at tracking the onset of an epileptic seizure. It has a higher temporal resolution and is able to follow the synchronization between two channels with complex activity patterns. This is an advantage when compared to the computation of coherence as a function of time and frequency. We have shown that the TF-SL is able to pick up completely different patterns at a distance of $W_1/2$, some patterns with high frequency components, others with low and also other patterns with a combination of high and low frequencies within the frequency band of interest. The results of the tests with the simulated data showed that the temporal resolution of the TF-SL allows the detection of sharp changes of coupling between nonlinear systems and the mean value reflects the strength of the coupling.

Nonlinear methods are needed for studying neuronal activity patterns related through nonlinear functions (Friston, 2000; Stam et al., 2003; Palva et al., 2005a). The complexity of the problem – to detect and quantify functional relationships of an arbitrary form in noisy signals from stochastic systems with nonlinear coupling – is probably so great that no single algorithm with a fixed set of parameters will ever suffice. Each method extracts different information from the data and the use of different measures might be an interesting approach in some cases. Phase synchronization, e.g., discloses correlations between the phases of systems independently from amplitude relationships (for a review, see Pereda et al., 2005). To discuss effects of amplitude on SL, two situations have to be considered: differences in amplitude within the same channel and between the channels. Within the channel, the sliding window might miss patterns with different amplitudes as recurrences at one time point, but at another time point those patterns will be used as the reference, and the comparison with the paired channel will be done again. Thus, if the channels continue to be synchronized, SL will not be affected. Differences in amplitudes between channels only cause problems with a constant critical distance and not with a fixed p_{ref}. Every analysis has assumptions concerning the relevant time scales of the dynamics. The present paper defines the synchronization likelihood parameters with explicit time-frequency priors, which clarifies the assumptions of the algorithm and facilitates future applications and interpretation of results.

Acknowledgments

T.M. is the recipient of a Praxis XXI doctoral fellowship from FCT, Ministry of Science, Portugal. K.L.-H. is funded by the Danish Research Agency and the Innovative Research Incentive Schemes of the Netherlands Organization for Scientific Research (NWO). This study was supported in part by a Neuro-Bsik grant to the Department of Experimental Neurophysiology, see www.mousephenomics.org. We thank Rik Jansen for comments on an earlier version of the manuscript, Jimmy Chui for an earlier version of the Matlab script used for computing the SL in the present paper and Andreas Daffertshofer for the Matlab script used for computing the time-frequency coherence. We thank the two anonymous reviewers for helpful comments on an earlier draft of this paper.

References

Arnhold, J., Grassberger, P., Lehnertz, K., Elger, C.E., 1999. A robust method for detecting interdependencies: application to intracranially recorded EEG. Physica D 134, 419–430.

Beggs, J.M., Plenz, D., 2004. Neuronal avalanches are diverse and precise activity patterns that are stable for many hours in cortical slice cultures. J. Neurosci. 24 (22), 5216–5229.

David, O., Cosmelli, D., Friston, K.J., 2004. Evaluation of different measures of functional connectivity using a neural mass model. NeuroImage 21, 659–673.

Dumont, M., Jurysta, F., Lanquart, J.P., Migeotte, P.F., van de Borne, P., Linkowsi, F., 2004. Interdependency between heart rate variability and sleep EEG: linear/non-linear? Clin. Neurophysiol. 115 (9), 2031–2040.

Fries, P., 2005. A mechanism for cognitive dynamics: neuronal communication through neuronal coherence. Trends Cogn. Sci. 9 (10), 474–480.

Friston, K.J., 2000. The labile brain. I. Neuronal transients and nonlinear coupling. Philos. Trans. R. Soc. London, B 355, 215–236.

Ikegaya, Y., Aaron, G., Cossart, R., Aronov, D., Lampl, I., Ferster, D., Yuste, R., 2004. Synfire chains and cortical songs: temporal modules of cortical activity. Science 304 (5670), 559–564.

Kalużny, P., Tarnecki, R., 1993. Recurrences plots of neuronal spike trains. Biol. Cybern. 68, 527–534.

Kenet, T., Bibitchkov, D., Tsodyks, M., Grinvals, A., Arieli, A., 2003. Spontaneous emerging cortical representations of visual attributes. Nature 425 (6961), 954–956.

Kennel, M.B., Brown, R., Abarbanel, H.D.I., 1992. Determining embedding dimension for phase-space reconstruction using a geometrical construction. Phys. Rev., A 45, 6.

Lee, L., Harrison, L.M., Mechelli, A., 2003. A report of the functional connectivity workshop, Dusseldorf 2002. NeuroImage 19, 457–465.

Nádasdy, Z., Hirase, H., Czurkó, A., Csicsvari, J., Buzsáki, G., 1999. Replay and time compression of recurring spike sequences in the hippocampus. J. Neurosci. 19 (21), 9497–9507.

Ott, E., 1993. Chaos in Dynamical Systems. Cambridge Univ. Press.

Palva, J.M., Palva, S., Kaila, K., 2005a. Phase synchrony among neuronal oscillations in the human cortex. J. Neurosci. 25 (15), 3962–3972.

Palva, S., Linkenkaer-Hansen, K., Näätänen, R., Palva, J.M., 2005b. Early neural correlates of conscious somatosensory perception. J. Neurosci. 25, 5248–5258.

Pereda, E., Rial, R., Gamundi, A., Gonzalez, J., 2001. Assessment of changing interdependencies between human electroencephalograms using nonlinear methods. Physica D 148, 147–158.

Pereda, E., Quiroga, R.Q., Bhattacharya, J., 2005. Nonlinear multivariate analysis of neurophysiological signals. Prog. Neurobiol. 77, 1–37.

Posthuma, D., de Geus, E.J., Mulder, E.J., Smit, D.J., Boomsma, D.I., Stam, C.J., 2005. Genetic components of functional connectivity in the brain: the heritability of synchronization likelihood. Hum. Brain Mapp. 26 (3), 191–198.

Prichard, D., Theiler, J., 1994. Generating surrogate data for time series with several simultaneously measured variables. Phys. Rev. Lett. 73, 951–954.

Quiroga, R.Q., Kraskov, A., Kreuz, T., Grassberger, G., 2002. Performance of different synchronization measures in real data: a case study on electroencephalographic signals. Phys. Rev., E Stat. Nonlinear Soft Matter Phys. 65, 041903.

Rosanova, M., Ulrich, D., 2005. Pattern-specific associative long-term potentiation induced by a sleep spindle-related spike train. J. Neurosci. 25 (41), 9398–9405.

Rulkov, N.F., Sushchik, M.M., Tsimring, L.S., Abarbanel, H.D.I., 1995. Generalized synchronization of chaos in directionally coupled chaotic systems. Phys. Rev., E Stat. Phys. Plasmas Fluids Relat. Interdiscip. Topics 51 (2), 980–994.

Sarnthein, J., Petsche, H., Rappelsberger, P., Shaw, G.L., von Stein, A., 1998. Synchronization between prefrontal and posterior association cortex during human working memory. Proc. Natl. Acad. Sci. U. S. A. 95, 7092–7096.

Schiff, S.J., So, P., Chang, T., Burke, R.E., Sauer, T., 1996. Detecting dynamical interdependence and generalized synchrony through mutual prediction in a neural ensemble. Phys. Rev., E 54, 6708.

Smith, S.W., 1999. The Scientist and Engineer's Guide to Digital Signal Processing. California Technical Publishing.

Stam, C.J., 2005. Nonlinear dynamical analysis of EEG and MEG: review of an emerging field. Clin. Neurophysiol. 116 (10), 2266–2301.

Stam, C.J., de Bruin, E.A., 2004. Scale-free dynamics of global functional connectivity in the human brain. Hum. Brain Mapp. 22 (2), 97–104.

Stam, C.J., van Dijk, B.W., 2002. Synchronization likelihood: an unbiased measure of generalized synchronization in multivariate data sets. Physica D 163, 236–241.

Stam, C.J., Breakspear, M., van Cappellen van Walsum, A.M., van Dijk, B.W., 2003. Nonlinear synchronization in EEG and whole-head MEG recordings of healthy subjects. Hum. Brain Mapp. 19, 63–78.

Stam, C.J., Montez, T., Jones, B.F., Rombouts, S.A., van der Made, Y., Pijnenburg, Y.A., Scheltens, P., 2005. Disturbed fluctuations of resting state EEG synchronization in Alzheimer's disease. Clin. Neurophysiol. 116 (3), 708–715.

Takens, F., 1981. Detecting strange attractors in turbulence. Lect. Notes Math. 898, 366–381.

Theiler, J., 1986. Spurious dimension from correlation algorithms applied to limited time-series data. Phys. Rev., A 34, 2427–2432.

Theiler, J., Eubank, S., Longtin, A., Galdrikian, B., Farmer, J.D., 1992. Testing for nonlinearity in time series: the method of surrogate data. Physica D 58, 77–94.

Varela, F., Lachaux, J.-P., Rodriguez, E., Martinerie, J., 2001. The brainweb: phase synchronization and large-scale integration. Nat. Rev., Neurosci. 2 (4), 229–239.

von Stein, A., Sarnthein, J., 2000. Different frequencies for different scales of cortical integration: from local gamma to long range alpha/theta synchronization. Int. J. Psychophysiol. 38 (3), 301–313.

Welch, P.D., 1967. The use of fast Fourier transform for the estimation of power spectra: a method based on time averaging over short, modified periodograms. IEEE Trans. Audio Electroacoust. AU-15, 70–73.

P2

ELSEVIER

NeuroImage

www.elsevier.com/locate/ynimg
NeuroImage 32 (2006) 1335 – 1344

Magnetoencephalographic evaluation of resting-state functional connectivity in Alzheimer's disease

C.J. Stam,[a,*] B.F. Jones,[b,f] I. Manshanden,[a] A.M. van Cappellen van Walsum,[c] T. Montez,[d] J.P.A. Verbunt,[a,e] J.C. de Munck,[e] B.W. van Dijk,[a,e] H.W. Berendse,[a] and P. Scheltens [b]

[a]*Department of Clinical Neurophysiology and MEG, VU University Medical Center, P.O. Box 7057 1007 MB Amsterdam, The Netherlands*
[b]*Alzheimer Center, Department of Neurology, VU University Medical Center, Amsterdam, Netherlands*
[c]*Radboud University Nijmegen Medical Centre, Department of Anatomy, Nijmegen, Netherlands*
[d]*Institute of Biophysics and Biomedical Engineering, Faculty of Sciences, University of Lisbon, Portugal*
[e]*Department of Medical Physics and Technology, VU University Medical Center, Amsterdam, Netherlands*
[f]*Dementia Research Centre, Institute of Neurology, UCL, London, UK*

Received 15 March 2006; revised 11 May 2006; accepted 15 May 2006
Available online 11 July 2006

Statistical interdependencies between magnetoencephalographic signals recorded over different brain regions may reflect the functional connectivity of the resting-state networks. We investigated topographic characteristics of disturbed resting-state networks in Alzheimer's disease patients in different frequency bands. Whole-head 151-channel MEG was recorded in 18 Alzheimer patients (mean age 72.1 years, SD 5.6; 11 males) and 18 healthy controls (mean age 69.1 years, SD 6.8; 7 males) during a no-task eyes-closed resting state. Pair-wise interdependencies of MEG signals were computed in six frequency bands (delta, theta, alpha1, alpha2, beta and gamma) with the synchronization likelihood (a nonlinear measure) and coherence and grouped into long distance (intra- and interhemispheric) and short distance interactions. In the alpha1 and beta band, Alzheimer patients showed a loss of long distance intrahemispheric interactions, with a focus on left fronto-temporal/parietal connections. Functional connectivity was increased in Alzheimer patients locally in the theta band (centro-parietal regions) and the beta and gamma band (occipito-parietal regions). In the Alzheimer group, positive correlations were found between alpha1, alpha2 and beta band synchronization likelihood and MMSE score. Resting-state functional connectivity in Alzheimer's disease is characterized by specific changes of long and short distance interactions in the theta, alpha1, beta and gamma bands. These changes may reflect loss of anatomical connections and/or reduced central cholinergic activity and could underlie part of the cognitive impairment.

Keywords: Alzheimer's disease; Resting state; Functional connectivity; MEG; Synchronization likelihood; Crosscorrelation; Coherence; Cognition

Introduction

The neurophysiological mechanisms that underlie cognitive and behavioral dysfunction in Alzheimer's disease (AD) are still incompletely understood. Despite an enormous increase in knowledge about the cellular, molecular, vascular (chronical cerebral hypoperfusion) and genetic processes involved in AD pathology, the relationship between these fundamental changes and abnormal functioning of large scale brain networks remains unclear.

One approach to this problem has concentrated on the idea that AD pathology at the cellular and molecular level could give rise to impaired activation of specific brain regions or a slowing down of local electrophysiological oscillatory activity. Evidence for such local abnormalities has been found with fMRI studies showing impaired activation, in particular, of the hippocampus and related areas during memory tasks (Rombouts et al., 2000). Neurophysiological techniques such as EEG and more recently MEG have also been used to identify local physiological abnormalities (for a review, see Jeong, 2004). EEG studies have demonstrated a slowing of the dominant rhythms, in particular, over the posterior temporal parietal and occipital brain areas (Boerman et al., 1994; Jeong, 2004; Jonkman, 1997). This EEG slowing has been correlated with brain atrophy, APOE genotype and low central cholinergic activity (Lehtovirta et al., 1996; Riekkinen et al., 1991). MEG studies have confirmed the notion of a slowing of brain rhythms and have also suggested an anterior displacement of the sources of these rhythms (Berendse et al., 2000; Fernandez et al., 2002, 2003, 2006; Maestu et al., 2001, 2003, 2004, 2005; Osipova et al., 2005). However, a limitation of these approaches is that it is unclear how these local abnormalities influence the functioning of the brain as an integrated system.

A promising alternative approach focuses on connections rather than on local dysfunction. A central problem in cognitive neuroscience is the question how different, widely distributed

* Corresponding author. Fax: +31 20 4444816.
E-mail address: CJ.Stam@VUmc.nl (C.J. Stam).
Available online on ScienceDirect (www.sciencedirect.com).

1053-8119/$ - see front matter © 2006 Elsevier Inc. All rights reserved.
doi:10.1016/j.neuroimage.2006.05.033

and specialized brain areas integrate their activity. It is widely believed that such large scale functional integration is crucial for higher cognitive and behavioral functioning (Fuster, 2003; Mesulam, 1990, 1998; Tononi et al., 1998). One candidate mechanism for large scale functional integration is the phenomenon of synchronization or temporal correlations between neural activity in different brain regions (Le van Quyen, 2003; Varela et al., 2001). Synchronization of brain regions can be studied by measuring statistical interdependencies (functional connectivity) between physiological signals such as fMRI BOLD, EEG or MEG from different brain regions either during a resting state or during a task (Lee et al., 2003; Fingelkurts et al., 2005; Pereda et al., 2005; Stam, 2005). Studies of functional connectivity have revealed the existence of synchronized neural networks in different frequency bands and involving different brain regions. For instance, working memory is associated with long distance interactions in the theta band, while gamma synchronization may be related to perception and consciousness (Rodriguez et al., 1999; Sarnthein et al., 1998; Stam et al., 2002a; Micheloyannis et al., 2005). Large scale low frequency synchronization has been associated with a context of cognition, while smaller scale high frequency synchronization might be related to content (Palva et al., 2005).

This raises the question whether AD is perhaps better characterized by abnormalities at the network level in addition to, or instead of, the well-known local disturbances. Disturbed functional connectivity would support a 'disconnection hypothesis' of cognitive dysfunction in AD (Delbeuck et al., 2003). Several EEG studies have demonstrated a lower coherence, a linear measure of functional connectivity, of EEG, especially in the alpha band, in AD (Adler et al., 2003; Babiloni et al., 2004a; Besthorn et al., 1994; Dunkin et al., 1994; Hogan et al., 2003; Jelic et al., 1996; Jiang, 2005; Koenig et al., 2005; Knott et al., 2000; Leuchter et al., 1992; Locatelli et al., 1998; Pogarell et al., 2005; Stevens et al., 2001). Changes in coherence outside the alpha band have been reported less frequently, and controversy exists about the question whether delta and theta band coherence are decreased or increased in AD.

Use of nonlinear measures has also suggested a loss of functional connectivity in AD, especially in the alpha and beta bands (Babiloni et al., 2004a,b; Jeong et al., 2001; Pijnenburg et al., 2004; Stam et al., 2003a). MEG may be more suitable than EEG to assess functional connectivity since MEG does not require the use of a reference and is more sensitive to nonlinear correlations (Stam et al., 2003b). In a pilot study, Berendse et al. showed a lower coherence in all frequency bands in AD patients (Berendse et al., 2000). More recently, we used the synchronization likelihood, a measure of generalized synchronization, to study functional connectivity in a larger group of AD subjects and controls (Stam and van Dijk, 2002; Stam et al., 2002b). This study revealed a lower level of synchronization in the upper alpha band, the beta and the gamma band in AD (Stam et al., 2002b). However, lower levels of functional connectivity per se may not yet explain why the large scale brain networks are functioning abnormally. Recently, we found that in AD abnormal topographic organization of large scale brain networks was present, with loss of so called 'small-world' features which correlated with MMSE scores (Stam et al., 2006). This points to the possibility that in AD a specific loss of certain long or short distance connections occurs, involving brain regions at risk in AD.

The present study was undertaken to study in more detail resting-state functional connectivity changes in AD. In particular, we addressed the question whether AD might be associated with a specific loss of either long distance or short distance interactions in particular regions and frequency bands. To this end, MEG was recorded during an eyes-closed no-task state in 18 AD patients and 18 healthy controls. The synchronization likelihood and coherence were computed between all pairs of sensors for signal filtered in delta, theta, alpha1, alpha2, beta and gamma bands. SL and coherence values were averaged for long distance (intra- and interhemispheric) and short distance local sensor pairs.

Methods

Subjects

The study involved 18 patients (mean age 72.1 years, SD 5.6; 11 males; mean MMSE 19.2, range: 13–25) with a diagnosis of probable AD according to the NINCDS-ADRDA criteria (McKhann et al., 1984) and 18 healthy control subjects (mean age 69.1 years, SD 6.8; 7 males; mean MMSE 29, range: 27–30), mostly spouses of the patients. Patients and control subjects were recruited from the Alzheimer Center of the VU University Medical Center. Subjects were assessed according to a clinical protocol, which involved history taking, physical and neurological examination, blood tests, MMSE (Folstein et al., 1975) neuropsychological work up (administration of a battery of neuropsychological tests), MRI of the brain according to a standard protocol and routine EEG. The final diagnosis was based upon a consensus meeting where all the available clinical data and the results of the ancillary investigations were considered. The study was approved by the Local Research Ethics Committee, and all patients or their caregivers had given written informed consent.

MEG recording

Magnetic fields were recorded while subjects were seated inside a magnetically shielded room (Vacuumschmelze GmbH, Hanau, Germany) using a 151-channel whole-head MEG system (CTF Systems Inc., Port Coquitlam, BC, Canada). Average distance between sensors in this system is 3.1 cm. A third-order software gradient (Vrba et al., 1999) was used with a recording pass band of 0.25 to 125 Hz. Sample frequency was 625 Hz. Fields were measured during a no-task eyes-closed condition. At the beginning and at the end of each recording, the head position relative to the coordinate system of the helmet was recorded by leading small alternating currents through three head position coils attached to the left and right pre-auricular points and the nasion on the subject's head. Head position changes during the recording up to approximately 1.5 cm were accepted. During the MEG recording, patients were instructed to close their eyes to reduce artefact signals due to eye movements.

For further off-line processing, the recordings were converted to ASCII files and down-sampled to 312.5 Hz. For each subject, three artefact-free epochs of 4096 samples (13,083 s) were selected by two of the investigators (BFJ and IM). Visual inspection and selection of epochs were done with the DIGEEGXP software (CS).

Nonlinear data analysis

Nonlinear correlations between all pair-wise combinations of MEG channels were computed with the synchronization

likelihood (Stam and van Dijk, 2002). Mathematical details can be found in Appendix A; here, we give a brief description. The synchronization likelihood (SL) is a general measure of the correlation or synchronization between two time series which is sensitive to linear as well as nonlinear interdependencies. The SL fluctuates around P_{ref} (a small positive number) in case of independent time series and reaches the value of 1 in case of maximally synchronous signals. P_{ref} is a parameter which has to be chosen; in the present study, P_{ref} was set at 0.01. The basic principle of the SL is to divide each time series into a series of 'patterns' (roughly, brief time intervals containing a few cycles of the dominant frequency) and to search for a recurrence of these patterns. The SL then is the chance that pattern recurrences in time series X coincide with pattern recurrences in time series Y; P_{ref} is the small but non-zero likelihood of coincident pattern recurrence in the case of independent time series. The end result of computing the SL for all pair-wise combinations of channels is an $N \times N$ matrix with N equal to 149 (sensor 150 and 151 were not used), where each entry $N_{i,j}$ contains the value of the SL for the channels i and j.

SL was computed for the following frequency bands: delta (0.5–4 Hz), theta (4–8 Hz), alpha1 (8–10 Hz), alpha2 (10–13 Hz), beta (13–30 Hz) and gamma (30–45 Hz). Digital, zero-phase lag filtering was done off-line. Results for the three epochs were averaged. Further averaging was done to obtain long distance intra- and interhemispheric and short distance local measures. For this, MEG channels were grouped into (left and right) central, frontal, occipital, parietal and temporal regions (based upon the naming of the CTF sensors). Long distances (8 intrahemispheric: fronto-temporal, fronto-parietal, parieto-occipital, occipito-temporal; 5 interhemispheric: central, frontal, occipital, parietal and temporal) involved correlations between two different regions (within one hemisphere and homologue regions of two hemispheres), and short distances involved correlations within one region. Midline sensors were not used. The procedure is illustrated in Fig. 1.

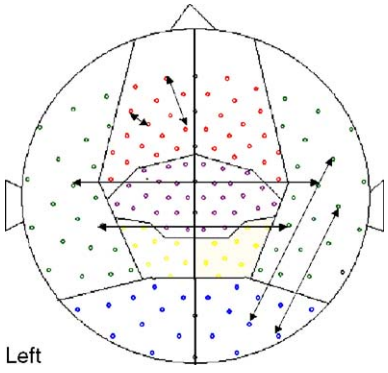

Fig. 1. Illustration of the allocation of sensor pairs to short and long distances. The figure shows the sensor positions of the CTF MEG system projected onto a two-dimensional surface. Sensors are grouped into frontal (red), central (purple), parietal (yellow), occipital (blue) and temporal (green) regions for both hemispheres. The short distance SL was computed as the average SL between all sensor pairs within one region (two such pairs are shown for the left frontal region). Long distance SL was computed from sensor pairs where one sensor was in one region, and the other sensor was in another region. This is illustrated for right occipito-temporal long distance SL and for temporal interhemispheric long distance SL.

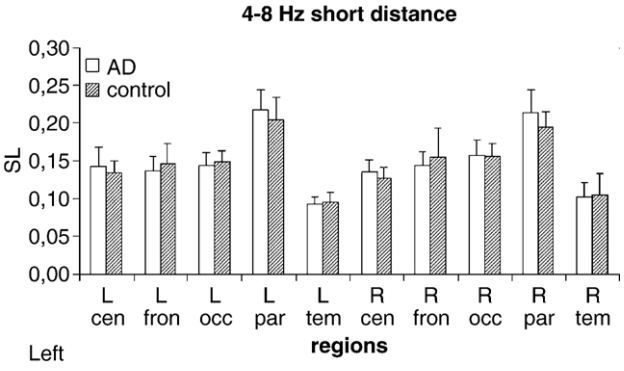

Fig. 2. Mean theta band SL (error bars indicate standard deviation) of Alzheimer patients and healthy controls for ten local regions (L = left; R = right hemisphere. cen = central; fron = frontal; occ = occipital; par = parietal; tem = temporal). For each region, the mean SL values obtained for all possible pairs of sensors within that region were averaged. SL was higher in Alzheimer patients at left and right central and parietal regions; in the other regions, SL in the patients was lower than or equal to that of the control subjects.

Linear analysis

Linear correlations between all pair-wise combinations of MEG channels were computed with coherence analysis (Nunez et al., 1997; Nolte et al., 2004).The complex coherency between two time series can be defined as the cross spectrum divided by the product of the two power spectra. As described by Nolte et al. (2004), its mean overall frequencies can alternatively be computed via the mean over time of the corresponding analytical signals like:

$$c = \frac{\langle A_1 A_2 e^{i\Delta\phi} \rangle}{\sqrt{\langle A_1^2 \rangle \langle A_2^2 \rangle}} \quad (1)$$

Here, A_1 and A_2 are the amplitudes of the two time series, and $\Delta\phi$ is the instantaneous phase difference between (the Hilbert transforms of) the two time series. The absolute value of coherency is coherence bounded between 0 and 1. Coherence was computed all for pairs of channels, for the six frequency bands described above. Results were averaged for long distance intra- and interhemispheric and short distance channel pairs as described for the synchronization likelihood. For the beta band, we also computed the crosscorrelation (correlation coefficient between the two time series) to check whether any significant effects detected by this basic measure would also be picked up by the coherence and SL analysis.

Statistical analysis

Statistical analysis was done with SPSS for Windows (version 10.0.7). For each frequency band, three separate repeated-measures ANOVAs were done, using Greenhouse–Geisser corrected degrees of freedom to correct for lack of sphericity. In some cases (when the ANOVA showed significant main effects or interactions), t test was used for detailed analysis. For the long distance intrahemispheric data, the repeated-measures factor had 8 levels (left and right fronto-temporal, fronto-parietal, parieto-occipital, occipito-temporal); for the long distance data, the repeated-measures factor had 5 levels (central, frontal, occipital, parietal and temporal) and for the short distance data the

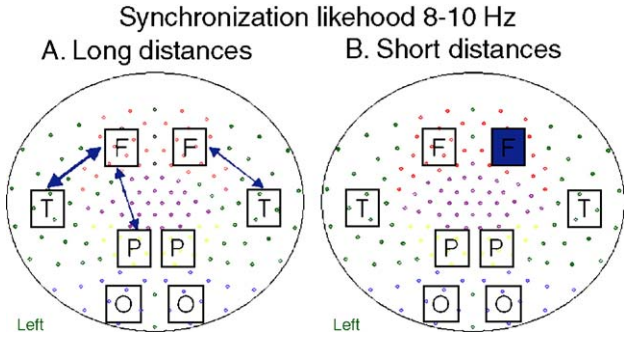

Fig. 3. Schematic illustration of SL (SL) results for the alpha1 band. A. Long distances. Decrease of bilateral fronto-temporal and left fronto-parietal SL in Alzheimer patients. B. Short distances. Local decrease of SL in right frontal region. Lines correspond to significant changes of average SL between two regions and squares to significant changes of local SL (thin line/light square: $P < 0.05$; thick line/dark square: $P < 0.01$; blue: Alzheimer lower than controls; red: Alzheimer higher than controls; significance is based upon two-tailed t tests and intended for illustration; formal testing was based upon a repeated-measures ANOVA).

repeated-measures factor had 10 levels (left and right central, frontal, occipital, parietal and temporal). The group factor had two levels (Alzheimer/control). Age was not used as a covariate since the age difference between the groups was not significant. A significance level of $P < 0.05$ was used.

Results

Nonlinear analysis

The delta band showed no significant effects involving the factor Group. In the theta band, a significant Group × Region interaction ($F[9,306] = 2.604$; $P = 0.029$) was found for short distances. This interaction effect is illustrated in Fig. 2. Inspection of Fig. 2 shows that the SL was higher in AD patients compared to controls in the right and left parietal and to a lesser extent central regions. This difference was significant for the right parietal region

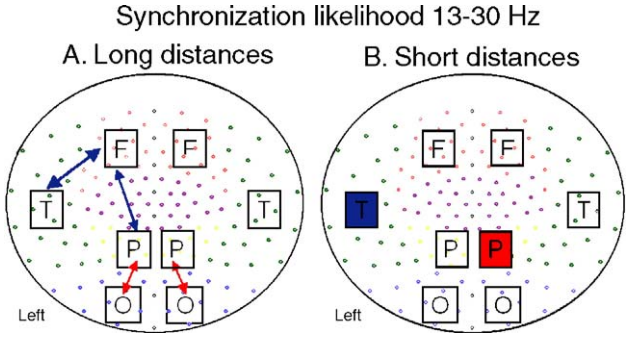

Fig. 4. Schematic illustration of SL (SL) results for the beta band. A. Long distances. Decrease of left fronto-temporal and fronto-parietal SL and increase in bilateral occipito-parietal SL in Alzheimer patients. B. Short distances. Local increase of SL in right parietal region and local decrease of SL in left temporal region. Lines correspond to significant changes of average SL between two regions and squares to significant changes of local SL (thin line/light square: $P < 0.05$; thick line/dark square: $P < 0.01$; blue: Alzheimer lower than controls; red: Alzheimer higher than controls; significance is based upon two-tailed t tests and intended for illustration; formal testing was based upon a repeated-measures ANOVA).

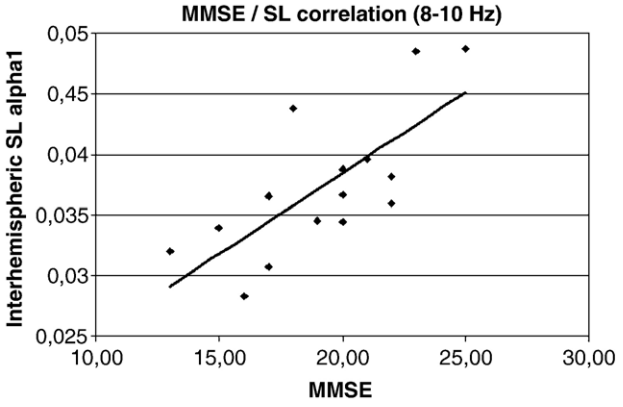

Fig. 5. Correlation between MMSE (15 Alzheimer patients for whom a score was available) score and averaged interhemispheric SL in the alpha1 band. $R = 0.727$; $P = 0.002$.

(two-sided t test, $P = 0.037$) In the other regions, SL was slightly lower in the AD group or comparable between the two groups. The interaction thus reflects a selective increase of SL in the central parietal areas in the AD patients.

In the alpha1 band, a significant main effect of Group was found ($F[1,34] = 5.745$; $P = 0.022$) for long distance intrahemispheric connections. This Group effect is illustrated schematically in Fig. 3. SL was lower in the AD group compared to the control group; the most significant changes involved the left fronto-temporal (t test: $P = 0.009$), left fronto-parietal (t test: $P = 0.012$) an the right fronto-temporal (t test: $P = 0.015$) connections.

The alpha2 band showed no significant effects involving the factor Group. In the beta band, two significant interactions were present: the first involved a significant Group × Region interaction ($F[7,238] = 4.042$; $P = 0.023$) for long distance intrahemispheric connections, and the second one a significant Group × Region interaction ($F[9,306] = 3.610$; $P = 0.006$) for short distance connections. These interaction effects are illustrated schematically in Fig. 4.

For all the frequency bands, correlations between SL measures and MMSE scores were computed. The correlations were computed for the AD subjects only. For the delta, theta and gamma bands, no significant correlations were found. For the alpha1 band, significant positive correlations were found between

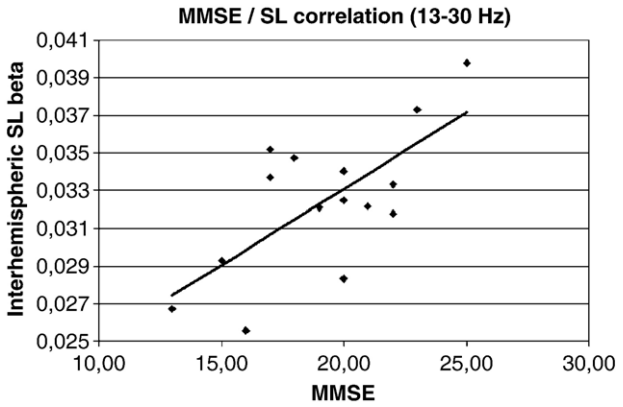

Fig. 6. Correlation between MMSE (15 Alzheimer patients for whom a score was available) score and averaged interhemispheric SL in the beta band. $R = 0.688$; $P = 0.005$.

the MMSE score and average interhemispheric SL ($R = 0.727$; $P = 0.002$), interhemispheric temporal SL ($R = 0.632$; $P = 0.011$), left frontal ($R = 0.673$; $P = 0.006$) and right frontal SL ($R = 0.551$; $P = 0.033$). The correlation between MMSE and average interhemispheric SL is shown in Fig. 5.

For the alpha2 band, significant positive correlations between SL and MMSE were found for interhemispheric connections ($R = 0.690$; $P = 0.005$), temporal interhemispheric connections ($R = 0.578$; $P = 0.024$), left frontal local connections ($R = 0.532$; $P = 0.041$) and left temporal local connections ($R = 0.526$; $P = 0.044$). In the beta band, significant positive correlations between SL and MMSE were found for right temporo-occipital connections ($R = 0.599$; $P = 0.018$), average interhemispheric SL ($R = 0.688$; $P = 0.005$) and interhemispheric temporal SL ($R = 0.619$; $P = 0.014$). The correlation between MMSE and average interhemispheric SL is shown in Fig. 6.

Linear analysis

Coherence showed no significant effects of Group or Group × Region interactions for the delta, theta and alpha1 bands. In the alpha2 band, there was a significant Group × Region interaction for short distances ($F[9,306] = 2.372$; $P = 0.033$). Post hoc t tests only showed a higher coherence in AD patients at the right parietal region (t test: $P = 0.026$). In the beta band, there was a significant Group × Region interaction for long intrahemispheric distances ($F[7,238] = 4.044$; $P = 0.012$) and for short distances ($F[9,306] = 4.700$; $P = 0.001$). These interactions are illustrated in Fig. 7. AD patients had a lower left fronto-temporal coherence (t test: $P = 0.010$) and a higher left (t test: $P = 0.038$) and right (t test: $P = 0.004$) parietal coherence. Short distance coherence was lower in the AD group in the left temporal region (t test: $P = 0.044$) and higher in left (t test: $P = 0.016$) and right (t test: $P = 0.001$) parietal regions. In the gamma band, there was a significant main effect of Group for long distances ($F[1,34] = 4.755$; $P = 0.036$). AD patients had higher left (t test, $P = 0.023$) and right (t test, $P = 0.003$) parieto-occipital coherence.

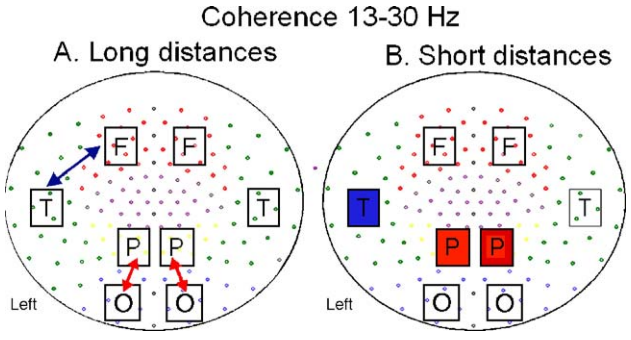

Fig. 7. Schematic illustration of coherence results for the beta band. A. Long distances. Decrease of left fronto-temporal coherence and increase in bilateral occipito-parietal coherence in Alzheimer patients. B. Short distances. Local increase of coherence in right and left parietal regions and local decrease of SL in left temporal region. Lines correspond to significant changes of average coherence between two regions and squares to significant changes of local coherence (thin line/light square: $P < 0.05$; thick line/dark square: $P < 0.01$; blue: Alzheimer lower than controls; red: Alzheimer higher than controls; significance is based upon two-tailed t tests and intended for illustration; formal testing was based upon a repeated-measures ANOVA).

For the beta band, results were checked with a crosscorrelation analysis. For long distance intrahemispheric crosscorrelations, there was a significant Group × Region interaction ($F[7,238] = 4.013$; $P = 0.005$). t tests showed a lower correlation in the AD group for left fronto-temporal connections (t test: $P = 0.006$) and higher correlations in the AD group for left (t test: $P = 0.010$) and right (t test: $P = 0.023$) parieto-occipital connections. For long distance, interhemispheric correlations no significant effects were found. For short distances, a significant Group × Region interaction was found ($F[9,306] = 4.009$; $P = 0.003$). The correlation was lower in the AD group at left temporal (t test: $P = 0.017$) and right frontal (t test: $P = 0.038$) locations; it was higher in the AD group at left (t test: $P = 0.012$) and right (t test: $P = 0.001$) parietal regions.

Discussion

This study demonstrated a specific pattern of changes in resting-state functional connectivity in AD patients. SL was increased in the theta band over the central and parietal areas and in the beta band over the parietal and occipital areas. Coherence showed a similar pattern of parieto-occipital increase in AD in alpha2, beta and gamma bands. In contrast, SL was decreased in the alpha1 band for long distance intrahemispheric sensor pairs, and both SL and coherence (and crosscorrelation) were decreased in the beta band for long distance frontal temporal/parietal and short distance left temporal sensor pairs. Lower SL, especially for temporal interhemispheric connections correlated with disease severity as expressed by a lower MMSE score.

In studies of this kind, it is always important to consider the question whether correlations between signals recorded at different sensors can be interpreted in terms of physiological interactions between different brain regions. In the case of EEG, an active reference electrode can cause spurious correlations between signals recorded at different electrodes (Guevara et al., 2005; Nunez et al., 1997). MEG does not require the use of a reference electrode and thus may be more suitable for estimating functional connectivity than EEG (Guevara et al., 2005). However, even with MEG correlations between signals from nearby sensors could be due to common sources rather than true interactions. Furthermore, the location of the sources giving rise to the signal recorded at the sensors is generally not known. This is the well-known problem of volume conduction that may give rise to spurious correlations in sensor space.

One possible solution is to estimate correlations between signals from reconstructed sources ('source space') rather than the actually recorded signal ('signal space') (David et al., 2002; Gross et al., 2001; Hadjipapas et al., 2005). However, no unique way exists to reconstruct the sources, and the source reconstruction algorithm used could influence the interdependencies between the sources (Hadjipapas et al., 2005). A possible alternative is the use of the imaginary component of the coherency, which is not sensitive to a linear mixing of independent sources (Nolte et al., 2004). However, even this approach may not always be effective (Wheaton et al., 2005). In the present study, we adopted a pragmatic approach, restricting the analysis to signal space, and grouping the sensor pairs in long and short distances. While SL and coherence estimated in this way will be influenced by volume conduction, it is less likely that volume conduction can explain group differences in SL between AD patients and controls.

Furthermore, several of our main results involve changes in long distance interactions which are less likely to be due to volume conduction. Note that changes observed in regions of the signal space cannot be interpreted as reflecting physiological changes in the brain regions underlying the sensors. Even so, we should stress that MEG is especially sensitive to superficial cortical sources. The changes over parietal regions we describe are supported by MRI findings with voxel-based morphometry (Karas et al., 2004).

Theoretically, estimates of statistical interdependencies between different channels could also be influenced by differences in signal power. Assuming a constant level of measurement/background noise, signals with lower power could be expected to have a lower signal-to-noise ration. A lower SNR ration might produce biased lower values of functional connectivity. However, we consider it unlikely that the main results of the present study can be explained in this way. The absolute signal power in the beta band in the AD group was either comparable to or lower than the power in the control group (Fig. 8). All three measures (SL, coherence and crosscorrelation) showed an increase of parieto-occipital connectivity in the AD group, while the power in the AD group was significantly lower in the parietal and occipital regions. Furthermore, the significant loss of connectivity in left fronto-temporal regions in the AD group was not associated with significant power changes at all. Thus, the assessment of functional connectivity provides information that is independent from signal power and is more likely related to functional interactions between brain regions.

Another methodological consideration concerns the use of drugs that influence the cholinergic system. In theory, such drugs could influence the EEG and the MEG, most likely by reverting the slowing and loss of connectivity due to the AD pathology (Adler and Brassen, 2001; Osipova et al., 2003). In our study, 6 of the 18 patients used cholinesterase inhibitors. To determine the possible influence of drug use on our results, we compared the SL (averaged over all possible pairs of sensors) in the theta, alpha1 and beta band between AD patients who did and who did not use cholinesterase inhibitors. No significant differences were found which suggests that our results are unlikely to be strongly influenced by medication effects.

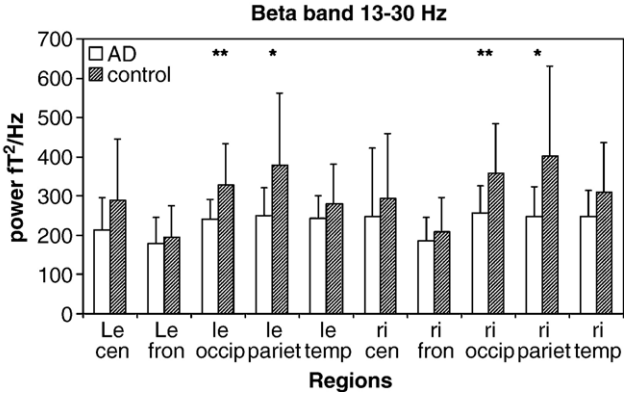

Fig. 8. Mean beta band absolute power (error bars indicate standard deviation) of Alzheimer patients and healthy controls for ten local regions (L = left; *R* = right hemisphere. cen = central; fron = frontal; occ = occipital; par = parietal; tem = temporal). For each region, the mean power values obtained for all sensors within that region were averaged. Power was significantly lower in Alzheimer patients at left and right parietal and occipital regions. **t* test: $P < 0.05$ ***t* test: $P < 0.01$.

Our study was conducted during an eyes-closed no-task condition. One might ask whether such a 'resting state' is the most effective condition for demonstrating abnormalities of functional connectivity in AD. For instance, a recent EEG study using spectral analysis and cognitive tasks has suggested that task-induced EEG changes might increase the discrimination between controls and MCI subjects (van der Hiele et al., 2006). However, a number of recent fMRI studies have shown that the resting state is a far more stable and active condition than has often been assumed (Gusnard and Raichle, 2001). The resting state is characterized by the activation of a 'default' network, which consists of frontal, posterior cingulate, parietal and medial temporal areas (Laufs et al., 2003). Abnormalities of this resting-state network have been demonstrated in AD (Lustig et al., 2003). Although the use of specific tasks, aimed at activating brain areas assumed to be involved in AD, might be expected to be more sensitive in demonstrating abnormalities, this is often not the case. One reason may be that the pathology may be associated with abnormally high as well as abnormally low task-related activation, which seriously complicates interpretation of the results (Osipova et al., 2005; Pijnenburg et al., 2004). Furthermore, the present study confirms that a simple resting-state condition is sufficient to demonstrate widespread changes in functional connectivity in AD. The relevance of resting-state SL for cognition is further supported by the fact that alpha1 and beta band SL, especially involving interhemispheric temporal connections, were positively correlated to MMSE scores.

The pattern of functional connectivity changes in the present study shows similarities as well as differences with previous EEG and MEG work. A lower level of synchronization in alpha band and beta band has been reported by most earlier EEG and MEG studies (Adler et al., 2003; Babiloni et al., 2004a; Besthorn et al., 1994; Dunkin et al., 1994; Hogan et al., 2003; Jelic et al., 1996; Jiang, 2005; Koenig et al., 2005; Knott et al., 2000; Leuchter et al., 1992; Locatelli et al., 1998; Pogarell et al., 2005; Stevens et al., 2001). In contrast to our previous MEG study (Stam et al., 2002b), we found a loss of lower instead of upper alpha band synchronization. Two factors may be involved in the differences between the present and previous MEG study: (i) the different way in which the embedding parameters L and M were chosen; (ii) the different choice of frequency bands.

In the 2002 study, the choice of L and M for the computation of the SL was still fairly arbitrary. Recently, it has been shown that an incorrect choice of L and M can result in unexpected frequency content of the patterns considered by the SL algorithm and that a proper choice of L and M should take into account the low and high frequency filters settings (Montez et al., submitted for publication). In the present study, we used a different approach to the choice of L and M based explicitly on the frequency content of the data (Montez et al., submitted for publication). There was also a different definition of the two alpha bands in the two studies: in the previous 2002 study, alpha1 was defined as 6–10 Hz and alpha2 as 10–14. Hz. Failure to find an effect in the lower alpha band in the 2002 study could be due to the fact that this band incorporated part of the theta band, where, as shown in the present study, changes are in the opposite direction. The significant effect in the upper alpha band in the 2002 study might be caused by incorporating part of the beta band, which showed a significant effect in both studies, as well as in EEG studies of SL (Stam et al., 2003a; Pijnenburg et al., 2004). In a similar way, the significant gamma band effects of the 2002 study partly overlap the beta band

results of the present study. With SL, we could not demonstrate significant effects in a higher gamma band of 30–45 Hz. In an EEG study, Babiloni et al. demonstrated a lower SL in a wide range of frequencies in AD patients (Babiloni et al., 2004b). This could be due to the much larger group size of this study, although the larger age difference between controls and patients might also have influenced the results. In the present study, no significant age effects were present between patients and controls.

The principal aim of the present study was to determine the relative contribution of long distance and short distance interactions in different frequency bands to impaired functional connectivity in AD. Short and long distance interactions might underlie local specialization and global integration of brain dynamics, which have to be balanced to ensure optimal information processing (Tononi et al., 1998; Van Cappellen van Walsum et al., 2003). We used the SL as well as the more commonly used coherence to study the contribution of short and long distance interactions. We expected SL to be sensitive to both nonlinear as well as linear aspects of a correlation, i.e. detects interdependencies between complex patterns that can be different in each channel and would not be detected by classical measures. In the present study, SL showed group differences in the theta and alpha1 that were not detected by coherence. In the beta band, both SL and coherence (as well as the crosscorrelation analysis) detected a similar pattern of fronto-temporal decrease and parieto-occipital increase in AD. In the alpha2 and gamma band, coherence revealed changes that were not picked up by SL. We have previously shown that SL may be more sensitive than coherence in detecting subtle differences between controls and AD patients (Stam et al., 2002b). Furthermore, SL can detect weak nonlinear coupling which has been demonstrated in MEG recordings (Stam et al., 2003b). The results of the present study show a more complex picture which might be due to the fact that we have now taken into account the spatial details of connectivity: in some cases, linear and nonlinear measures perform equally well, in other cases, one of the two approached may reveal information not picked up by the other approach.

Lower SL in the alpha1 band was restricted to long distance, intrahemispheric fronto-temporal and fronto-parietal interactions. This might reflect loss of long distance association fibers connecting frontal, temporal, parietal and occipital areas. The beta band also showed a loss of long distance intrahemispheric linear and nonlinear connectivity, involving especially left frontal, temporal and parietal connections. Although interhemispheric correlations were not significantly lower in AD subjects, the SL did show a strong correlation with lower MMSE scores. Of interest, lower interhemispheric coherence in AD has been shown to be correlated with atrophy of the corpus callosum (Pogarell et al., 2005). This further supports the concept that lower long distance synchronization might reflect loss of anatomical connections. Two studies suggest that the relationship between long distance anatomical connections and functional connectivity could be partly genetically determined. In a large study in twins, it was shown that alpha band SL was strongly inherited (Posthuma et al., 2005). Lower EEG coherence in AD has been associated with the e4 allele of the APOE genotype (Jelic et al., 1997).

Short distance linear and nonlinear interactions in the beta band were mainly impaired in the left temporal region. The activity recorded by the MEG sensors mainly originates in the superficial neocortical temporal areas. Activity from the medial hippocampal and entorhinal cortex will have a much smaller amplitude at the scalp surface. However, both areas are strongly connected and abnormal temporal connectivity may reflect the primary pathology of the medial temporal lobe. Other MEG studies in AD have also stressed the importance of the (left) temporal region (Maestu et al., 2004, 2005). Left temporal disturbances have been associated with a higher chance of conversion to MCI (Maestu et al., 2006).

A surprising finding in the present study was the increase in SL and coherence of occipito-parietal connections and the right parietal region in the beta band and for coherence also in the alpha2 and gamma band. These regions may be relatively spared in the early stages of AD. Thus, it seems unlikely that this local increase in connectivity is due to loss of association fibers or lower acetylcholine levels. A possible, but at this stage highly speculative explanation could be that the parieto-occipital connectivity reflects a compensation mechanism in a relatively healthy part of the network. That the functional architecture of widespread brain networks can be influenced even at sites far away from local pathology has recently been demonstrated in patients with brain tumors (Bartolomei et al., 2006). Future studies will have to confirm the existence of the compensation mechanism and the possible influence of treatment on this phenomenon. More generally, it would be of interest to back up the correlations between impaired functional connectivity described in the present study by a more causal approach. The hypothesis is that the extent to which treatment with cholinesterase inhibitors or even rTMS restores normal functional connectivity would predict their favorable impact on cognitive functioning in AD.

Acknowledgments

The study was financially supported by a grant from Alzheimer Nederland. T.M. is the recipient of a Praxis XXI doctoral fellowship from FCT, Ministry of Science, Portugal.

Appendix A. Mathematical background of synchronization likelihood

The synchronization likelihood (SL) is a measure of the *generalized synchronization* between two dynamical systems X and Y (Stam and van Dijk, 2002). Generalized synchronization (Rulkov et al., 1995) exists between X and Y of the state of the response system is a function of the driver system: $Y = F(X)$. The first step in the computation of the SL is to convert the time series X_i and Y_i recorded from X and Y as a series of state space vectors using the method of time delay embedding (Takens, 1982):

$$X_i = \left(X_i, X_{i+L}, X_{i+2\times L}, X_{i+3\times L} \ldots, X_{i+(m-1)\times L}\right) \quad (1)$$

where L is the time lag and m the embedding dimension. From a time series of N samples, $N-(m \times L)$ vectors can be reconstructed. State space vectors Y_i are reconstructed in the same way.

SL is defined as the conditional likelihood that the distance between Y_i and Y_j will be smaller than a cutoff distance r_y, given that the distance between X_i and X_j is smaller than a cutoff distance r_x. In the case of maximal synchronization, this likelihood is 1; in the case of independent systems, it is a small, but nonzero number, namely P_{ref}. This small number is the likelihood that two randomly

chosen vectors Y (or X) will be closer than the cut-off distance r. In practice, the cut-off distance is chosen such that the likelihood of random vectors being close is fixed at P_{ref}, which is chosen the same for X and for Y. To understand how P_{ref} is used to fix r_x and r_y, we first consider the correlation integral:

$$C_r = \frac{2}{N(N-w)} \sum_{i=1}^{N} \sum_{j=i+w}^{N-w} \theta\left(r - |X_i - X_j|\right) \quad (2)$$

Here, the correlation integral C_r is the likelihood that two randomly chosen vectors X will be closer than r. The vertical bars represent the Euclidian distance between the vectors. N is the number of vectors, w is the Theiler correction for autocorrelation (Theiler, 1986), and θ is the Heaviside function: $\theta(X) = 0$ if $X \geq 0$ and $\theta(\mathrm{X}) = 1$ if $X < 0$. Now, r_x is chosen such that $\mathrm{Cr}_x = P_{\mathrm{ref}}$ and r_y is chosen such that $\mathrm{Cr}_y = P_{\mathrm{ref}}$. The SL between X and Y can now be formally defined as:

$$\mathrm{SL} = \frac{2}{N(N-w)P_{\mathrm{ref}}} \times \sum_{i=1}^{N} \sum_{j=i+w}^{N-w} \theta\left(r_x - |X_i - X_j|\right)\theta\left(r_y - |Y_i - Y_j|\right) \quad (3)$$

SL is a symmetric measure of the strength of synchronization between X and Y ($\mathrm{SL}_{XY} = \mathrm{SL}_{YX}$). In Eq. (3), the averaging is done over all i and j; by doing the averaging only over j, SL can be computed as a function of time i. From Eq. (3), it can be seen that in the case of complete synchronization SL = 1; in the case of complete independence, SL = P_{ref}. In the case of intermediate levels of synchronization, $P_{\mathrm{ref}} < \mathrm{SL} < 1$.

In the present paper, the choice of the two most important embedding parameters L and m was based upon the frequency content of the time series (Montez et al., submitted for publication). L is chosen small enough to over-sample the highest frequencies present in the signal, and the embedding window $L \times m$ long enough to capture the period of the slowest frequency. For a given sample frequency in Hz and low frequency (LF) and high frequency (HF) filters in Hz, L (expressed in samples) is chosen such that L = sample frequency / (HF × 4). The embedding dimension m (expressed in samples) follows from: m = sample frequency / (LF × L). The Theiler correction w was chosen equal to the embedding window $L \times m$ and $P_{\mathrm{ref}} = 0.01$.

References

Adler, G., Brassen, S., 2001. Short-term rivastigmine treatment reduces EEG slow-wave power in Alzheimer patients. Neuropsychobiology 43, 273–276.

Adler, G., Brassen, S., Jajcevic, A., 2003. EEG coherence in Alzheimer's dementia. J. Neural Transm. 110, 1051–1058.

Babiloni, C., Miniussi, C., Moretti, D.V., Vecchio, F., Salinari, S., Rossini, P.M., 2004a. Cortical networks generating movement-related EEG rhythms in Alzheimer's disease: an EEG coherence study. Behav. Neurosci. 118, 698–706.

Babiloni, C., Ferri, F., Moretti, D.V., Strambi, A., Binetti, G., Dal Forno, G., Ferreri, F., Lanuzza, B., Bonato, C., Nobili, F., Rodriguez, G., Salinari, S., Passero, S., Rocchi, R., Stam, C.J., Rossini, P.M., 2004b. Abnormal fronto-parietal coupling of brain rhythms in mild Alzheimer's disease: a multicentric EEG study. Eur. J. Neurosci. 19, 1–9.

Bartolomei, F., Bosma, I., Klein, M., Baayen, J.C., Reijneveld, J.C., Postma, T.J., Heimans, J.J., van Dijk, B.W., de Munck, J.C., de Jongh, A., Cover, K.S., Stam, C.J., 2006. How do brain tumors alter functional connectivity? A magnetoencephalography study. Ann. Neurol. 59, 128–138.

Berendse, H.W., Verbunt, J.P.A., Scheltens, Ph., van Dijk, B.W., Jonkman, E.J., 2000. Magnetoencephalographic analysis of cortical activity in Alzheimer's disease. A pilot study. Clin. Neurophysiol. 111, 604–612.

Besthorn, C., Forstl, H., Geiger-Kabisch, C., Sattel, H., Gasser, T., Schreiter-Gasser, U., 1994. EEG coherence in Alzheimer disease. Electroencephalogr. Clin. Neurophysiol. 90, 242–245.

Boerman, R.H., Scheltens, P., Weinstein, H.C., 1994. Clinical neurophysiology in the diagnosis of Alzheimer's disease. Clin. Neurol. Neurosurg. 96, 111–118.

David, O., Garnero, L., Cosmelli, D., Varela, F.J., 2002. Estimation of neural dynamics from MEG/EEG cortical current density maps: application to the reconstruction of large-scale cortical synchrony. IEEE Trans. Biomed. Eng. 49, 975–987.

Delbeuck, X., Van der Linder, M., Colette, F., 2003. Alzheimer's disease as a disconnection syndrome? Neuropyschol. Rev. 13, 79–92.

Dunkin, J.J., Leuchter, A.F., Newton, T.F., Cook, I.A., 1994. Reduced EEG coherence in dementia: state or trait marker? Biol. Psychiatry 35, 870–879.

Fernandez, A., Maestu, F., Amo, C., Gil, P., Fehr, Th., Wienbruch, Ch., Rockstroh, B., Elbert, Th., Ortiz, T., 2002. Focal temporoparietal slow activity in Alzheimer's disease revealed by magnetoencephalography. Biol. Psychiatry 52, 764–770.

Fernandez, A., Arazzola, J., Maestu, F., Amo, C., Gil-Gregorio, P., Wienbruch, C., Ortiz, T., 2003. Correlations of hippocampal atrophy and focal low-frequency magnetic activity in Alzheimer disease: volumetric MR imaging–magnetoencephalographic study. Am. J. Neuroradiol. 24, 481–487.

Fernandez, A., Hornero, R., Mayo, A., Poza, J., Gil-Gregorio, Ortiz, T., 2006. MEG spectral profile in Alzheimer's disease and mild cognitive impairment. Clin. Neurophysiol. 117, 306–314.

Fingelkurts, A.A., Fingelkurts, A.A., Kahkonen, S., 2005. Functional connectivity in the brain—Is it a elusive concept? Neurosci. Biobehav. Rev. 28, 827–836.

Folstein, M.F., Folstein, S.E., McHugh, P.R., 1975. "Mini-mental state". A practical method for grading the cognitive state of patients for the clinician. J. Psychiatr. Res. 12, 189–198.

Fuster, J.M., 2003. Cortex and Mind. Unifying Cognition. Oxford Univ. Press, New York.

Gross, J., Kujala, J., Hamalainen, M., Timmermann, L., Schnitzler, A., Salmelin, R., 2001. Dynamic imaging of coherent sources: studying neural interactions in the human brain. Proc. Natl. Acad. Sci. 98, 694–699.

Guevara, R., Velazguez, J.L.P., Nenadovic, V., Wennberg, R., Senjanovic, G., Dominguez, L.G., 2005. Phase synchronization measurements using electroencephalographic recordings. What can we really say about neuronal synchrony?. Neuroinformatics 3, 301–314.

Gusnard, D.A., Raichle, M.E., 2001. Searching for a baseline: functional imaging and the resting brain. Nat. Rev., Neurosci. 2, 685–694.

Hadjipapas, A., Hillebrand, A., Holliday, I.E., Singh, K., Barnes, G., 2005. Assessing interactions of linear and nonlinear neuronal sources using MEG beamformers: a proof of concept. Clin. Neurophysiol. 116, 1300–1313.

Hogan, M.J., Swanwick, G.R.J., Kaiser, J., Rowan, M., Lawlor, B., 2003. Memory-related EEG power and coherence reductions in mild Alzheimer's disease. Int. J. Psychophysiol. 49, 147–163.

Jelic, V., Shigeta, M., Julin, P., Almkvist, O., Winblad, B., Wahlung, W.O., 1996. Quantitative electroencephalography power and coherence in Alzheimer's disease and mild cognitive impairment. Dementia 7, 314–323.

Jelic, V., Julin, P., Shigeta, M., Lannfelt, A., Winblad, L., Wahlund, B., 1997. Apolipoprotein E e4 allele decreases functional connectivity in Alzheimer's disease as measured by EEG coherence. J. Neurol. Neurosurg. Psychiatry 63, 59–65.

Jeong, J., 2004. EEG dynamics in patients with Alzheimer's disease. Clin. Neurophysiol. 115, 1490–1505.

Jeong, J., Gore, J.C., Peterson, B.S., 2001. Mutual information analysis of the EEG in patients with Alzheimer's disease. Clin. Neurophysiol. 112, 827–835.

Jiang, Z.Y., 2005. Abnormal cortical functional connections in Alzheimer's disease: analysis of inter- and intra-hemispheric EEG coherence. J. Zhejiang Univ. Sci., B 6, 259–264.

Jonkman, E.J., 1997. The role of the electroencephalogram in the diagnosis of dementia of the Alzheimer type: an attempt at technology assessment. Neurophysiol. Clin. 27, 211–219.

Karas, G.B., Scheltens, P., Rombouts, S.A., Visser, P.J., van Schijndel, R.A., Fox, N.C., Barkhof, F., 2004. Global and local gray matter loss in mild cognitive impairment and Alzheimer's disease. NeuroImage 23, 708–716.

Knott, V., Mohr, E., Mahoney, C., Ilivitsky, V., 2000. Electroencephalographic coherence in Alzheimer's disease: comparisons with a control group and population norms. J. Geriatr. Psychiatry Neurol. 13, 1–8.

Koenig, T., Prichep, L., Dierks, T., Hubl, D., Wahlund, L.O., John, E.R., Jelic, V., 2005. Decreased EEG synchronization in Alzheimer's disease and mild cognitive impairment. Neurobiol. Aging 26, 165–171.

Laufs, H., Krakow, K., Sterzer, P., Eger, E., Beyerle, A., Salek-Haddadi, A., Kleinschmidt, A., 2003. Electroencephalographic signatures of attentional and cognitive default modes in spontaneous brain activity fluctuations at rest. Proc. Natl. Acad. Sci. 100, 11053–11058.

Lee, L., Harrison, L.M., Mechelli, A., 2003. A report of the functional connectivity workshop, Dusseldorf 2002. NeuroImage 19, 457–465.

Le van Quyen, M., 2003. Disentangling the dynamic core: a research program for a neurodynamics at the large scale. Biol. Res. 36, 67–88.

Lehtovirta, M., Partanen, J., Kononen, M., Soininen, H., Helisalmi, S., Mannermaa, A., Ryynanen, M., Hartikainen, P., Riekkinen Sr., P., 1996. Spectral analysis of EEG in Alzheimer's disease: relation to Apolipoprotein E polymorphism. Neurobiol. Aging 4, 523–526.

Leuchter, A.F., Newton, T.F., Cook, A.A., Walter, D.O., 1992. Changes in brain functional connectivity in Alzheimer-type and multi-infarct dementia. Brain 115, 1543–1561.

Locatelli, T., Cursi, M., Liberati, D., Francheschi, M., Comi, G., 1998. EEG coherence in Alzheimer's disease. Electroencephalogr. Clin. Neurophysiol. 106, 229–237.

Lustig, C., Snyder, A.Z., Bhakta, M., O'Brien, K.C., AcAvoy, M., Raichle, M.E., Morris, J.C., Buckner, R.L., 2003. Functional deactivations: change with age and dementia of the Alzheimer type. Proc. Natl. Acad. Sci. 100, 14504–14509.

Maestu, F., Fernandez, A., Simos, P.G., Gil-Gregorio, P., Amo, C., Rodriguez, R., Arrazola, J., Ortiz, T., 2001. Spatio-temporal patterns of brain magnetic activity during a memory task in Alzheimer's disease. NeuroReport 12, 3917–3922.

Maestu, F., Arrazola, J., Fernandez, A., Simos, P.G., Amo, C., Gil-Gregorio, P., Fernandez, S., 2003. Do cognitive patterns of brain magnetic activity correlate with hippocampal atrophy in Alzheimer's disease? J. Neurol. Neurosurg. Psychiatry 74, 208–212.

Maestu, F., Fernandez, A., Simos, P.G., Lopez-Ibor, M.I., Campo, P., Criado, J., Rodriguez-Palancas, A., Ferre, F., Amo, C., Ortiz, T., 2004. Profiles of brain magnetic activity during a memory task in patients with Alzheimer's disease and in non-demented elderly subjects, with or without depression. J. Neurol. Neurosurg. Psychiatry 75, 1160–1162.

Maestu, F., Garcia-Segura, J., Ortiz, T., Montoya, J., Fernandez, A., Gil-Gregorio, P., Campo, P., Fernandez, S., Viano, J., Portera, A., 2005. Evidence of biochemical and biomagnetic interactions in Alzheimer's disease: an MEG and MR spectroscopic study. Dement. Geriatr. Cogn. Disord. 20, 145–152.

Maestu, F., Campo, P., Gil-Gregorio, P., Fernandez, S., Fernandez, A., Ortiz, T., 2006. Medial temporal lobe neuromagnetic hypoactivation and risk for developing cognitive decline in elderly population: a 2-year follow-up study. Neurobiol. Aging 27, 32–37.

McKhann, G., Drachman, D., Folstein, M., Katzman, R., Price, D., Stadlan, E.M., 1984. Clinical diagnosis of Alzheimer's disease: report of the NINCDS-ADRDA Work Group under the auspices of Department of Health and Human Services Task Force on Alzheimer's Disease. Neurology 34, 939–944.

Mesulam, M.M., 1990. Large-scale neurocognitive networks and distributed processing for attention, language, and memory. Ann. Neurol. 28, 597–613.

Mesulam, M.M., 1998. From sensation to cognition. Brain 121, 1013–1052.

Micheloyannis, S., Sakkalis, V., Vourkas, M., Stam, C.J., Simos, P.G., 2005. Neural networks involved in mathematical thinking: evidence for linear and non-linear analysis of electroencephalographic activity. Neurosci. Lett. 373, 212–217.

Montez, T., Linkenkaer-Hansen, K., van Dijk, B.W., Stam, C.J., submitted for publication. Synchronization likelihood with explicit time–frequency priors (revised manuscript).

Nolte, G., Wheaton, O.B.L., Mari, Z., Vorbach, S., Hallett, M., 2004. Identifying true brain interaction from EEG data using the imaginary part of coherency. Clin. Neurophysiol. 115, 2292–2307.

Nunez, P.L., Srinivasan, R., Westdorp, A.F., Wijesinghe, R.S., Tucker, D.M., Silberstein, R.B., Cadusch, P.J., 1997. EEG coherency I: statistics, reference electrode, volume conduction, Laplacians, cortical imaging, and interpretation at multiple scales. Electroencephalogr. Clin. Neurophysiol. 103, 499–515.

Osipova, D., Ahveninen, J., Kaakkola, S., Jaaskelainen, I.P., Huttunen, J., Pekkonen, E., 2003. Effects of scopolamine on MEG spectral power and coherence in elderly subjects. Clin. Neurophysiol. 114, 1902–1907.

Osipova, D., Ahveninen, J., Jensen, O., Ylikoski, A., Pekkonen, E., 2005. Altered generation of spontaneous oscillations in Alzheimer's disease. NeuroImage 27, 835–841.

Palva, J.M., Palva, S., Kaila, K., 2005. Phase synchrony among neuronal oscillations in the human cortex. J. Neurosci. 25, 3962–3972.

Pereda, E., Quian Quiroga, R., Bhattacharya, J., 2005. Nonlinear multivariate analysis of neurophysiological signals. Prog. Neurobiol. 77, 1–37.

Pijnenburg, Y.A.L., van de Made, Y., van Cappellen van Walsum, A.M., Knol, D.L., Scheltens, Ph., Stam, C.J., 2004. EEG synchronization likelihood in mild cognitive impairment and Alzheimer's disease during a working memory task. Clin. Neurophysiol. 115, 1332–1339.

Pogarell, O., Teipel, S.J., Juckel, G., Gootjes, L., Moller, T., Burger, K., Leinsinger, G., Moller, H.J., Hegerl, U., Hampel, H., 2005. EEG coherence reflects regional corpus callosum area in Alzheimer's disease. J. Neurol. Neurosurg. Psychiatry 76, 109–111.

Posthuma, D., de Geus, E.J.C., Mulder, E.J.C.M., Smit, D.J.A., Boomsma, D.I., Stam, C.J., 2005. Genetic components of functional connectivity in the brain: the heritability of synchronization likelihood. Hum. Brain Mapp. 26, 191–198.

Riekkinen, P., Buzsaki, G., Riekkinen Jr., P., Soininen, H., Partanen, J., 1991. The cholinergic system and EEG slow waves. Electroencephalogr. Clin. Neurophysiol. 78, 89–96.

Rodriguez, E., George, N., Lachauz, J.P., Martinerie, J., Renault, B., Varela, F.J., 1999. Perception's shadow: long distance synchronization of human brain activity. Nature 397, 430–433.

Rombouts, S.A.R.B., Barkhof, F., Veltman, D.J., Machielsen, W.C.M., Witter, M.P., Bierlaagh, M.A., Lazeron, R.H.C., Valk, J., Scheltens, P., 2000. Functional MR imaging in Alzheimer's disease during memory encoding. Am. J. Neuroradiol. 21, 1869–1875.

Rulkov, N.F., Sushchik, M.M., Ysimring, L.S., Abarbanel, H.D.I., 1995. Generalized synchronization of chaos in directionally coupled chaotic systems. Phys. Rev., E 51, 980–994.

Sarnthein, J., Petsche, H., Rappelsberger, P., Shaw, G.L., von Stein, A., 1998. Synchronization between prefrontal and posterior association cortex during human working memory. Proc. Natl. Acad. Sci. 95, 7092–7096.

Stam, C.J., 2005. Nonlinear dynamical analysis of EEG and MEG: review of an emerging field. Clin. Neurophysiol. 116, 2266–2301.

Stam, C.J., van Dijk, B.W., 2002. Synchronization likelihood: an unbiased measure of generalized synchronization in multivariate data sets. Physica, D 163, 236–241.

Stam, C.J., van Cappellen van Walsum, A.M., Micheloyannis, S., 2002a. Variability of EEG synchronization during a working memory task in healthy subjects. Int. J. Psychophysiol. 46, 53–66.

Stam, C.J., van Cappellen van Walsum, A.M., Pijnenburg, Y.A.L., Berendse, H.W., de Munck, J.C., Scheltens, Ph., van Dijk, B.W., 2002b. Generalized synchronization of MEG recordings in Alzheimer's disease: evidence for involvement of the gamma band. J. Clin. Neurophysiol. 19, 562–574.

Stam, C.J., van der Made, Y., Pijnenburg, Y.A.L., Scheltens, Ph., 2003a. EEG synchronization in mild cognitive impairment and Alzheimer's disease. Acta Neurol. Scand. 108, 90–96.

Stam, C.J., Breakspear, M., van Cappellen van Walsum, A.M., van Dijk, B.W., 2003b. Nonlinear synchronization in EEG and whole-head MEG recordings of healthy subjects. Hum. Brain Mapp. 19, 63–78.

Stam, C.J., Jones, B.F., Nolte, G., Breakspear, M., Scheltens, Ph., 2006. Small-world networks and functional connectivity in Alzheimer's disease. Cerebral Cortex. doi:10.1093/cercor/bhj127. [electronic publication ahead of print].

Stevens, A., Kircher, T., Nickola, M., Bartels, M., Rosellen, N., Wormstall, H., 2001. Dynamic regulation of EEG power and coherence is lost early and globally in probable DAT. Eur. Arch. Psychiatry Clin. Neurosci. 251, 199–204.

Takens, F., 1982. Detecting strange attractors in turbulence. Lect. Notes Math. 898, 366–381.

Theiler, J., 1986. Spurious dimension from correlation algorithms applied to limited time-series data. Phys. Rev., A 34, 2427–2432.

Tononi, G., Edelman, G.M., Sporns, O., 1998. Complexity and coherency: integrating information in the brain. TICS 2, 474–484.

Van Cappellen van Walsum, A.-M., Pijnenburg, Y.A.L., Berendse, H.W., van Dijk, B.W., Knol, D.L., Scheltens, Ph., Stam, C.J., 2003. A neural complexity measure applied to MEG data in Alzheimer's disease. Clin. Neurophysiol. 114, 1034–1040.

van der Hiele, K., Vein, A.A., Kramer, C.G., Reijntjes, R.H., van Buchem, M.A., Westendorp, R.G., Bollen, E.L., van Dijk, J.G., Middelkoop, H.A., 2006. Memory activation enhances EEG abnormality in mild cognitive impairment. Neurobiol. Aging ([electronic publication ahead of print] PMID: 16406153).

Varela, F., Lachaux, J.-P., Rodriguez, E., Martinerie, J., 2001. The brainweb: phase synchronization and large-scale integration. Nat. Rev., Neurosci. 2, 229–239.

Vrba, J., Anderson, G., Betts, K., et al., 1999. 151-Channel whole-cortex MEG system for seated or supine positions. In: Yoshimoto, T., Kotani, M., Kuriki, S., et al., (Eds.), Recent Advances in Biomagnetism. Tohoku Univ. Press, Sendai, Japan, pp. 93–96.

Wheaton, L.A., Nolte, G., Bohlhalter, S., Fridman, E., 2005. Synchronization of parietal and premotor areas during preparation an execution of praxis hand movement. Clin. Neurophysiol. 116, 1382–1390.

P3

Impaired temporal correlations in temporo-parietal oscillations in early-stage Alzheimer's disease

Teresa Montez [a,b], Simon-Shlomo Poil[e], Bethany F. Jones[b], Ilonka Manshanden[b], Jeroen P. A. Verbunt[b,d] , Bob W. van Dijk[b,d], Arjen B Brussaard[e], Arjen van Ooyen[e], Cornelis J. Stam[b], Philip Scheltens[c], Klaus Linkenkaer-Hansen[e¶]

[a] Institute of Biophysics and Biomedical Engineering, Faculty of Sciences of the University of Lisbon, Campo Grande, 1749-016 Lisbon, Portugal.

[b] Department of Clinical Neurophysiology and MEG Centre, VU University Medical Center, PO Box 7057, 1007 MB Amsterdam, The Netherlands.

[c] Alzheimer Center and Department of Neurology, VU University Medical Center, PO Box 7057, 1007 MB Amsterdam, The Netherlands

[d] Department of Physics and Medical Technology, VU University Medical Center, De Boelelaan 1117, 1081 HV Amsterdam, The Netherlands.

[e] Department of Experimental Neurophysiology, Center for Neurogenomics and Cognitive search (CNCR), VU University Amsterdam, De Boelelaan 1085, 1081 HV Amsterdam, The Netherlands.

Corresponding author:
Klaus Linkenkaer-Hansen, Dr.
Department of Experimental Neurophysiology
Center for Neurogenomics and Cognitive Research (CNCR)
VU University Amsterdam
De Boelelaan 1085
1081 HV Amsterdam, The Netherlands
Phone (office): +31 20 5986479
Fax: +31 20 5987112
E-mail: klaus.linkenkaer@cncr.vu.nl

Classification: Biological sciences

Text pages	23
Figures	4
Tables	0
Abstract word count	229
Character count (including character equivalents of figures)	48981

Author contributions:
B.J. and Ph.S. were involved in patient recruitment.
I.M., J.P.A.V, and B.W.v.D helped with acquisition and pre-processing of the data.
T.M., S.-S.P., and K.L.-H. analyzed data.
C.J.S., Ph.S., A.B.B., A.v.O., and K.L.-H. designed research and supervised the project.
K.L.-H. wrote the first draft of the MS. All authors commented on the manuscript.

Abstract

Encoding and retention of information in memory modulate the amplitude of neuronal oscillations up to several seconds. Interestingly, during resting-state conditions, which are known to be associated with prominent mnemonic activity, ongoing oscillations also exhibit amplitude modulations on multiple time scales, as indicated by long-range temporal correlations (LRTC) up to tens of seconds. We reasoned that correlations in oscillations over time might be important for memory and could therefore be abnormal in Alzheimer's disease (AD). To test this hypothesis, we measured magnetoencephalography (MEG) during eyes-closed rest in 19 patients diagnosed with early-stage AD and 16 age-matched control subjects and characterized temporal correlations in ongoing oscillations using detrended fluctuation analysis and a novel "avalanche analysis" that quantifies the life- and waiting-time probability distributions of oscillation bursts. We found that Alzheimer's patients had markedly weaker long-range temporal correlations in the alpha band (6-13 Hz) over temporo-parietal regions on time scales of 1–25 seconds. On shorter time scales (< 1 second), abnormal dynamics of alpha oscillations in AD patients were expressed as a strongly reduced probability for the occurrence of oscillation bursts with long life- or waiting-times in the temporo-parietal regions. These regions have been associated with mnemonic functions in healthy subjects and show metabolic and structural deficits in AD, suggesting that the tendency for ongoing alpha oscillations to carry a memory of their own amplitude dynamics is important for cognition.

Introduction

Psychological and neuroimaging data suggest that the brain performs many important functions during rest, such as retrieval and manipulation of information in short-term memory, and problem solving and planning (1, 2). These resting-state functions may represent an essential aspect of human self-awareness and are susceptible to impairment in brain-related disorders including dementia, depression, and schizophrenia (3).

Neuroimaging has identified anatomical patterns of activity that are remarkably consistent across resting-state experiments, most notably in the precuneus, lateral parietal and medial prefrontal cortices (4, 5). The existence of such a "resting-state network" may suggest that the brain has a "default mode" of operation in the absence of goal-directed behavior (6). Connectivity analysis has aimed at understanding the integrity of the distributed resting-state network using metabolic, hemodynamic or electrophysiological techniques. This has revealed disturbances in the resting-state networks in Alzheimer's disease (7-9) and other pathologies (4, 10).

Functional connectivity has traditionally been considered a phenomenon in the spatial domain (11-13), and it is widely accepted that correlations between neuronal activities in anatomically distributed networks are important for cognition (14-16). Correlations over time, however, may be equally important for brain function; e.g., cognitive functions typically involve a series of operations requiring temporal coordination of neuronal activity across many time scales (17, 18). This is true particularly during rest where thoughts unfold on time scales of several seconds and, thus, require ongoing mnemonic activity and "binding" in the temporal domain to ensure continuity and integrity of conscious experiences (3). In experiments where the timing of such mnemonic operations is explicitly known, a sustained increase in the oscillation amplitude has been observed for several seconds in multiple brain areas and

frequency bands during information encoding and retention (19-21). These results suggest that oscillations related to ongoing mnemonic operations during rest are amplitude modulated on long time scales and that a slow modulation of oscillatory activity may serve a "binding" function in the temporal domain.

We and others have recently shown that ongoing oscillations during rest are modulated in amplitude on multiple time scales, as reflected in the slow power-law decay of autocorrelations of up to several tens of seconds, also known as "long-range temporal correlations" (LRTC) (22-25). This indicates that oscillations may carry a "memory" of their own dynamics. It remains unknown, however, whether this physiological memory is related to cognitive memory. If this were the case, one would expect a memory disease like Alzheimer's to show abnormally weak temporal correlations in oscillations that have been implicated with mnemonic operations (19-21). To test this we measured ongoing activity with whole-scalp magnetoencephalography (MEG) in patients diagnosed with early-stage Alzheimer's disease (AD) and in age-matched control subjects. We have identified four complementary biomarkers of temporal correlations in ongoing oscillations that point to an impaired physiological memory of alpha oscillations over temporo-parietal cortices in AD.

Results

Spectral analysis revealed prominent oscillations in the alpha-frequency band in the occipito-parietal region in all subjects, albeit that the AD patients had peak frequencies in the range of 6.3–10.0 Hz, which is lower than the age-matched control subjects (7.1–10.7 Hz, $p < 0.05$, two-tailed t-test, Fig. 1 *A* and 2 *D*). This is in agreement with the well-known slowing of the alpha rhythm in AD (26-28). Thus, to avoid confounding

frequency and amplitude effects, we defined the alpha-frequency band to be 6–13 Hz. Alpha oscillations in both groups exhibited erratic fluctuations in amplitude (Fig. 1 *D* and *E*) and a high signal-to-noise ration relative to the background noise in the MEG recording room (Fig. 1 *F*), which is important for an accurate estimation of temporal correlations (29). We used three complementary methods to test whether the temporal correlations of these fluctuations carry functionally relevant information about the state of the underlying networks.

On long time scales (1–25 s), we used detrended fluctuation analysis (DFA) (Fig. 1 *G*), which has previously been shown to robustly estimate the strength of long-range temporal correlations of a power-law form (22, 29). The DFA analysis identified a highly significant drop in LRTC in several channels over temporo-parietal regions (Fig. 2 *A–C*, DFA exponents 0.66 ± 0.01 in AD and 0.71 ± 0.01 in the control group, $p < 0.005$ for the mean DFA exponent across 33 channels, two-tailed t-test, see Methods). This is particularly interesting in view of the lack of a group effect on oscillation amplitudes (Fig. 2 *E*). Note that the MEG data were transformed to planar synthetic gradiometers, which are maximally sensitive to neuronal currents immediately below the sensor (see Methods).

The DFA exponent being larger than 0.5 on time scales of 1–25 seconds clearly indicates that the oscillations do not wax and wane randomly. The DFA analysis, however, is not suitable for quantifying the dynamics on time scales shorter than 1 second (see Methods). Hence, to further understand the meta-stable dynamics of the oscillations on short to intermediate time scales, we therefore adopted an "avalanche analysis" from the study of critical phenomena (30, 31). We quantified the time periods that oscillation amplitudes stayed above or below the median level in individual channels (Fig. 1 *B*, see Methods). These periods are termed "oscillation life- and

waiting-times", respectively, and their probability distributions decayed as power-laws (Fig. 1 *H* and *I*). The corresponding power-law exponents, τ and τ_w, therefore provide a convenient index of the variation in oscillation-burst life-times: the less likely the occurrence of a long-lasting oscillation, the larger the life-time exponent. A random signal that is filtered and analyzed identically to the MEG signal is characterized by rapidly decreasing life- and waiting-time distributions (Fig. 1 *H* and *I*). Interestingly, and in line with the analysis of LRTC, group differences in life-time exponents were identified in the temporo-parietal regions (Fig. 3 *C*), with life-time exponents 1.91 ± 0.06 in AD and 1.68 ± 0.04 in the control group (Fig. 3 *B*; $p < 0.005$). A different way of illustrating the lower capacity of AD patients to generate long-lasting oscillations is to compute the cumulative probability distribution of life-times, which showed significant differences at percentiles around 88–100%. The 95%-percentile, e.g., was 383 ± 11 ms in AD and 439 ± 12 ms in controls (Fig. 3 *D* and *E*; $p < 0.005$). Surprisingly, also the waiting times were highly affected with waiting-time exponents 1.77 ± 0.04 in AD and 1.60 ± 0.04 in the control group (Fig. 3 *G* and *H*; $p < 0.005$), which further supports the conclusion that oscillatory dynamics is considerably more random in Alzheimer's patients than in age-matched control subjects.

Finally, we correlated the exponents from the analysis of LRTC and oscillation life- and waiting-times. The group effect for both DFA, life- and waiting-time exponents may lead to the impression that these exponents are correlated; however, the Pearson correlation analysis did not indicate a significant linear correlation in any of the groups for any of the measures (r in the range of –0.42 to –0.32 with $p > 0.05$, Fig. 4). This reflects the different time scales that the methods are sensitive to, and suggest that Alzheimer's patients have abnormal temporal structure of oscillations both within and across multiple bursts.

Discussion

Resting-state alpha oscillations carry a memory of their own amplitude dynamics for tens of seconds, as reflected by long-range temporal correlations (LRTC) (22, 29). We investigated whether this physiological memory may be impaired in a disease of cognitive memory. Here, we report that patients with early-stage Alzheimer's disease (AD) have impaired temporal correlations in temporo-parietal alpha oscillations. These brain regions have been implicated with mnemonic operations in normal subjects and exhibit structural, metabolic, and blood-flow deficits in AD. Taken together with previous electrophysiological data from working memory tasks (19-21), our results suggest that the capacity to modulate neuronal oscillations on multiple time scales may be important for memory.

Biomarkers of pathology derived from amplitude dynamics of oscillations

The DFA analysis of LRTC in ongoing oscillations has previously been shown to identify pathophysiological states with spectral and anatomical specificity. In major depressive disorder, temporal correlations were selectively attenuated in the theta band (17), whereas abnormally strong correlations were found near the seizure zone in epilepsy patients primarily in the beta band (32, 33). Here, we identified a pattern of weaker LRTC in alpha oscillations in AD extending from the parietal region and bilaterally towards the temporal lobes. This is particularly interesting in view of the insignificant effect of AD on oscillation amplitude at 6–13 Hz and in line with a recent study in twins showing that power and LRTC convey complementary information (29). The analysis of oscillation life-times complemented the DFA in identifying impaired

temporal correlation properties of temporo-parietal oscillations in AD. This topography agrees remarkably well with previously identified anatomical regions expressing Alzheimer's associated pathologies based on reductions in blood flow and metabolism during rest (34, 35), cortical atrophy (36), or amyloid deposition (34).

Together, these findings suggest that the amplitude modulation of temporo-parietal alpha oscillations on both short to intermediate (< ~1 s) and long (1–25 s) time scales represents a physiological memory that is important for cognitive memory. Further, the lack of an amplitude effect suggests that temporal correlations may be more important for mnemonic operations than the capacity to generate large-amplitude oscillations. This highlights the importance of quantifying the amplitude dynamics of oscillations in fundamental and clinical research on ongoing oscillations.

Mnemonic processing and temporal correlation properties of oscillations

Electrophysiological studies using intracranial electrode recordings, EEG, or MEG have identified a sustained increase in parietal alpha activity as a hallmark of mnemonic activity in humans (19-21). We have previously proposed that the amplitude modulation of oscillations and their temporal correlations on time scales of seconds to tens of seconds may provide a temporal dimension to functional connectivity that is important for the temporal integrity of working-memory (17). In other words, higher cognitive functions, such as maintaining continuity of thoughts during rest, require integrity of neuronal processing over time to make sense (18) and this may require correlated activity on multiple time scales. Interestingly, psychological and fMRI studies have pointed to prominent mnemonic activity during rest (1), and brain regions involved in mnemonic tasks (34, 37) overlap considerably with those showing high activity during rest (4). Thus, converging functional and anatomical evidence suggests that one indeed

would expect impaired amplitude dynamics of temporo-parietal alpha oscillations as we have reported here.

Functional connectivity and temporal correlation properties of oscillations

Memory is believed to depend on the functional connectivity between different brain areas, and the cognitive symptoms of AD have therefore been proposed to reflect a "disconnection syndrome" (38). Indeed, there is considerable evidence pointing to deficits in the functional connectivity of resting-state networks in AD, especially a reduced involvement of parietal cortices as revealed by functional magnetic resonance imaging (7, 8, 39). In electrophysiological recordings, linear (40) and non-linear measures of synchronization (41-43) have been used to identify reduced interregional correlations, in particular between frontal and parietal regions. Impaired functional connections in AD may be related to structural atrophy (34), but most likely also include deficits in cholinergic or other neurotransmitter systems (27, 38, 44, 45).

Failures in any of the components of a large-scale circuit are expected to disrupt its reverberating activity (14, 46) and to affect the temporal dynamics of activity also locally. It is therefore plausible that the abnormally weak correlations in alpha oscillations on time scales up to 25 seconds are in part caused by a "disconnection" in a large-scale network. It is increasingly being recognized that resting-state activity in neurocognitive networks have a multi-scale spatio-temporal structure (47); however, only few studies have explicitly addressed the time-scale dependence of functional connectivity (48, 49).

Summary and outlook

We have shown that temporal correlations in alpha oscillations, as characterized by LRTC, life- and waiting-time statistics, are abnormal in temporo-parietal regions in AD. These brain regions have been implicated with mnemonic processing and exhibit deficits in blood-flow and metabolism in Alzheimer's patients during rest. To our knowledge, this is the first study to identify an electrophysiological memory that operates on time scales up to tens of seconds and that is impaired in a disease of cognitive memory. We propose that non-invasive mapping of LRTC and other indices of temporal correlations may provide important biological markers in pre-clinical trials aimed at investigating the progression and treatment response of patients with AD or other memory disorders (50).

Methods

Subjects

The study involved 19 patients (73.9 ± 6.4 years (mean ± standard deviation); 11 males) with a diagnosis of probable AD according to the NINCDS-ADRDA criteria (51) and 16 healthy control subjects (70 ± 6.2 years; 7 males), mostly spouses of the patients. Patients and control subjects were recruited from the Alzheimer Center at the VU University Medical Center. Subjects were assessed according to a clinical protocol, which involved history taking, physical and neurological examination, blood tests, mini-mental state examination (MMSE) (52), several neuropsychological tests, and routine EEG. The final diagnosis was based upon a consensus meeting where all the available clinical data and the results of the ancillary investigations were considered. Mean MMSE of patients was 21.3 (range: 14–28) and five controls were tested with MMSE (mean score 29, range: 26–30). Ten patients were taking cholinesterase inhibitors: seven

were taking 24 mg/d of galantamine and three were taking 12 mg/d of rivastigmine. The same patients and MEG recordings were used in the study of Stam et al. (43). The study was approved by the Local Research Ethics Committee, and all patients or their caregivers had given written informed consent.

MEG recording

Four minutes of data were acquired in a 151-channel MEG system (CTF Systems Inc., Vancouver, Canada) at 625 Hz and band-pass filtered from 0.25 to 125 Hz. The subjects were comfortably seated and were instructed to close their eyes. The same acquisition settings were used for an empty-room recording without a subject in the MEG device to estimate the background noise of the laboratory.

Data analysis

The recordings were down-sampled off-line to 125 Hz, high-pass filtered at 1 Hz and low-pass filtered at 45 Hz using finite impulse response filters. The broadband data were visually inspected in segments of 5 seconds in the EEGLAB (53) data scroll viewer and segments containing non-periodic artifacts were marked and omitted from the analysis. Independent component analysis was performed with EEGLAB and components representing ECG, eye movements or muscular artifacts were removed. Bad channels were repaired by replacing them with the average of their neighbors, and planar synthetic gradiometers (for two orthogonal directions giving 300 synthetic sensors) were computed using the Fieldtrip toolbox (http://www.ru.nl/fcdonders/fieldtrip/) and the method described in (54). The planar gradient fields are typically largest in magnitude directly above a given source (21, 54) and, therefore, provide an interpretation of topographic distributions that is analogous to

projections of statistical maps onto the surface of the brain in PET and fMRI. The amplitude envelope in the alpha-frequency band was extracted using bandpass filters at 6–13 Hz (finite impulse response filters with a Hamming window and filter order 28) and the Hilbert transform (Fig. 1C). In this study, we focus on alpha oscillations because of their known amplitude modulation in mnemonic tasks (19-21) and the importance of a high signal-to-noise ratio for a robust estimation of temporal correlations (29).

Analysis of oscillation power and long-range temporal correlations. The decay of temporal (auto-)correlations in the time range of 1–25 s was estimated with detrended fluctuation analysis (DFA). The DFA was introduced as a method to quantify correlations in complex data with less strict assumptions about the stationarity of the signal than the classical auto-correlation function or power spectral density (55). An additional advantage of DFA is the greater accuracy in the estimates of correlations, which facilitates a reliable analysis of LRTC up to time scales of at least 10% of the duration of the signal (56). The main steps from the broadband MEG signal to the quantification of LRTC using DFA have been explained in detail elsewhere (22-24). In brief, the DFA measures the scaling of the root-mean-square fluctuation of the integrated and linearly detrended signals, $F(t)$, as a function of time window size, t (Fig. 1G). For signals that are uncorrelated or have persistent power-law correlations, the average fluctuation $\langle F(t) \rangle$ is of the form $\langle F(t) \rangle = t^{\alpha}$, where α is the DFA scaling exponent. If $0.5 < \alpha \leq 1.0$, this indicates power-law scaling behavior and the presence of temporal correlations, whereas $\alpha = 0.5$ indicates the ideal case of an uncorrelated signal. The amplitude of oscillations was computed as the mean amplitude envelope after bandpass filtering and Hilbert transform.

Analysis of oscillation life- and waiting times. For each synthetic sensor and subject, we computed the median amplitude and used this as the threshold for defining the beginning and end of an oscillation burst. The periods of the amplitude envelope remaining above and below this median level were termed life- and waiting-times, respectively (Fig. 1B). Probability distributions of oscillation life- and waiting-times were computed using equidistant binning on a logarithmic axis with 10 bins per decade. Based on visual inspection of probability distributions from MEG channels in the parietal region, which have a high signal-to-noise ratio, it was found that all subjects had probability distributions that decayed as a power-law in the range of 119–538 ms (Fig. 3A). The power-law exponents that characterize the life- and waiting-time distributions are denoted τ and τ_w, respectively. The exponents were computed using least-square fitting of the 8 bins corresponding to the time range 119–538 ms in all synthetic sensors and subjects. The average R^2 was 0.97 across the n = 10500 channels. Further details on this method and its theoretical basis will be published elsewhere (Poil S.-S., van Ooyen A., Linkenkaer-Hansen K., unpublished data).

Statistical analysis. The biomarker value in each channel was computed as the average across the two orthogonal synthetic sensors. Two-tailed t-tests between patient and control groups were performed; p-values below 0.05 and 0.01 are indicated on topographic plots. A correction for multiple comparisons was not necessary, because the number of channels with p-values below 0.05 ranged from 18 and 45 channels and the likelihood of having this many channels out of 150 channels by chance is less than 0.0006 (cf. binomial distribution). Furthermore, the channels were anatomically clustered in topographic plots (Figs. 2 and 3). Biomarker values of patient and control

groups are reported as mean ± standard error of mean (SEM) based on the average values across channels with $p < 0.05$ in the initial two-tailed t-test. Group differences in these cross-channel means were computed using two-tailed t-test.

Acknowledgements. T.M. was the recipient of a doctoral fellowship from FCT, Ministry of Science, Portugal financed by POCI 2010 and FSE and a grant from the Calouste Gulbenkian Foundation. K.L.-H. received funding from the Danish Research Agency and the Innovative Research Incentive Schemes of the Netherlands Organization for Scientific Research (NWO).

References

1. Binder R*, et al.* (1999) Conceptual Processing during the Conscious Resting State: A Functional MRI Study. *J Cognit Neurosci* 11**:**80-93.
2. Mason MF*, et al.* (2007) Wandering Minds: The Default Network and Stimulus-Independent Thought. *Science* 315**:**393-395.
3. Smallwood J & Schooler JW (2006) The Restless Mind. *Psychological Bulletin* 132**:**946-95813.
4. Fox MD & Raichle ME (2007) Spontaneous fluctuations in brain activity observed with functional magnetic resonance imaging. *Nature Rev Neurosci* 8**:**700-711.
5. Damoiseaux JS*, et al.* (2006) Consistent resting-state networks across healthy subjects. *Proc Natl Acad Sci USA* 103**:**13848-13853.

6. Gusnard DA & Raichle ME (2001) Searching for a baseline: functional imaging and the resting human brain. *Nature Rev Neurosci* 2**:**685-694.

7. Greicius MD, Srivastava G, Reiss AL, & Menon V (2004) Default-mode network activity distinguishes Alzheimer's disease from healthy aging: Evidence from functional MRI. *Proc Natl Acad Sci USA* 101**:**4637-4642.

8. Rombouts SA*, et al.* (2005) Altered resting state networks in mild cognitive impairment and mild Alzheimer's disease: an fMRI study. *Hum Brain Mapp* 26**:**231-239.

9. Babiloni C*, et al.* (2004) Abnormal fronto-parietal coupling of brain rhythms in mild Alzheimer's disease: a multicentric EEG study. *Eur J Neurosci* 19**:**2583-2590.

10. Greicius MD*, et al.* (2007) Resting-State Functional Connectivity in Major Depression: Abnormally Increased Contributions from Subgenual Cingulate Cortex and Thalamus. *Biol Psych* 62**:**429-437.

11. Aertsen AM, Gerstein GL, Habib MK, & Palm G (1989) Dynamics of neuronal firing correlation: modulation of "effective connectivity". *J Neurophysiol* 61**:**900-917.

12. Friston KJ (1994) Functional and effective connectivity in neuroimaging: A synthesis. *Hum Brain Mapp* 2**:**56-78.

13. Sporns O, Chialvo DR, Kaiser M, & Hilgetag CC (2004) Organization, development and function of complex brain networks. *Trends Cogn Sci* 8**:**418-425.

14. Varela F, Lachaux J-P, Rodriguez E, & Martinerie J (2001) The brainweb: Phase synchronization and large-scale integration. *Nature Rev Neurosci* 2**:**229-239.

15. Singer W (1999) Neuronal Synchrony: A Versatile Code Review for the Definition of Relations? *Neuron* 24**:**49-65.

16. Fries P (2005) A mechanism for cognitive dynamics: neuronal communication through neuronal coherence. *Trends Cogn Sci* 9**:**474-480.

17. Linkenkaer-Hansen K*, et al.* (2005) Breakdown of Long-Range Temporal Correlations in Theta Oscillations in Patients with Major Depressive Disorder. *J Neurosci* 25**:**10131-10137.

18. Cowan N (1998) Visual and auditory working memory capacity. *Trends Cogn Sci* 2**:**77-77.

19. Raghavachari S*, et al.* (2001) Gating of Human Theta Oscillations by a Working Memory Task. *J Neurosci* 21**:**3175-3183.

20. Jensen O, Gelfand J, Kounios J, & Lisman JE (2002) Oscillations in the Alpha Band (9-12 Hz) Increase with Memory Load during Retention in a Short-term Memory Task. *Cereb Cortex* 12**:**877-882.

21. Jokisch D & Jensen O (2007) Modulation of Gamma and Alpha Activity during a Working Memory Task Engaging the Dorsal or Ventral Stream. *J Neurosci* 27**:**3244-3251.

22. Linkenkaer-Hansen K, Nikouline VV, Palva JM, & Ilmoniemi RJ (2001) Long-Range Temporal Correlations and Scaling Behavior in Human Brain Oscillations. *J Neurosci* 21**:**1370-1377.

23. Linkenkaer-Hansen K*, et al.* (2004) Stimulus-induced change in long-range temporal correlations and scaling behaviour of sensorimotor oscillations. *Eur J Neurosci* 19**:**203-218.

24. Nikulin VV & Brismar T (2005) Long-range temporal correlations in electroencephalographic oscillations: Relation to topography, frequency band, age and gender. *Neuroscience* 130**:**549-558.

25. Leopold DA, Murayama Y, & Logothetis NK (2003) Very Slow Activity Fluctuations in Monkey Visual Cortex: Implications for Functional Brain Imaging. *Cereb Cortex* 13**:**422-433.

26. Jeong J (2004) EEG dynamics in patients with Alzheimer's disease. *Clinical Neurophysiology* 115**:**1490-1505.

27. Osipova D*, et al.* (2005) Altered generation of spontaneous oscillations in Alzheimer's disease. *NeuroImage* 27**:**835-841.

28. Fernandez A*, et al.* (2002) Focal temporoparietal slow activity in Alzheimer's disease revealed by magnetoencephalography. *Biol Psych* 52**:**764-770.

29. Linkenkaer-Hansen K*, et al.* (2007) Genetic Contributions to Long-Range Temporal Correlations in Ongoing Oscillations. *J Neurosci* 27**:**13882-13889.

30. Harris TE (2002) *The Theory of Branching Processes* (Courier Dover Publications).

31. Plenz D & Thiagarajan TC (2007) The organizing principles of neuronal avalanches: cell assemblies in the cortex? *Trends Neurosci* 30**:**101-110.

32. Monto S, Vanhatalo S, Holmes MD, & Palva JM (2007) Epileptogenic Neocortical Networks Are Revealed by Abnormal Temporal Dynamics in Seizure-Free Subdural EEG. *Cereb Cortex* 17**:**1386-1393.

33. Parish LM*, et al.* (2004) Long-range temporal correlations in epileptogenic and non-epileptogenic human hippocampus. *Neuroscience* 125**:**1069-1076.

34. Buckner RL (2004) Memory and Executive Function in Aging and AD: Multiple Factors that Cause Decline and Reserve Factors that Compensate. *Neuron* 44**:**195-208.

35. Johannsen P, Jakobsen J, & Gjedde A (2000) Statistical maps of cerebral blood flow deficits in Alzheimer's disease. *Eur J Neurol* 7**:**385-392.

36. Thompson PM*, et al.* (2003) Dynamics of Gray Matter Loss in Alzheimer's Disease. *J Neurosci* 23**:**994-1005.

37. Kuhl BA, Dudukovic NM, Kahn I, & Wagner AD (2007) Decreased demands on cognitive control reveal the neural processing benefits of forgetting. *Nature Neurosci* 10**:**908-914.

38. Delbeuck X, Van der Linden M, & Collette F (2003) Alzheimer' Disease as a Disconnection Syndrome? *Neuropsych Rev* 13**:**79-92.

39. Lustig C*, et al.* (2003) Functional deactivations: Change with age and dementia of the Alzheimer type. *Proc Natl Acad Sci USA* 100**:**14504-14509.

40. Dunkin JJ, Leuchter AF, Newton TF, & Cook IA (1994) Reduced EEG coherence in dementia: State or trait marker? *Biol Psych* 35**:**870-879.

41. Babiloni C*, et al.* (2004) Abnormal fronto-parietal coupling of brain rhythms in mild Alzheimer's disease: a multicentric EEG study. *European Journal of Neuroscience* 19**:**2583-2590.

42. Stam CJ*, et al.* (2005) Disturbed fluctuations of resting state EEG synchronization in Alzheimer's disease. *Clin Neurophysiol* 116**:**708-715.

43. Stam CJ*, et al.* (2006) Magnetoencephalographic evaluation of resting-state functional connectivity in Alzheimer's disease. *NeuroImage* 32**:**1335-1344.

44. Osipova D*, et al.* (2003) Effects of scopolamine on MEG spectral power and coherence in elderly subjects. *Clinical Neurophysiology* 114**:**1902-1907.

45. Maxim V*, et al.* (2005) Fractional Gaussian noise, functional MRI and Alzheimer's disease. *NeuroImage* 25**:**141-158.

46. Maestu F*, et al.* (2003) Do cognitive patterns of brain magnetic activity correlate with hippocampal atrophy in Alzheimer's disease? *J Neurol Neurosurg Psychiatry* 74**:**208-212.

47. Bressler SL & Tognoli E (2006) Operational principles of neurocognitive networks. *Int J Psychophysiol* 60**:**139-148.

48. Honey CJ, Kotter R, Breakspear M, & Sporns O (2007) Network structure of cerebral cortex shapes functional connectivity on multiple time scales. *Proc Natl Acad Sci USA* 104**:**10240.

49. Nikouline VV, Linkenkaer-Hansen K, Huttunen J, & Ilmoniemi RJ (2001) Interhemispheric phase synchrony and amplitude correlation of spontaneous beta oscillations in human subjects: a magnetoencephalographic study. *NeuroReport* 12**:**2487-2491.

50. Thal LJ*, et al.* (2006) The role of biomarkers in clinical trials for Alzheimer disease. *Alzheimer Dis Assoc Disord* 20**:**6-15.

51. McKhann G (1984) (AAN Enterprises), pp. 939-944.

52. Folstein MF, Folstein SE, & McHugh PR (1975) "Mini-mental state": A practical method for grading the cognitive state of patients for the clinician. *J Psych Res* 12**:**189-198.

53. Delorme A & Makeig S (2004) EEGLAB: an open source toolbox for analysis of single-trial EEG dynamics including independent component analysis. *J Neurosci Meth* 134**:**9-21.

54. Bastiaansen MCM & Knosche TR (2000) Tangential derivative mapping of axial MEG applied to event-related desynchronization research. *Clinical Neurophysiology* 111**:**1300-1305.

55. Peng CK*, et al.* (1994) Mosaic organization of DNA nucleotides. *Physical Review E* 49**:**1685.

56. Gao J*, et al.* (2006) Assessment of long-range correlation in time series: How to avoid pitfalls. *Physical Review E (Statistical, Nonlinear, and Soft Matter Physics)* 73**:**016117-016110.

Figure 1. Three power-law scaling exponents for characterizing the amplitude dynamics of alpha-band oscillations.

The grand-average amplitude spectra of a mid-parietal planar synthetic gradiometer exhibit a clear shift towards lower frequencies in AD patients (*thick red line*) compared to control subjects (*thin blue line*) (A). To characterize the amplitude dynamics of alpha oscillations, the MEG signals were band-pass filtered from 6–13 Hz (*thin green line*) and the amplitude envelope of the oscillations (*thick blue line*) extracted with the Hilbert transform (B, C). Non-random fluctuations are qualitatively identified as a tendency for oscillations to exhibit amplitude modulations on multiple time scales, as seen in the control subject (D), as opposed to rapidly changing amplitude levels even on short time scales, as seen in the AD patient (E) and the MEG recording without a subject in the device (F). The DFA exponent, α, provides a quantitative measure of the temporal structure on long time scales (1–25 s): the stronger correlations in the control subject (G, *blue circles*) compared with the AD patient (G, *red diamonds*) is reflected in a value of α closer to 1 (0.81 vs. 0.58). The lack of temporal correlations in (F) is reflected in the DFA exponent having the value of ~0.5, which is characteristic of an uncorrelated random process (G, *black dots*). To quantify differences in oscillatory dynamics on short to intermediate time scales (< 1 s), we introduced a threshold at the median amplitude (*horizontal dashed line* in B) and defined the start and end of an oscillation burst as the time points of crossing this threshold. The probability distributions of oscillation-burst "life-times" and "waiting-times" decayed as power-laws with exponents τ and τ_w, respectively (H, I). All data were taken from a parietal channel.

Figure 2. Impaired long-range temporal correlations in temporo-parietal oscillations in Alzheimer's disease.

(A) Grand-average DFA plot of a parietal channel for AD (*red diamonds*), control group (*blue circles*), and a recording without a subject in the MEG device (*black dots*). Data were band-pass filtered 6–13 Hz and the amplitude envelope extracted with the Hilbert transform. (B) Individual-subject values and mean ± SEM of DFA exponents ($p < 0.005$) averaged over the 33 channels marked with white circles in (C). (C) Topography of DFA exponents in the alpha-frequency band for patients (*left column*), controls (*middle column*), and controls minus patients (*right column*). White circles denote channels with $p < 0.05$ (*open*), and $p < 0.01$ (*filled*). (D) Individual peak frequencies in the broad alpha band (6–13 Hz) in a parietal channel for patients (*red diamonds*) and control subjects (*blue circles*), and their mean ± SEM ($p < 0.05$). (E) Individual amplitudes averaged over the 12 channels showing the largest group difference and mean ± SEM of the two groups. (F) Topography of mean amplitude in the alpha-frequency band for AD patients (*left column*), controls (*middle column*), and controls minus patients (*right column*).

Figure 3. Altered life- and waiting-times of temporo-parietal oscillations in Alzheimer's disease.

(A) Grand-average probability distribution function (PDF) of oscillation life-times for AD patients (*red diamonds*), control group (*blue circles*), and an empty-room recording (*black dots*). (B) Individual-subject values and mean ± SEM of the life-time exponents τ ($p < 0.005$) averaged over the 25 channels marked with white circles in (C). (C) Grand average topographies of τ for AD patients (*left column*), controls (*middle column*), and controls minus patients (*right column*). White circles denote channels with $p < 0.05$

(*open*), and $p < 0.01$ (*filled*) in all topographic plots. (D) Cumulative probability distribution function (CDF) of oscillation life-times for AD (*red line*) and control group (*blue line*). The grand-average 95%-percentiles are marked with vertical lines. (E) Individual values and means ± SEM of cumulative life-times averaged over the 45 channels marked with white circles in (F) ($p < 0.005$). (F) Grand average topographies of cumulative life-times at the 95%-percentile for AD patients (*left column*), controls (*middle column*), and controls minus patients (*right column*). (G) Grand-average probability distribution of waiting-times for channels with a significant group difference for AD (*red diamonds*), control group (*blue circles*), and the empty-room recording (*black dots*). (H) Individual values and means ± SEM of τ_w averaged over the 18 channels marked with white circles in (I) ($p < 0.005$). (I) Grand-average topography of waiting-times for AD patients (*left column*), controls (*middle column*), and controls minus patients (*right column*).

Figure 4. Temporal correlation properties of alpha oscillations are different on short and long time scales.

Scatter plots showing insignificant correlations between DFA exponents and power-law exponents of oscillation life-times (A) and waiting-times (B) for AD patients (*red diamonds*) and control group (*blue circles*).

Figure 1

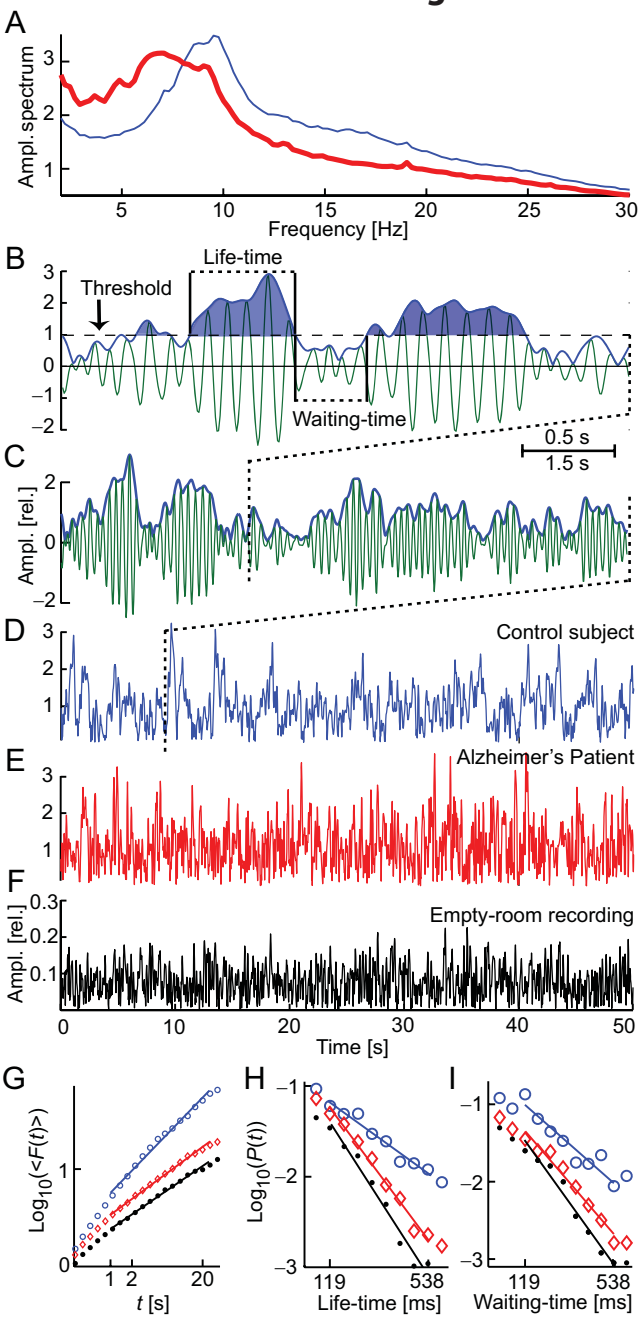
A
Ampl. spectrum
Frequency [Hz]
B
Life-time
Threshold
Waiting-time
0.5 s
1.5 s
C
Ampl. [rel.]
D
Control subject
E
Alzheimer's Patient
F
Empty-room recording
Ampl. [rel.]
Time [s]
G
Log10(<F(t)>)
t [s]
H
Log10(P(t))
Life-time [ms]
I
Waiting-time [ms]

Figure 2

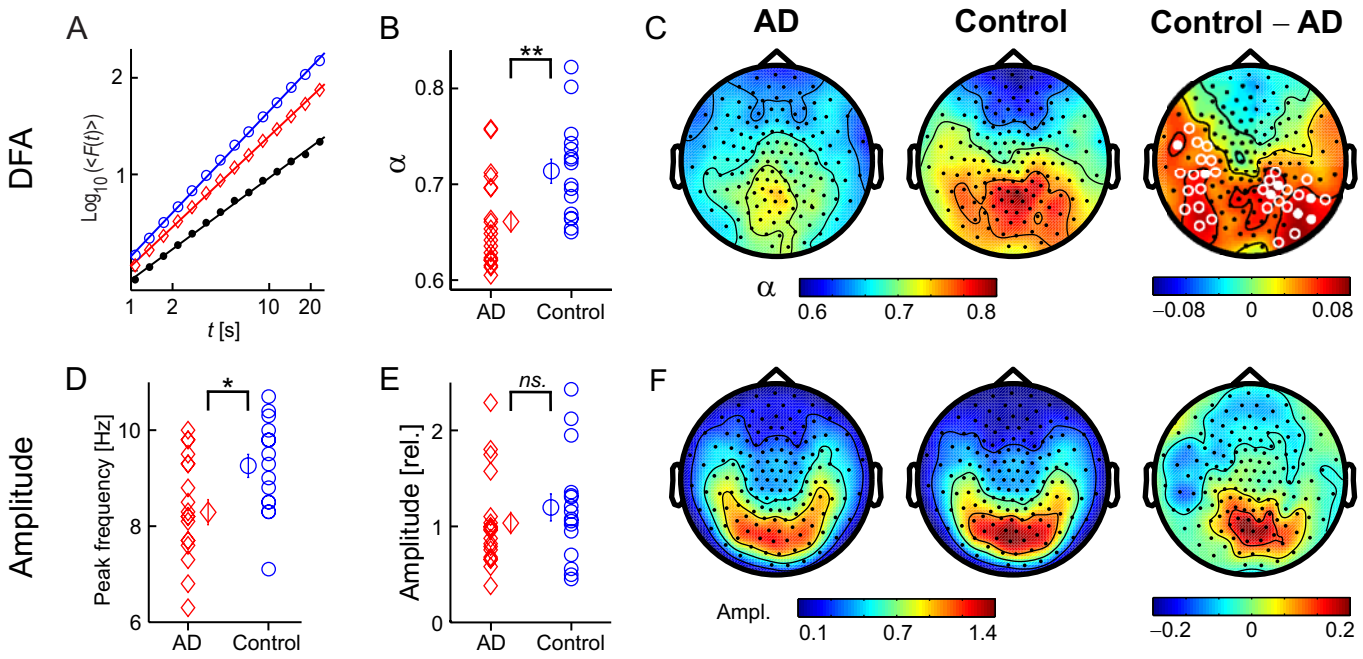
DFA
Amplitude
A
B
C
D
E
F
AD
Control
Control – AD
t [s]
α
Peak frequency [Hz]
Amplitude [rel.]
Ampl.
*
**
ns.

Figure 3

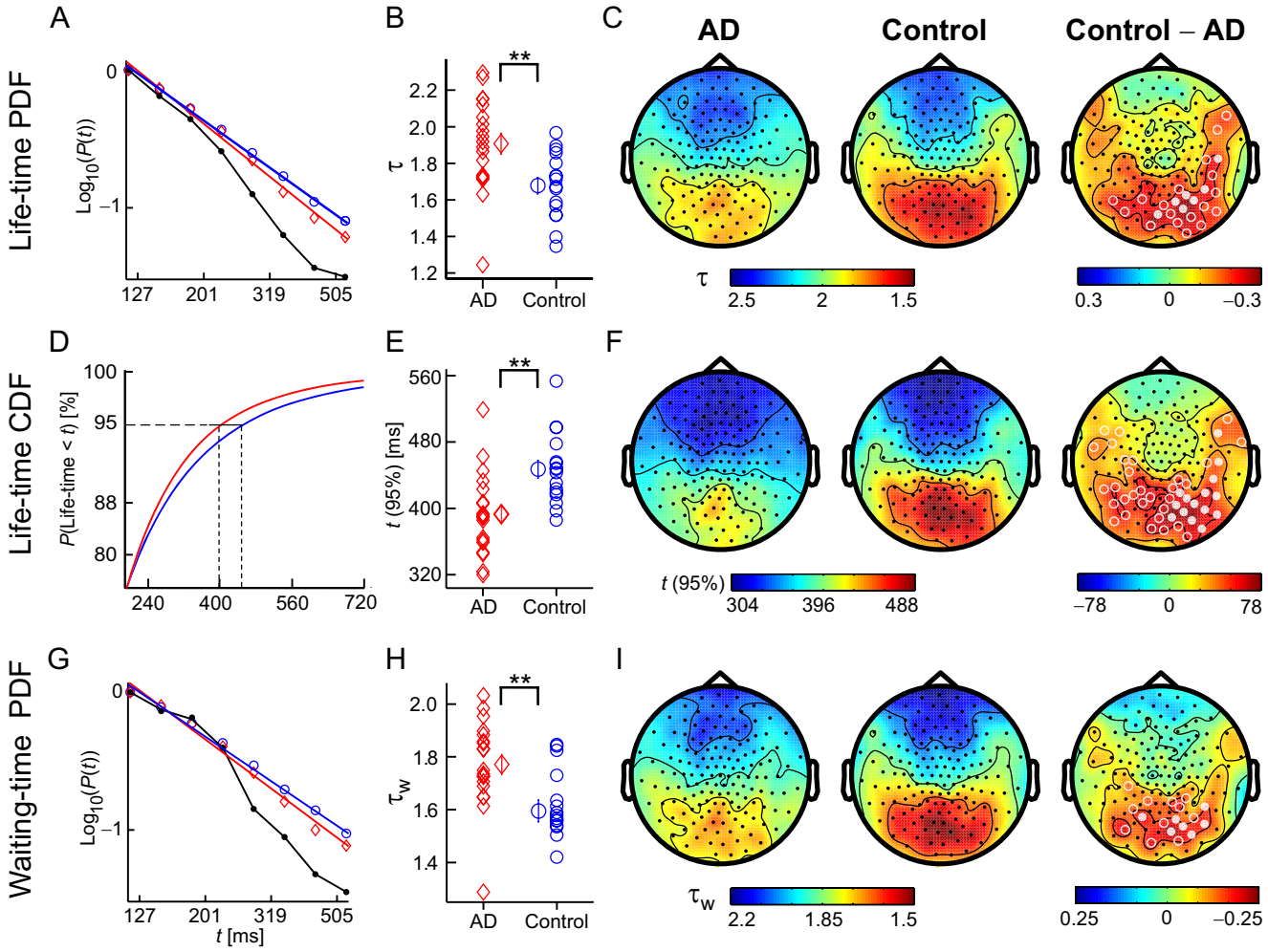
A
B
C
AD
Control
Control – AD
Life-time PDF
Log10(P(t))
0
−1
127
201
319
505
τ
2.2
2.0
1.8
1.6
1.4
1.2
**
AD
Control
τ
2.5
2
1.5
0.3
0
−0.3
D
E
F
Life-time CDF
P(Life-time < t) [%]
100
95
88
80
240
400
560
720
t (95%) [ms]
560
480
400
320
t (95%)
304
396
488
−78
0
78
G
H
I
Waiting-time PDF
t [ms]
τw
2.0
1.8
1.6
1.4
2.2
1.85
1.5
0.25
−0.25

Figure 4

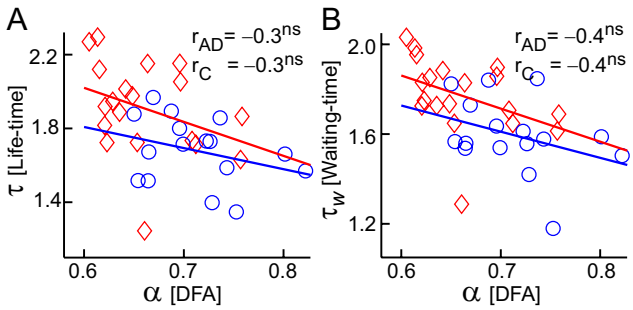
A
B
r_{AD}= –0.3^{ns}
r_C = –0.3^{ns}
r_{AD}= –0.4^{ns}
r_C = –0.4^{ns}
τ [Life-time]
τ_w [Waiting-time]
α [DFA]
α [DFA]
2.2
1.8
1.4
2.0
1.6
1.2
0.6
0.7
0.8
0.6
0.7
0.8

P4

ELSEVIER

Clinical Neurophysiology 116 (2005) 708–715

www.elsevier.com/locate/clinph

Disturbed fluctuations of resting state EEG synchronization in Alzheimer's disease

C.J. Stam[a,*], T. Montez[b,e], B.F. Jones[a,c], S.A.R.B. Rombouts[d], Y. van der Made[a], Y.A.L. Pijnenburg[c], Ph. Scheltens[c]

[a]*Alzheimer Centre, Department of Clinical Neurophysiology, VU University Medical Centre, P.O. Box 7057, 1007 MB Amsterdam, The Netherlands*
[b]*MEG Centre, VU University Medical centre, P.O. Box 7057, 1007 MB Amsterdam, The Netherlands*
[c]*Alzheimer Centre, Department of Neurology, VU University Medical Centre, P.O. Box 7057, 1007 MB Amsterdam, The Netherlands*
[d]*Department of Physics & Medical Technology, VU University Medical Centre, P.O. Box 7057, 1007 MB Amsterdam, The Netherlands*
[e]*Institute of Biophysics and Biomedical Engineering, Faculty of Sciences, University of Lisbon, Portugal*

Accepted 25 September 2004
Available online 28 October 2004

Abstract

Objective: We examined the hypothesis that cognitive dysfunction in Alzheimer's disease is associated with abnormal spontaneous fluctuations of EEG synchronization levels during an eyes-closed resting state.

Methods: EEGs were recorded during an eyes-closed resting state in Alzheimer patients ($N=24$; 9 males; mean age 76.3 years; SD 7.8; range 59–86) and non-demented subjects with subjective memory complaints ($N=19$; 9 males; mean age 76.1 years; SD 6.7; range: 67–89). The mean level of synchronization was determined in different frequency bands with the synchronization likelihood and fluctuations of the synchronization level were analysed with detrended fluctuation analysis (DFA).

Results: The mean level of EEG synchronization was lower in Alzheimer patients in the upper alpha (10–13 Hz) and beta (13–30 Hz) band. Spontaneous fluctuations of synchronization were diminished in Alzheimer patients in the lower alpha (8–10 Hz) and beta bands. In patients as well as controls the synchronization fluctuations showed a scale-free pattern.

Conclusions: Alzheimer's disease is characterized both by a lower mean level of functional connectivity as well as by diminished fluctuations in the level of synchronization. The dynamics of these fluctuations in patients and controls was scale-free which might point to self-organized criticality of neural networks in the brain.

Significance: Impaired functional connectivity can manifest itself not only in decreased levels of synchronization but also in disturbed fluctuations of synchronization levels.

Keywords: Alzheimer's disease; EEG synchronization; Detrended fluctuation analysis; Functional connectivity; Resting state; Self-organized criticality

1. Introduction

The exact nature of the neurophysiological processes underlying cognitive dysfunction in Alzheimer's disease is still incompletely understood. Many EEG studies have shown a slowing of the dominant rhythms in Alzheimer's disease (for a recent review see Jeong, 2004). This EEG slowing is usually interpreted as an indication of impaired activity of neural networks, possibly due to a lack of the excitatory neurotransmitter acetylcholine (Francis et al., 1999). Studies with functional MRI also point in the direction of impaired activity, especially during tasks that involve the medial temporal lobe memory systems (Rombouts et al., 2000). However, a simple relation between EEG slowing/impaired activity and cognitive dysfunction does not exist. For instance, there is no correlation between the frequency of the dominant alpha rhythm and intelligence (Posthuma et al., 2001).

Another approach focuses on the notion that higher brain functions invariably require cooperation of widely distributed specialized brain regions. According to this view,

* Corresponding author. Tel.: +31 20 4440727; fax: +31 20 4444816.
E-mail address: cj.stam@vumc.nl (C.J. Stam).

1388-2457/$30.00
doi:10.1016/j.clinph.2004.09.022

cognitive dysfunction in Alzheimer's disease might be due to a disturbance of these functional interactions between different brain regions. The idea that Alzheimer's disease is a disconnection syndrome is supported by neuropsychological, neuroanatomical and neurophysiological data (Delbeuck et al., 2003). Because of their high temporal resolution, EEG and MEG (magneto encephalography) are particularly suited for studying functional interactions between brain regions, although interpretation of such studies is complicated by the influence of volume conduction (Nolte et al., 2004). Abnormalities in coherence, which is a linear measure of the frequency dependent correlation between different EEG channels, support the notion of a disconnection syndrome in Alzheimer's disease (Adler et al., 2003; Berendse et al., 2000; Besthorn et al., 1994; Dunkin et al., 1994; Knott et al., 2000; Leuchter et al., 1987, 1992; Locatelli et al., 1998). Recently, these results have been confirmed with nonlinear measures of correlation between EEG and MEG signals such as the mutual information (Jeong et al., 2001) and the synchronization likelihood (Pijnenburg et al., 2004; Stam et al., 2002b, 2003b).

However, a decrease in the mean level of functional interactions between different brain regions may reflect only part of the abnormalities in Alzheimer's disease. There is increasing support for the notion that cognition is essentially a dynamic process which requires the constant creation and destruction of different synchronized neural networks (Breakspear and Terry, 2002; Freeman and Rogers, 2002; Friston, 2000; Rodriguez et al., 1999). This process of formation and destruction of synchronous networks is reflected in spontaneous fluctuations in the mean level of synchronization. A promising method to characterize these spontaneous fluctuations in the mean level of synchronization is detrended fluctuation analysis (Peng et al., 1992, 1995). This method characterizes the relation between the variance of some measure (after correction for the local linear trend) as a function of time scale. In complex dynamical systems this relation often obeys a power law. Consequently, in this case, the logarithm of the fluctuations is a simple linear function of the logarithm of the time scale and can be characterized completely by its slope (DFA exponent) and its intercept with the *Y*-axis. Systems that display this kind of behaviour are said to be 'scale free'. Such systems do not have one characteristic time scale, but show similar statistical properties on all timescales. Several studies have applied detrended fluctuation analysis to single channel EEG analysis and have found indications for scale free fluctuations (Linkenkaer-Hansen et al., 2001; Worrell et al., 2002). Recently, we have shown that spontaneous fluctuations of synchronization between EEG channels in healthy subjects also display scale free characteristics (Stam and de Bruin, 2004).

The present study was undertaken to examine the hypothesis that Alzheimer's disease is characterized not only by a decrease in the mean level of synchronization, but also by abnormalities in the spontaneous fluctuations of the synchronization level. For this purpose we examined resting state EEG recordings of 24 patients with Alzheimer's disease and 19 non-demented subjects with subjective memory complaints. Global levels of EEG synchronization in different frequency bands were quantified with the synchronization likelihood (Stam and van Dijk, 2002). Time series of spontaneous fluctuations in the synchronization likelihood level were examined with detrended fluctuation analysis.

2. Methods and materials

2.1. Subjects

The study involved consecutive subjects referred to the Alzheimer Centre at the VU university medical centre (Y.P.; P.S.). All subjects were studied according to a protocol which involved history taking, physical and neurological examination, blood tests (ESR, hemoglobin, white cell count, serum electrolytes, glucose, BUN, creatinine, liver function tests, TSH and free thyroid hormone, vitamin B1 and B6 levels, syphilis serology), MMSE, neuropsychological examination, MRI of the brain and a quantitative EEG. The final diagnosis was based upon a consensus meeting where all the available clinical data and the results of the ancillary investigations were considered. A diagnosis of probable Alzheimer's disease was based upon the McKhann criteria (McKhann et al., 1984).

The present study concerns 43 subjects, 24 with a diagnosis of probable Alzheimer's disease (9 males; mean age 76.3 years; SD 7.8; range 59–86); and 19 control subjects with only subjective memory complaints ('SC'; 9 males; mean age 76.1 years; SD 6.7; range: 67–89). Mean MMSE score of the Alzheimer patients was 18.8 (SD 3.8; range 10–26); mean MMSE score of the SC subjects was 27.6 (SD 2.5; range 22–30).

2.2. EEG recording

EEGs were recorded in all subjects as part of the examination protocol. EEGs were recorded (against C3–C4) with a Nihon Kohden digital EEG apparatus (EEG 2100) at the following positions of the 10–20 system: Fp2, Fp1, F8, F7, F4, F3, A2, A1, T4, T3, C4, C3, T6, T5, P4, P3, O2, O1, Fz, Cz, Pz. ECG was recorded in a separate channel. Electrode impedance was below 5 kOhm. Initial filter settings were: time constant, 1 s; low pass filter, 70 Hz. Sample frequency was 200 Hz and A–D precision 12 bit. EEGs were recorded in a sound attenuated, dimly lit room while patients sat in a slightly reclined chair. Care was taken by the EEG technicians to keep the patients awake during the whole recording. For the present analysis artefact-free epochs (containing no eye-blinks, slow eye-movements, excess muscle activity, ECG artefacts etc.) of 4096 samples (20.475 s) were selected off-line. These epochs were re-referenced to an average reference electrode, involving all

electrodes except Fp2 and Fp1. Computation of the synchronization likelihood and detrended fluctuation analysis were done with the DIGEEGXP software written by one of the authors (CS). The synchronization likelihood time series was determined and the detrended fluctuation analysis was done on this time series. All analyses were done separately for the following frequency bands: delta (0.5–4 Hz); theta (4–8) Hz, lower alpha or alpha1 (8–10 Hz), upper alpha or alpha 2 (10–13 Hz), beta (13–30 Hz) and gamma (30–48 Hz).

2.3. Synchronization likelihood

The synchronization likelihood (SL) is a measure of the statistical interdependencies between two time series, for instance two EEG channels. The synchronization likelihood takes on values between P_{ref} (a small number close to 0) in the case of independent time series and one in the case of fully synchronized time series. The synchronization likelihood is sensitive to linear as well as non-linear interdependencies and can be computed for each time sample, making it suitable for tracking time-dependent changes in the synchronization level. For a technical description of the method and its properties we refer to Stam and van Dijk (2002). Here we explain the general principles.

Assume we have two time series x_i and y_i, where the index i denotes discrete time. From each of these time series and for each time i we construct m dimensional vectors X_i and Y_i in state space with the method of time-delay embedding (Takens, 1981) as follows:

$$X_i = (x_i, x_{i+L}, x_{i+2L}, x_{i+3L}, \ldots, x_{i+(m-1)L}) \quad (1)$$

where L is the time lag, and m the embedding dimension. These m-dimensional vectors X_i (Y_i is defined similarly) can be thought of as representing the 'state' of the system underlying the time series at a moment in time. Synchronization likelihood is now defined as the conditional likelihood that Y_i and Y_j will be very close together ('close together' means that the distance between Y_i and Y_j in state space is smaller than the critical cut-off distance), given that X_i and X_j are very close together. In other words, the synchronization likelihood is the likelihood that if system X is (almost) in the same state at two different times i and j, that system Y will also be (almost) in the same state at i and j. In the case of maximal synchronization this chance is 1; in the case of independent systems, it is a small, but non-zero number, namely P_{ref}. This small number is the likelihood that two randomly chosen vectors Y (or X) will be closer than the cut-off distance. In practice, the cut-off distance is chosen such that the likelihood of random vectors being close is fixed at P_{ref}, which is chosen the same for X and for Y.

In the computation of distances between the vectors X_i, X_j and Y_i, Y_j, further restrictions are involved: only those vectors are used where the time indices fall in a range determined by two windows: ($w1 < |i-j| < w2$) (|| denotes absolute values). The first window $w1$, also termed Theiler correction, excludes vector pairs from the calculations that are close together simply due to autocorrelation properties of the time series (Theiler, 1986). The second window $w2$ increases the time resolution of the SL computation by excluding vector pairs that are too far away in time. In the present study $w1 = 100$ and $w2$ was 1/10 of the length of the EEG time series. The other parameters were set as follows: log $L = 10$; embedding dimension $m = 10$; $P_{\text{ref}} = 0.01$. With the exception of P_{ref}, these choices were the same as in a number of previous studies (Stam et al., 2002a,b, 2003a,b).

In the present study we computed the synchronization likelihood averaged over all possible pairs of channels ($19 \times 18/2$) for each 16th time sample of the EEG time series. This resulted in a 'time series' of SL values with a length of $4096/16 = 256$ samples (the length of the EEG time series was 4096 samples). This time series of synchronization values was subjected to detrended fluctuation analysis.

2.4. Detrended fluctuation analysis

Detrended fluctuation analysis (DFA) is a technique used to characterize the correlation structure of non-stationary time series. DFA studies investigate how the variance in a time series depends upon the timescale used to determine this variance; this dependence is characterized by the exponent of a linear fit through a double logarithmic plot of variance as a function of timescale. It was initially introduced to characterize long-range correlations between nucleotide sequences (Peng et al., 1992). Here we closely follow the description of the method as given by Peng et al. (1995). A schematic representation is shown in Fig. 1 of Stam and de Bruin (2004).

The analysis is applied to a discrete time series $x(i)$, $i = \{1 \ldots N\}$, which in the present study represents

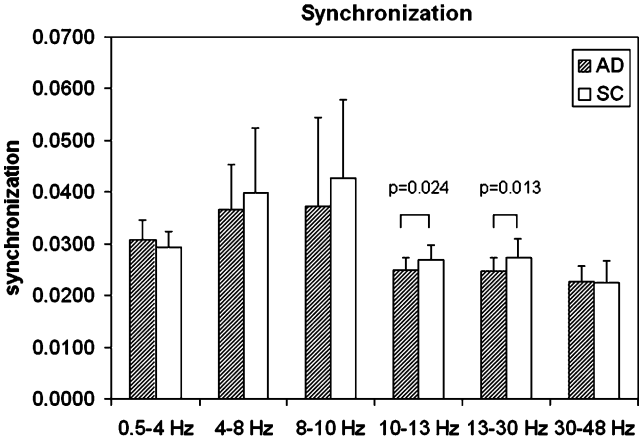

Fig. 1. Mean synchronization likelihood (error bars denote standard deviations) of Alzheimer patients (AD; $N = 24$) and subjects with subjective memory complaints (SC; $N = 19$) for different frequency bands. Alzheimer patients had a significantly lower synchronization in the upper alpha and beta band. P values in plot correspond to two-tailed t-test.

the synchronization likelihood averaged over all pairs of channels for each time sample ($N=4096/16=256$). In the first step, the mean is subtracted from this time series and the time series is integrated

$$y(k) = \sum_{i=1}^{k} [x(i) - \langle x \rangle] \quad (2)$$

where $\langle x \rangle$ is the average of the synchronization likelihood time series. Next, the de-meaned, integrated time series $y(k)$ is divided in a number of segments with length n (n represents the time scale of observation). In this study we used the following segment lengths: 4, 8, 16, 32, 64 and 128 samples. For each of these segments, the local least-squares linear fit is determined. The ensuing piece-wise linear fit is designated $y_n(k)$. Then, the integrated time series $y(k)$ is detrended by subtracting the local linear fit $y_n(k)$ for each segment. The root mean square fluctuation of this integrated and detrended time series is given by:

$$F(n) = \sqrt{\frac{1}{N} \sum_{k=1}^{N} [y(k) - y_n(k)]^2} \quad (3)$$

Subsequently, this determination of $F(n)$ is repeated for a range of different scales n (in the present study n ranged from 4 samples to 128 samples). In a final step, the logarithm of $F(n)$ is plotted as a function of the logarithm of the time scale n (we used logarithms with a base of 2). If the time series $x(i)$ has self-similar, scale-free (fractal) properties, this plot will display a linear scaling region with a certain scaling exponent. The exponent of the plot of $\mathrm{Log}_2(F(n))/\mathrm{Log}_2(n)$ is called the scaling or self-similarity coefficient. This exponent is 0.5 if $x(i)$ is uncorrelated white noise; it is 1.5 if $x(i)$ is Brownian noise (which is highly correlated), and it is 1 if $x(i)$ is $1/f$ noise.

However, it cannot be excluded that the exponent will be influenced by such factors as finite data length, filtering and computation of the synchronization likelihood (which involves several windows). To determine the extent to which this is the case, and to allow a statistical test of the hypothesis that the DFA exponent > exponent of noise, 20 control data sets were generated. These data sets had the same dimensions (data length; number of channels) as the EEG data, but all channels were filled with white noise, and there were no correlations between the channels. These 20 data sets were analysed in the same way as the EEG data.

In the present study the linear fit was determined from 6 points of the DFA plot. From this fit the exponent, the intercept with the Y-axis and the goodness of fit (expressed as the squared correlation coefficient R^2) were determined.

2.5. Statistical analysis

Statistical analysis was done with SPSS for Windows, version 10.0.7. Differences in group means were tested with independent samples t-tests. Correlations between MMSE scores and EEG measures (mean synchronization, DFA exponent, intercept and R^2 for all frequency bands) were determined with Pearson correlation coefficients. The significance level was set at $P<0.05$.

3. Results

The mean synchronization likelihood (averaged over all pair-wise combinations of channels and all time points) for both groups and all frequency bands is shown in Fig. 1. Differences between Alzheimer patients and subjects with subjective complaints were tested with independent samples t-tests (equal variances not assumed) for each frequency band. Mean synchronization was significantly lower in the Alzheimer group in the alpha 2 band ($t[41]=-2.362$; $P=0.024$) and in the beta band ($t[41]=-2.630$; $P=0.013$). Group differences in the other frequency bands were not significant.

The mean results of the DFA analysis are shown in Table 1. In all frequency bands the 3 DFA measures (exponent, intercept and goodness of fit) were compared

Table 1
Mean results (SD in brackets) of the detrended fluctuation analysis of the synchronization likelihood time series in different frequency bands

Measure	Group	Frequency band					
		0.5–4 Hz	4–8 Hz	8–10 Hz	10–13 Hz	13–30 Hz	30–48 Hz
Exponent	AD	0.841* (0.092)	0.900* (0.117)	0.970*$^{\&}$ (0.134)	0.842*$^{\#}$ (0.104)	0.690* (0.091)	0.618* (0.070)
	SC	0.838* (0.087)	0.959* (0.139)	1.031*$^{\&}$ (0.093)	0.786*$^{\#}$ (0.077)	0.707* (0.091)	0.639* (0.092)
	Noise	0.673 (0.083)	0.710 (0.061)	0.716 (0.074)	0.681 (0.076)	0.580 (0.058)	0.551 (0.068)
Intercept	AD	−8.493 (0.192)	−8.814 (0.262)	−9.096 (0.432)	−9.312$^{\#}$ (0.180)	−9.361$^{\&}$ (0.241)	−9.410 (0.254)
	SC	−8.528 (0.272)	−8.852 (0.339)	−8.920 (0.481)	−9.085$^{\#}$ (0.218)	−9.180$^{\&}$ (0.342)	−9.470 (0.219)
	Noise	−9.232 (0.213)	−9.652 (0.131)	−9.900 (0.198)	−9.875 (0.178)	−10.044 (0.151)	−9.98 (0.166)
R^2	AD	0.990$^{\$}$ (0.007)	0.984 (0.011)	0.994 (0.005)	0.992 (0.0112)	0.988 (0.008)	0.988 (0.112)
	SC	0.989 (0.011)	0.988 (0.010)	0.996$^{\$}$ (0.004)	0.987 (0.014)	0.987 (0.014)	0.992$^{\$}$ (0.006)
	Noise	0.984 (0.011)	0.980 (0.015)	0.990 (0.012)	0.987 (0.015)	0.987 (0.013)	0.981 (0.019)

'Exponent', exponent of the linear fit through the DFA plot; 'Intercept', intercept of the linear fit; 'R^2', squared correlation coefficient as a measure of the goodness of fit; AD, Alzheimer patients ($N=24$); SC, subjects with subjective memory complaints ($N=19$); Noise, uncorrelated noise data sets ($N=20$). *$P<0.001$ (significant difference compared with noise); $^{\$}P<0.05$ (significant difference compared with noise); $^{\#}P<0.05$ (significant difference AD–SC); $^{\&}P<0.10$ (trend AD–SC).

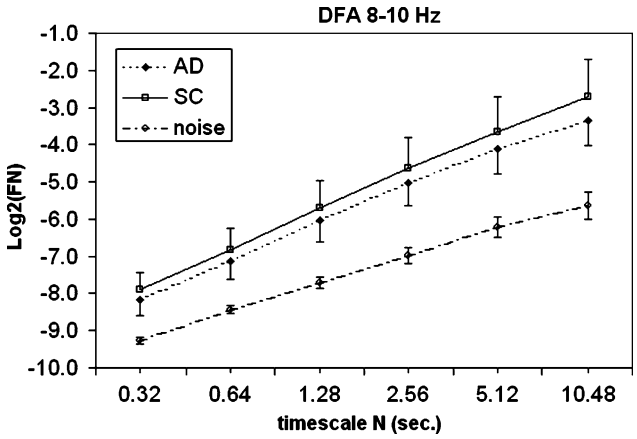

Fig. 2. Mean DFA plots (error bars denote standard deviations) of Alzheimer patients (AD; $N=24$) and subjects with subjective memory complaints (SC; $N=19$) for the lower alpha band (8–10 Hz). The plot shows the LOG_2 of the detrended fluctuation F_N as a function of time scale N (s). For comparison the results of a control data set of 20 white noise epochs subjected to the same analysis (filtering, SL computation and DFA analysis of the SL time series) as the EEG data are shown.

between AD patients, subjects with subjective complaints and noise control data (however, for the noise control data the intercep was not considered in the statistical analysis since it is arbitrary). Although the exponent for the noise data was higher than 0.5, the exponent of the EEG data (both AD and SC) was significantly larger compared to the exponent of the noise data in all frequency bands ($P<$ 0.001 for all comparisons). The goodness of fit for the noise data was close to 1 in all frequency bands, but it was significantly smaller (implying a worse linear fit) compared to the fit for the AD group in the delta band, and compared to the fit for the SC group in the lower alpha and the gamma band.

In the lower alpha band there was a trend in the direction of a smaller DFA exponent for the AD group compared to the SC group ($P=0.085$); in the upper alpha band the DFA exponent was significantly larger in the AD group compared to the SC group ($P=0.048$). The DFA intercept was smaller in the AD group compared to the SC group in the upper alpha band, ($P=0.008$) and there was a trend in the same direction in the beta band ($P=0.059$). Detailed results for the lower alpha band are shown in Fig. 2, for the upper alpha band in Fig. 3 and for the beta band in Fig. 4. In the theta band there was a positive correlation between the DFA exponent and the MMSE score.

In the upper alpha band a significant negative correlation was found between DFA exponent, goodness of fit and the MMSE score.

4. Discussion

The most important finding of the present study is that Alzheimer's disease is characterized not only by a decrease in mean levels of EEG synchronization, but also by changes in the spontaneous fluctuations of EEG synchronization. Mean levels of synchronization were decreased in Alzheimer patients in the upper alpha band and the beta band. Spontaneous fluctuations of the synchronization level were diminished in Alzheimer patients in the upper alpha band and to a lesser extent in the beta band. In the upper alpha band, the DFA exponent was larger in the Alzheimer group for the upper alpha band. Finally, both mean synchronization level as well as DFA parameters showed correlations with the MMSE score.

The changes in mean synchronization level in the present study are largely in agreement with the results of earlier studies using synchronization likelihood to characterize statistical interdependencies between EEG or MEG signals in early and mild Alzheimer's disease (Stam et al., 2002b, 2003b; Pijnenburg et al., 2004). The general pattern in these studies in early and mild Alzheimer patients was a preferential involvement of the upper alpha and especially the beta band. Loss of synchronization in the gamma band could only be shown in the MEG study, and this might be due to the higher sensitivity of MEG compared to EEG for subtle, possibly nonlinear coupling at higher frequencies (Stam et al., 2002b; 2003a). Another recent study that used synchronization likelihood reported a lower synchronization in Alzheimer patients in the delta, theta, alpha and beta bands (Babiloni et al., 2004). The involvement of lower frequency bands in this study could be due to the fact that the control subjects were healthy subjects without memory complaints, whereas the other studies as well as the present one used non-demented subjects with subjective memory complaints as controls. Furthermore, in the Babiloni et al. study the control subjects were significantly younger than the patients, requiring a statistical correction for age effects. Finally, in contrast to the other studies in which an average reference was used, Babiloni et al. used a source montage (determined from the local average of the surrounding electrodes) which will result in different and lower synchronization values (Babiloni et al., 2004; Stam and de Bruin, 2004). In the present study Alzheimer patients and subjects with subjective memory complaints were carefully matched for age (AD, mean age 76.3 year; SD 7.8; range 59–86; SC, mean age 76.1 year; SD 6.7; range, 67–89). Consequently, the synchronization loss in the upper alpha and beta band may well represent the first change in Alzheimer's disease.

Other studies using different nonlinear measures (Jeong et al., 2001) or the more usual coherence analysis have also reported loss of functional connectivity in Alzheimer's disease in different frequency bands (Adler et al., 2003; Berendse et al., 2000; Besthorn et al., 1994; Dunkin et al., 1994; Knott et al., 2000; Leuchter et al., 1987, 1992; Locatelli et al., 1998). Although these studies vary greatly in terms of characteristics of patient and control groups, choice of electrode pairs and montage, and choice of frequency

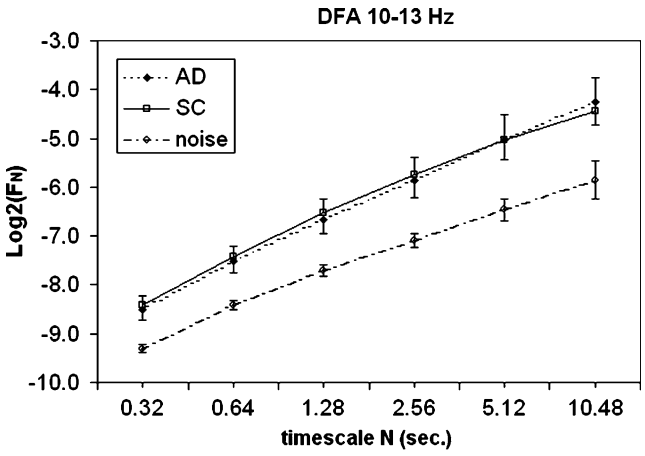

Fig. 3. Mean DFA plots (error bars denote standard deviations) of Alzheimer patients (AD; $N=24$) and subjects with subjective memory complaints (SC; $N=19$) for the upper alpha band (10–12 Hz). The plot shows the LOG_2 of the detrended fluctuation F_N as a function of time scale N (s). For comparison the results of a control data set of 20 white noise epochs subjected to the same analysis (filtering, SL computation and DFA analysis of the SL time series) as the EEG data are shown.

bands, the general pattern of loss of synchronization in Alzheimer's disease seems consistent and the alpha band is nearly always involved. The present study is in agreement with these findings but stresses the importance of distinguishing between lower and upper alpha band processes.

Although there seems to be widespread agreement in the literature that linear and nonlinear measures reflect lower levels of statistical interdepence between EEG and MEG time series in Alzheimer's patients, any interpretation of such findings in terms of true loss of functional connectivity in the underlying networks can only be tentative. Volume conduction strongly affects EEG recordings, and may produce spurious correlations, especially between nearby channels. To avoid this problem one could consider correlations between time series of reconstructed sources, but this approach presents its own problems, since there is no unique solution to the inverse problem. One promising solution is to consider the imaginary component of the coherence, which is insensitive to contributions from volume conduction (Nolte et al., 2004). Future studies should consider approaches along these lines to determine whether lower levels of statistical interdependencies in Alzheimer's disease reflect true loss of functional connectivity.

The main goal of the present study was the characterization of spontaneous fluctuations in the global level of synchronization in Alzheimer patients and non-demented control subjects. Detrended fluctuation analysis of synchronization time series always showed a good to perfect linear relation between the strength of the fluctuations and the time scale on a double logarithmic plot. The squared correlation coefficient of this linear fit was very high in all frequency bands, and in both groups (Table 1). This finding, in combination with the DFA exponents (see below), is an indication that the spontaneous fluctuations of the synchronization in different frequency bands has a scale-free character, at least on the time scales studied, that is from 0.32 to 10.24 s. Also, the goodness of fit was similar in Alzheimer patients and subjects with subjective memory complaints in all frequency bands. The scale-free fluctuations of synchronization in the present study are in agreement with the findings of a previous study in young, healthy subjects, and extend these observations to longer time scales (Stam and de Bruin, 2004).

The slope of the linear fit through the DFA plots (the DFA exponent) was similar in both groups and all frequency bands, with the exception of the upper alpha band where the slope was larger in the AD group (Table 1). The values of the DFA exponent for the delta, theta and alpha band were all very close to 1. The values of the exponent for higher frequency bands were somewhat lower, and decreased from the upper alpha band to the gamma band. However, in all frequency bands the exponent was larger than the slope of a set of random control data subjected to the same filtering, SL computation and DFA analysis, which suggests the existence of significant long range correlations in the global level of synchronization. The DFA also showed a significant difference between the two groups. In the upper alpha and the beta band the intercept was smaller in the Alzheimer group (Table 1). A smaller intercept indicates that the fluctuations of EEG synchronization in the upper alpha and the beta band are smaller in the Alzheimer group. In other words, the DFA plot in Alzheimer patients is shifted as a whole to a lower level (see Fig. 4).

Scale-free fluctuations, like those detected for spontaneous fluctuations of EEG synchronization levels in the present study, can be found in many types of complex systems (Bak and Paczuski, 1995). Despite its ubiquity, a generally accepted universal explanation of scale-free dynamics does not yet exist. The most ambitious attempt to

Table 2
Correlations between MMSE score, synchronization, and DFA parameters (exponent, intercept and R^2)

	Frequency band					
	0.5–4 Hz	4–8 Hz	8–10 Hz	10–13 Hz	13–30 Hz	30–48 Hz
Synchronization	−0.313*	0.310*	0.271	0.175	0.358*	−0.150
Exponent	−0.165	0.386*	0.238	−0.443**	−0.077	0.038
Intercept	−0.024	0.104	−0.260	0.050	0.272	−0.229
R^2	−0.097	0.215	−0.152	−0.419**	−0.080	0.297

*$P<0.05$; **$P<0.01$ (two-tailed).

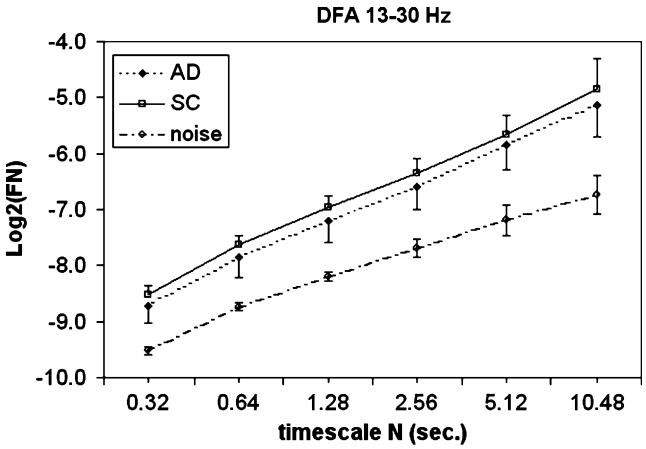

Fig. 4. Mean DFA plots (error bars denote standard deviations) of Alzheimer patients (AD; $N=24$) and subjects with subjective memory complaints (SC; $N=19$) for the beta band (13–30 Hz). The plot shows the LOG_2 of the detrended fluctuation F_N as a function of time scale N (s). For comparison the results of a control data set of 20 white noise epochs subjected to the same analysis (filtering, SL computation and DFA analysis of the SL time series) as the EEG data are shown.

provide a general explanation is the theory of self-organized criticality (SOC) introduced by Per Bak (Bak et al., 1987, 1988). Self-organized criticality refers to large systems with local non-linear interactions in which a slow build-up of some energy value is alternated with brief bursts ('ava-avalanches') of energy redistribution. Such systems evolve to a critical state without tuning, which is characterized by spatial and temporal power laws and scale-free dynamics. The critical state of this type of system is very robust (it is a powerful attractor of the dynamics), and is associated with an optimal response to outside disturbances.

Several models have been proposed for self-organized criticality (Turcotte, 1999). Neurons can be modelled as integrate-and-fire oscillators, where the integration (slow changes in the membrane potential) corresponds with the slow build-up of energy, and the firing (action potential) corresponds with the fast energy redistribution. Consequently, large networks of interconnected neurons are likely candidates for self-organized criticality. Evidence for SOC has been found in models of neural networks as well as in neural networks cultured in vitro (Beggs and Plens, 2003; Corral et al., 1995). Several studies of EEG and MEG provide further support for the hypothesis that the neural networks of the brain also display SOC at a macroscopic level (Linkenkaer-Hansen et al., 2001; Nikulin and Brismar, 2004; Stam and de Bruin, 2004; Worrell et al., 2002).

The present study suggests that self-organized criticality might explain normal as well as abnormal brain dynamics, since scale-free dynamics was equally clear in control subjects and Alzheimer patients. Apparently, the self-organized state is very robust, and persists even in the case of neural loss and changes in levels of neurotransmitters. This resistance of the SOC against small parameter changes was also reported for cultured neural networks (Beggs and Plens, 2003). However, even though the general pattern of SOC may persist in Alzheimer's disease, we could show that its specific parameters are changed, and that the magnitude of synchronization fluctuations is shifted to a lower level in patients in the upper alpha and to a lesser extent in the beta band, at least on the time scales studied. A possible interpretation of this finding is that larger fluctuations of EEG synchronization reflect stronger and more rapid creation and destruction of subsequent synchronous neural networks. Disruption of this process might be associated with a loss of cognitive flexibility and processing speed in Alzheimer's disease, and may manifest itself in the 'downward shift' of the DFA plot, at least in the upper alpha and beta band. This interpretation is supported by the finding that the strongest correlation between any EEG measure and an estimate of cognition was that between a higher upper alpha band DFA intercept (implying stronger synchronization fluctuations) and the MMSE score (Table 2, Fig. 3).

In this context it is important to stress that the 'eyes-closed, resting state' we studied is more closely related to cognition than is often appreciated. Using fMRI Greicius et al. showed that during such a resting state a complex network involving the posterior cingulate gyrus, bilateral inferior parietal cortex, left inferolateral temporal cortex, and ventral anterior cingulated cortex, is active (Greicius et al., 2003). In a recent study the same group showed that this resting state network is disrupted in Alzheimer's disease (Greicius et al., 2004). This supports an interpretation of the synchronization and DFA findings of the present study in terms of a disrupted 'default network'. Functional MRI and EEG are complementary in demonstrating spatial and time dependent characteristics of the default network and its abnormalities in Alzheimer's disease. Integrated EEG/fMRI will become available soon and may enable further exploring the pathophysiology of neural networks involved in cognitive dysfunction in Alzheimer's disease.

Acknowledgements

TM is the recipient of a Praxis XXI doctoral fellowship from FCT, Ministry of Science, Portugal. SARB R is supported by a grant of the Netherlands Organisation for Scientific Research (NWO). The authors would like to thank the two anonymous referees for valuable comments on an earlier draft of this paper.

References

Adler G, Brassen S, Jajcevic A. EEG coherence in Alzheimer's dementia. J Neural Transm 2003;110:1051–8.

Babiloni C, Ferri F, Moretti DV, Strambi A, Binetti G, Dal Forno G, Ferreri F, Lanuzza B, Bonato C, Nobili F, Rodriguez G, Salinari S,

Passero S, Rocchi R, Stam CJ, Rossini PM. Abnormal fronto–parieto coupling of brain rhythms in mild Alzheimer's disease: a multicentric EEG study. Eur J Neurosci 2004;19:1–9.

Bak P, Paczuski M. Complexity, contingency, and criticality. Proc Natl Acad Sci 1995;92:6689–96.

Bak P, Tang Ch, Wiesenfeld K. Self-organized criticality: an explanation of 1/*f* noise. Phys Rev Lett 1987;59:381–4 [83].

Bak P, Tang Ch, Wiesenfeld K. Self-organized criticality. Phys Rev A 1988;38:364–74.

Beggs JM, Plens D. Neuronal avalanches in neocortical circuits. J Neurosci 2003;23:11167–77.

Berendse HW, Verbunt JPA, Scheltens Ph, van Dijk BW, Jonkman EJ. Magnetoencephalographic analysis of cortical activity in Alzheimer's disease. A pilot study. Clin Neurophysiol 2000;111:604–12.

Besthorn C, Forstl H, Geiger-Kabisch C, Sattel H, Gasser T, Schreiter-Gasser U. EEG coherence in Alzheimer disease. Electroencephal Clin Neurophysiol 1994;90:242–5.

Breakspear M, Terry JR. Nonlinear interdependence in neural systems: motivation, theory, and relevance. Int J Neurosci 2002;112:1263–84.

Corral A, Perez J, Diaz-Guilera A, Arenas A. Self-organized criticality and synchronization in a lattice model of integrate-and-fire oscillators. Phys Rec Lett 1995;74:118–21.

Delbeuck X, Van der Linder M, Colette F. Alzheimer's disease as a disconnection syndrome? Neuropyschol Rev 2003;13:79–92.

Dunkin JJ, Leuchter AF, Newton TF, Cook IA. Reduced EEG coherence in dementia: state or trait marker? Biol Psychiatry 1994;35:870–9.

Francis PT, Palmer AM, Snape M, Wilcock GK. The cholinergic hypohtesis of Alzheimer's disease: a review of the progress. J Neurol Neurosurg Psychiatry 1999;66:137–47.

Freeman WJ, Rogers LJ. Fine temporal resolution of analytic phase reveals episodic synchronization by state transitions in gamma EEGs. J Neurophysiol 2002;87:937–45.

Friston KJ. The labile brain. I. Neuronal transients and nonlinear coupling. Phil Trans R Soc Lond B 2000;355:215–36.

Greicius MD, Krasnow B, Reiss AL, Menon V. Functional connectivity in the resting brain: a network analysis of the default mode hypothesis. Proc Natl Acad Sci 2003;100:253–8.

Greicius MD, Srivastava G, Reiss AL, Menon V. Default-mode network activity distinguishes Alzheimer's disease from healthy aging: evidence from functional MRI. Proc Natl Acad Sci 2004;101:4637–42.

Jeong J. EEG dynamics in patients with Alzheimer's disease. Clin Neurophysiol 2004;115:1490–505.

Jeong J, Gore JC, Peterson BS. Mutual information analysis of the EEG in patients with Alzheimer's disease. Clin Neurophysiol 2001;112: 827–35.

Knott V, Mohr E, Mahoney C, Ilivitsky V. Electroencephalographic coherence in Alzheimer's disease: comparisons with a control group and population norms. J Geriatr Psychiatry Neurol 2000;13:1–8.

Leuchter AF, Spar JE, Walter DO, Weiner H. Electroencephalographic spectra and coherence in the diagnosis of Alzheimer's-type and multi-infarct dementia. A pilot study. Arch Gen Psychiatry 1987;44:993–8.

Leuchter AF, Newton TF, Cook AA, Walter DO. Changes in brain functional connectivity in Alzheimer-type and multi-infarct dementia. Brain 1992;115:1543–61.

Linkenkaer-Hansen K, Nikouline VV, Palva JM, Ilmoniemi RJ. Long-range temporal correlations and scaling behavior in human brain oscillations. J Neurosci 2001;21:1370–7.

Locatelli T, Cursi M, Liberati D, Francheschi M, Comi G. EEG coherence in Alzheimer's disease. Electroencephal Clin Neurophysiol 1998;106: 229–37.

McKhann G, Drachman D, Folstein M, Katzman R, Price D, Stadlan EM. Clinical diagnosis of Alzheimer's disease: report of the NINCDS-ADRDA Work Group under the auspices of Department of Health and Human Services Task Force on Alzheimer's disease. Neurology 1984; 34:939–44.

Nikulin VV, Brismar T. Long-range temporal correlations in alpha and beta oscillations: effect of arousal level and test–retest reliability. Clin Neurophysiol 2004;115:1896–908.

Nolte G, Wheaton OBL, Mari Z, Vorbach S, Hallett M. Identifying true brain interaction from EEG data using the imaginary part of coherency. Clin Neurophysiol 2004;115:2292–307.

Peng CK, Buldyrev SV, Goldberger AL, Havlin S, Sciortino F, Simons M, Stanley HE. Long-range correlations in nucleotide sequences. Nature 1992;356:168–70.

Peng CK, Havlin S, Stanley HE, Goldbergeer AL. Quantification of scaling exponents and crossover phenomena in nonstationary hearbeat time series. Chaos 1995;5:82–7.

Pijnenburg YAL, van de Made Y, van Cappellen van Walsum AM, Knol DL, Scheltens Ph, Stam CJ. EEG synchronization likelihood in mild cognitive impairment and Alzheimer's disease during a working memory task. Clin Neurophysiol 2004;115:1332–9.

Posthuma D, Neale MC, Boomsma DI, de Geus EJC. Are smarter brains running faster? Heritability of alpha peak frequency, IQ, and their interrelation Behav Genet 2001;31:567–79.

Rodriguez E, George N, Lachauz JP, Martinerie J, Renault B, Varela FJ. Perception's shadow: long distance synchronization of human brain activity. Nature 1999;397:430–3.

Rombouts SARB, Barkhof F, Veltman DJ, Machielsen WCM, Witter MP, Bierlaagh MA, Lazeron RHC, Valk J, Scheltens P. Functional MR imaging in Alzheimer's disease during memory encoding. Am J Neuroradiol 2000;21:1869–75.

Stam CJ, de Bruin EA. Scale-free dynamics of global functional connectivity in the human brain. Hum Brain Mapp 2004;22:97–109.

Stam CJ, van Dijk BW. Synchronization likelihood: an unbiased measure of generalized synchronization in multivariate data sets. Physica D 2002; 163:236–41.

Stam CJ, van Cappellen van Walsum AM, Micheloyannis S. Variability of EEG synchronization during a working memory task in healthy subjects. Int J Psychophysiol 2002a;46:53–66.

Stam CJ, van Cappellen van Walsum AM, Pijnenburg YAL, Berendse HW, de Munck JC, Scheltens Ph, van Dijk BW. Generalized synchronization of MEG recordings in Alzheimer's disease: evidence for involvement of the gamma band. J Clin Neurophysiol 2002b;19: 562–74.

Stam CJ, Breakspear M, van Cappellen van Walsum AM, van Dijk BW. Nonlinear synchronization in EEG and whole-head MEG recordings of healthy subjects. Hum Brain Mapp 2003a;19:63–78.

Stam CJ, van der Made Y, Pijnenburg YAL, Scheltens Ph. EEG synchronization in mild cognitive impairment and Alzheimer's disease. Acta Neurol Scand 2003b;108:90–6.

Takens F. Detecting strange attractors in turbulence. Lect Note Math 1981; 898:366–81.

Theiler J. Spurious dimension from correlation algorithms applied to limited time-series data. Phys Rev A 1986;34:2427–32.

Turcotte DL. Self-organized criticality. Rep Prog Phys 1999;62:1377–429.

Worrell GA, Craunstoun SD, Echauz J, Litt B. Evidence for self-organized criticality in human epileptic hippocampus. NeuroReport 2002;13: 2017–21.